2023

THE DISCOVERY AND CHARACTERIZATION OF NOVEL POTENT 5-SUBSTITUTED 3, 3', 4', 7-TETRAMETHOXYFLAVONOID DNA TRIPLEX SPECIFIC BINDING LIGANDS

Vanessa Marie Rangel
University of the Pacific

Recommended Citation

THE DISCOVERY AND CHARACTERIZATION OF NOVEL POTENT
5-SUBSTITUTED 3, 3', 4', 7-TETRAMETHOXYFLAVONOID DNA TRIPLEX SPECIFIC
BINDING LIGANDS

By

Vanessa M. Rangel

A Dissertation Submitted

In Partial Fulfillment of the

Requirements for the Degree of

DOCTOR OF PHILOSOPHY

Thomas J. Long School of Pharmacy and Health Sciences
Pharmaceutical and Chemical Sciences

University of the Pacific
Stockton, California

2023

THE DISCOVERY AND CHARACTERIZATION OF NOVEL POTENT
5-SUBSTITUTED 3, 3', 4', 7-TETRAMETHOXYFLAVONOID DNA TRIPLEX SPECIFIC
BINDING LIGANDS

By

Vanessa M. Rangel

APPROVED BY:

Dissertation Advisor: Liang Xue, Ph.D.

Committee Member: George Pantouris, Ph.D.

Committee Member: Andreas Franz, Ph.D.

Committee Member: Wade Russu, Ph.D.

Committee Member: Craig Vierra, Ph.D.

Department Chair: Jerry Tsai, Ph.D.

THE DISCOVERY AND CHARACTERIZATION OF NOVEL POTENT
5-SUBSTITUTED 3, 3', 4', 7-TETRAMETHOXYFLAVONOID DNA TRIPLEX SPECIFIC
BINDING LIGANDS

Copyright 2023

By

Vanessa M. Rangel

Acknowledgments

I would first like to thank my advisor Dr. Liang Xue. It is because of him that I joined the PCSP program. I would not have reached this accomplishment without his guidance and support.

I would like to thank Dr. Andy Franz, Dr. George Pantouris, Dr. Wade Russu, and Dr. Craig Vierra for agreeing to be on my dissertation committee. Their feedback and assistance to my dissertation writing are appreciated.

My sincerest thank you goes to Faith Keith, Dr. Brett Williams, and Karen Johnson. Without them the chemistry department and my doctoral study would not have run smoothly.

Thank you to all the members of the Xue lab. Dr. Mandeep Sign, Landy Gu, and Nghia Tran. Their willingness to lend a helping hand has greatly aided the success of my doctoral studies. Additionally, thank you to all the undergraduates who have joined the group throughout the years. Especially, Justin Shen who has made my last year a pleasant and funny experience.

I would like to thank my parents Maria E Rangel and Mike Rangel for their unconditional love, support, and encouragement.

Lastly, I am grateful for financial support from the University of the Pacific and support for purchasing an isothermal titration calorimeter and a differential scanning calorimeter from the National Science Foundation (MRI-1828179). I am also grateful for financial support for this project from the National Institutes of Health (1R15GM148914-01).

THE DISCOVERY AND CHARACTERIZATION OF NOVEL POTENT
5-SUBSTITUTED 3, 3', 4', 7-TETRAMETHOXYFLAVONOID DNA TRIPLEX SPECIFIC
BINDING LIGANDS

Abstract

By Vanessa M. Rangel

University of the Pacific
2023

Chemotherapy works by killing fast dividing cells. Unfortunately, these drugs are not specific to cancer tissue and can damage normal cells. Chemotherapy is like taking poison and hoping it kills the cancer cells before it kills you. As an alternative, many researchers have investigated the use of antigene therapy to selectively target cancer causing genes to avoid off target effects. Although promising, the theory is limited by the stability of the triplex structure. Here, we report the discovery of potent triplex binding ligands derived from the natural product quercetin. Chemical derivatives of 5-substituted 3, 3', 4', 7-tetramethoxyquercetin derivatives were characterized using several biophysical methods: thermal denaturation monitored by UV, circular dichroism, viscometry, differential scanning calorimetry, and isothermal titration calorimetry. The data revealed that these derivatives specifically stabilize triplex DNA and do not influence the stability of duplex DNA, triple RNA, or duplex RNA. Structurally, the amino containing side chains at the 5-position and the linker length are critical for the observed binding affinity and specificity. Two derivatives, 5 and 7, are comparable (if not better) to the triplex groove binder Neomycin. Our data confirm the binding mode as enthalpically driven intercalation. Piperidine or pyrrolidine 5-substituted 3, 3', 4', 7-tetramethoxyquercetin derivatives with a three-carbon linker are the lead compounds for development as a potential antigene enhancer.

Table of Contents

List of Tables

Table

List of Figures

Figure

List of Abbreviations

A	Adenine
BBB	Blood Brain Barrier
C	Cytosine
˚C	Degree Celsius
CD	Circular Dichroism
DNA	Deoxyribonucleic Acid
ds	Double Strand
DSC	Differential Scanning Calorimetry
EDTA	Ethylenediaminetetraacetic Acid
G	Guanine
G4	G-Quadruplex
HBA	Hydrogen Bond Acceptor
HBD	Hydrogen Bond Donor
HPV	Human Papillomavirus
ITC	Isothermal Titration Calorimetry
KCl	Potassium Chloride
K_d	Dissociation Constant
mM	Millimolar
miRNA	Micro Ribonucleic Acid
mRNA	Messenger Ribonucleic Acid
NaCl	Sodium Chloride

PEG   Polyethylene Glycol

pre-mRNA   Premature Messenger Ribonucleic Acid

PNA   Peptide Nucleic Acid

RISC   Ribonucleic Acid Induced Silencing Complex

RNA   Ribonucleic Acid

RNAi   Ribonucleic Acid Interference

rRNA   Ribosomal Ribonucleic Acid

SARS-CoV-2   Severe Acute Respiratory Syndrome–Related Coronavirus

siRNA   Small Interfering Ribonucleic Acid

T   Thymine

TFO   Triplex Forming Oligonucleotide

T_m Melting Temperature

U   Uracil

UTR   Untranslated Region

UV-Vis   Ultraviolet-Visible Spectroscopy

WNA   W-Shaped Nucleic Acids

List of Symbols

α Alpha

Å Angstrom

Β Beta

Δ Delta

> Greater Than

μ micro

% Percent

π Pi

± Plus or Minus

CHAPTER 1: DNA INTRODUCTION

DNA Basics

The Discovery of DNA

Friedrich Miescher was the first person reported in the literature to isolate DNA in 1869 during a time when proteins were thought to be the source of genetic material.[1] While determined to understand cellular composition, he worked with lymphocytes and noticed precipitation in his test solution under acidic conditions but when alkali was added it redissolved. This was the first-time crude DNA had been extracted from cells and because of the histochemical facts he noted he determined the precipitate must be attributed to the nuclei. Due to its presence in the nuclei, he termed the precipitate "nuclein," which we now call deoxyribonucleic acids (DNA). By burning the DNA, he determined it contained carbon, hydrogen, oxygen, nitrogen, and a large amount of phosphorus which was the key difference indicating it was not protein. After Miescher, a small number of scientists started researching nuclein.

Among this small fraction of scientists embarking on research involving nuclein was the renowned Albrecht Kossel who was granted the Nobel Prize in Medicine for discovering that DNA contains four bases; adenine, guanine, cytosine, and either thymine or uracil (Figure 1-1) depending on the pentose sugar molecule.[2] DNA contains a 2'-deoxyribose sugar whereas ribonucleic acids (RNA) contain ribose. DNA uses thymine as a pyrimidine base and RNA uses uracil in place of thymine.

Figure 1-1

Nucleic Acid Basic Structures
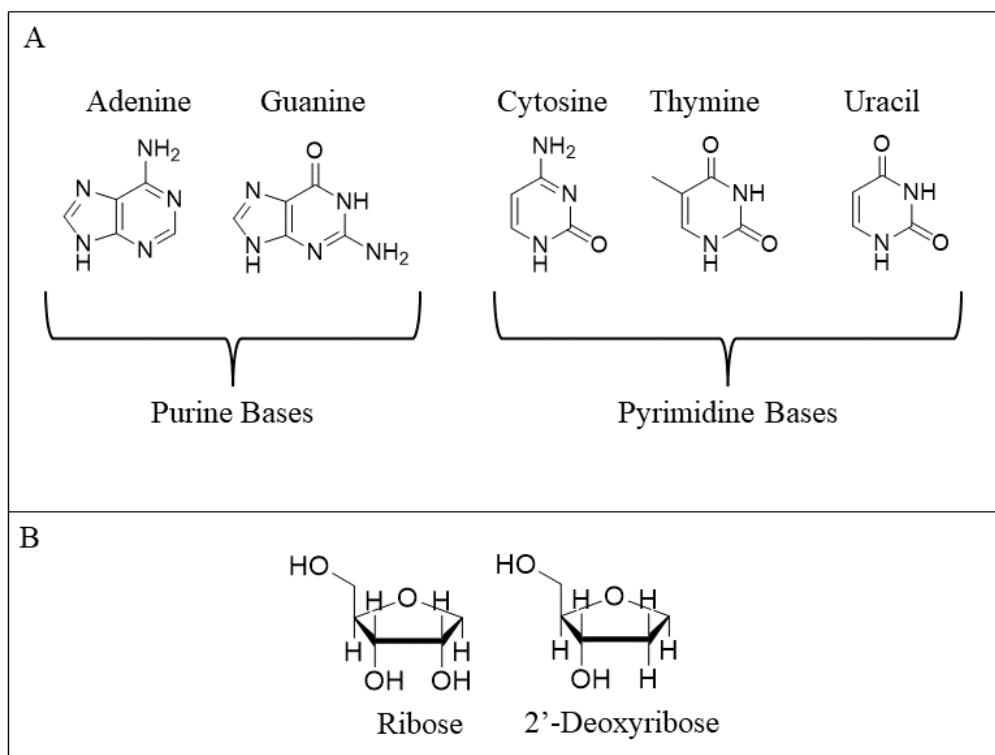
(A) Structures of the naturally occurring purine and pyrimidine bases. (B) Structures of ribose sugar (RNA) and 2'-deoxyribose sugar (DNA).

However, it wasn't until 1944 that DNA research became of significant interest when Oswald T. Avery, Colin M. MacLeod, and Maclyn McCarty "proved beyond a reason of doubt" that DNA is responsible for heredity. While studying the transformation of *Pneumococcus* Type III they determined DNA was the fundamental unity for genetic information. [2,3]

Nine years later, on April 25, 1953, a Nature article titled "Molecular Structure of Nucleic Acids" revolutionized nucleic acid research. [4] J.D. Watson and F.H.C. Crick reported on several key DNA structural features. First, DNA is made of two right-handed helical strands coiled around the same axis, but running in opposite directions, one 5'→3' and the other 3'→5'.

The bases (A, T, G, C) are contained within the center of the helix, while phosphate diester groups are on the outside, exposed to the hydrophilic environment. These phosphate diester groups are joined with β-D-deoxyribofuranose residues via 3', 5' linkages. The deoxyribofuranose sugar is perpendicular to the attached base and there is a residue (sugar and base) every 3.4 Å in the z-direction. Additionally, each phosphate atom is at a distance of 10 Å from the axis. The novel feature that they determined is that the two helical strands were held together via hydrogen bonding of the bases between strands. A single base from one strand binds with a single base from the other strand via H-bonding. Purine bases A and G bind with a pyrimidine base either T or C, respectively, by purine position 1 and 6 to pyrimidine position 2 and 3 (Figure 1-2). This structure determination was partly due to Rosalind Franklin, as she had demonstrated via X-Ray diffraction the helical structure of A and B DNA. [5]

Figure 1-2

Watson and Crick Base Pairing
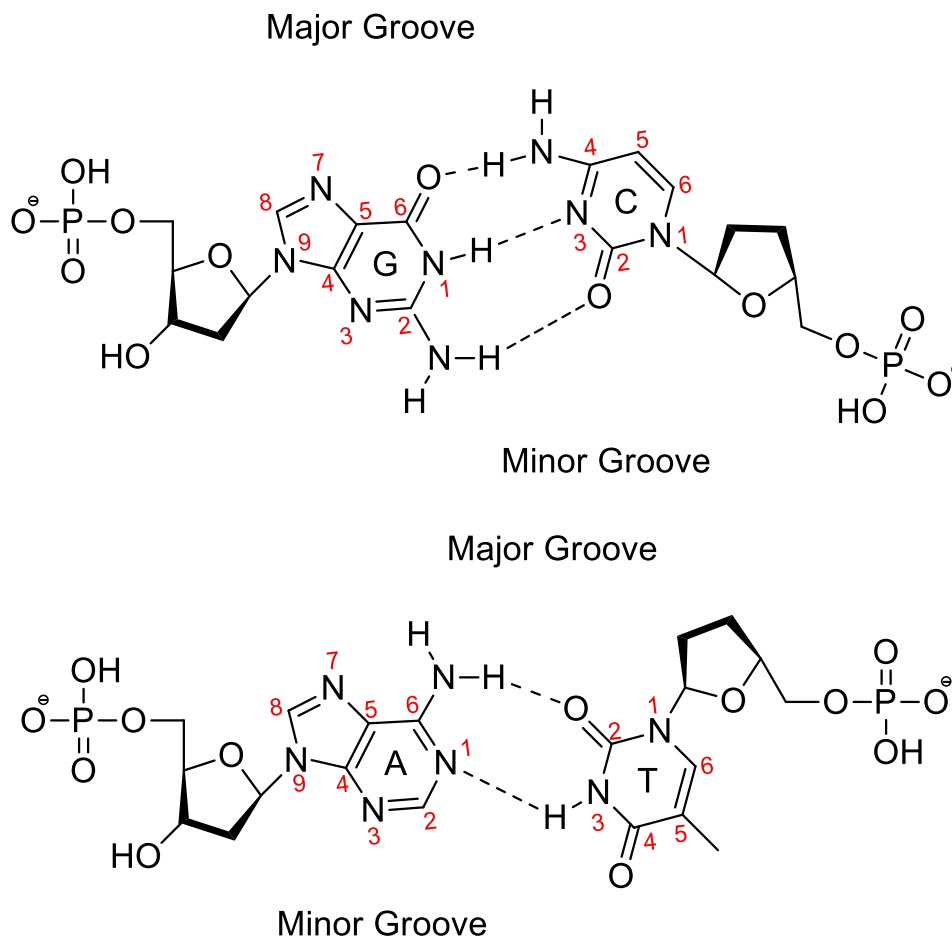
Central Dogma

Once the discovery of DNA was reported and accepted as the source of genetic heredity, Crick was able to propose a more accurate central dogma than what was previously established. He proposed that in all cells three "general transfers" can occur, which are the replication of parent DNA to daughter DNA, the transcription of DNA to RNA, and the translation of RNA to protein. [6] He then proposed that under special circumstances "special transfers" may occur: RNA to RNA, reverse transcription of RNA to DNA, and a direct transfer from DNA to protein

(Figure 1-3). The third, however, there was no evidence for other than an *in vitro* cell free experiment involving neomycin. Today, it is accepted that protein-coding DNA is transcribed to produce RNA which is then translated to produce protein.

Figure 1-3

The Central Dogma Proposed by Crick[7]
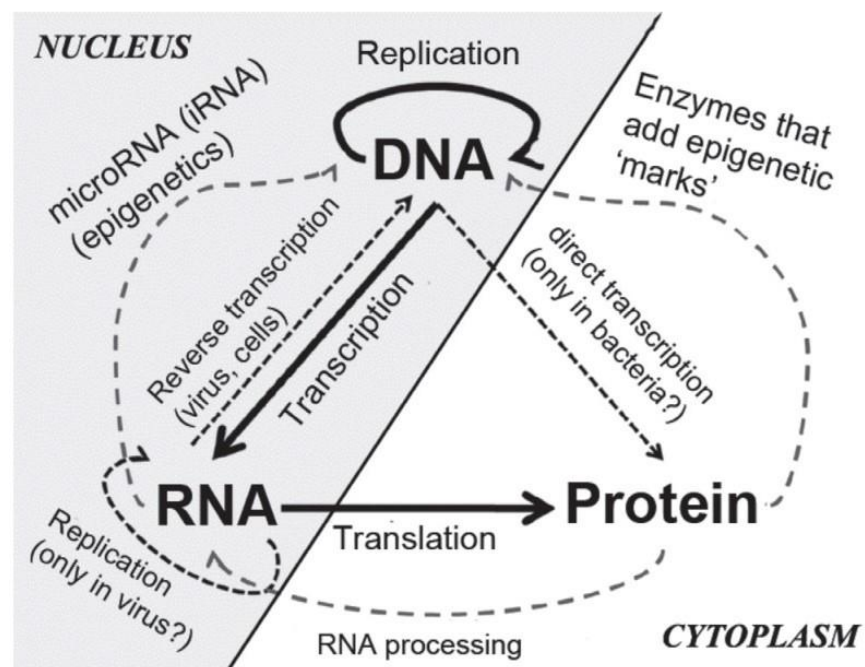
In eukaryotic cells, transcription occurs in the nucleus and is the first step in converting genetic material into functional proteins. Within the nucleus, transcription factors and RNA polymerase are recruited to the promoter region of a given gene causing a bend that separates the duplex strands. The non-coding strand is used as the template to first produce premature messenger RNA, pre-mRNA. [8] The pre-mRNA is then processed before the mature mRNA is transported into the cytoplasm. This processing includes splicing to remove intron sequences that would not play a role in protein formations as well as adding a 5' cap, specifically a 7-

methylguanosine cap to prevent degradation and aid in initiating translation. Processing ends

with elongating the 3' end with a poly-A tail, again to prevent degradation, but also to signal for

exportation to the cytoplasm. Once in the cytoplasm, ribosomal RNA (rRNA) decodes the

mRNA by inducing the binding of a translational RNA (tRNA) which holds the correct

complementary anticodon sequence. These tRNAs are carriers of specific amino acids that help

couple together a growing chain polypeptide, which folds to form active proteins. [8]

Structures and Functions

Duplex Structures

There are three duplex structures that DNA can form: B-DNA, A-DNA, and Z-DNA

(Figure 1-4). The most common form of DNA is B-DNA which was described by Watson and

Crick in 1953. B-DNA is described by its right-handed double helix around the same axis, the

two strands running antiparallel to each other. [4] The two strands are held together via hydrogen

bonding of the purine to the pyrimidine bases both in anti-conformation perpendicular to the axis

and the ribose sugar pucker conformation is 2'-endo (Figure 1-5). The dimensions of B-DNA

are as follows: 0.34 nm between base pairs, 3.4 nm per turn and 10 base pairs per turn. The

diameter of a B-DNA duplex is about 20Å. The major and minor grooves of B-DNA are

comparable in depth; however, the major groove is wider than the minor groove. The difference

in width makes the major groove a target for proteins and therefore the minor groove can be used

as an allosteric site for small molecules drugs. This is different from the A-form DNA.

Figure 1-4.

Three Helical Structures of DNA[9]

A-DNA   **B-DNA**   **Z-DNA**
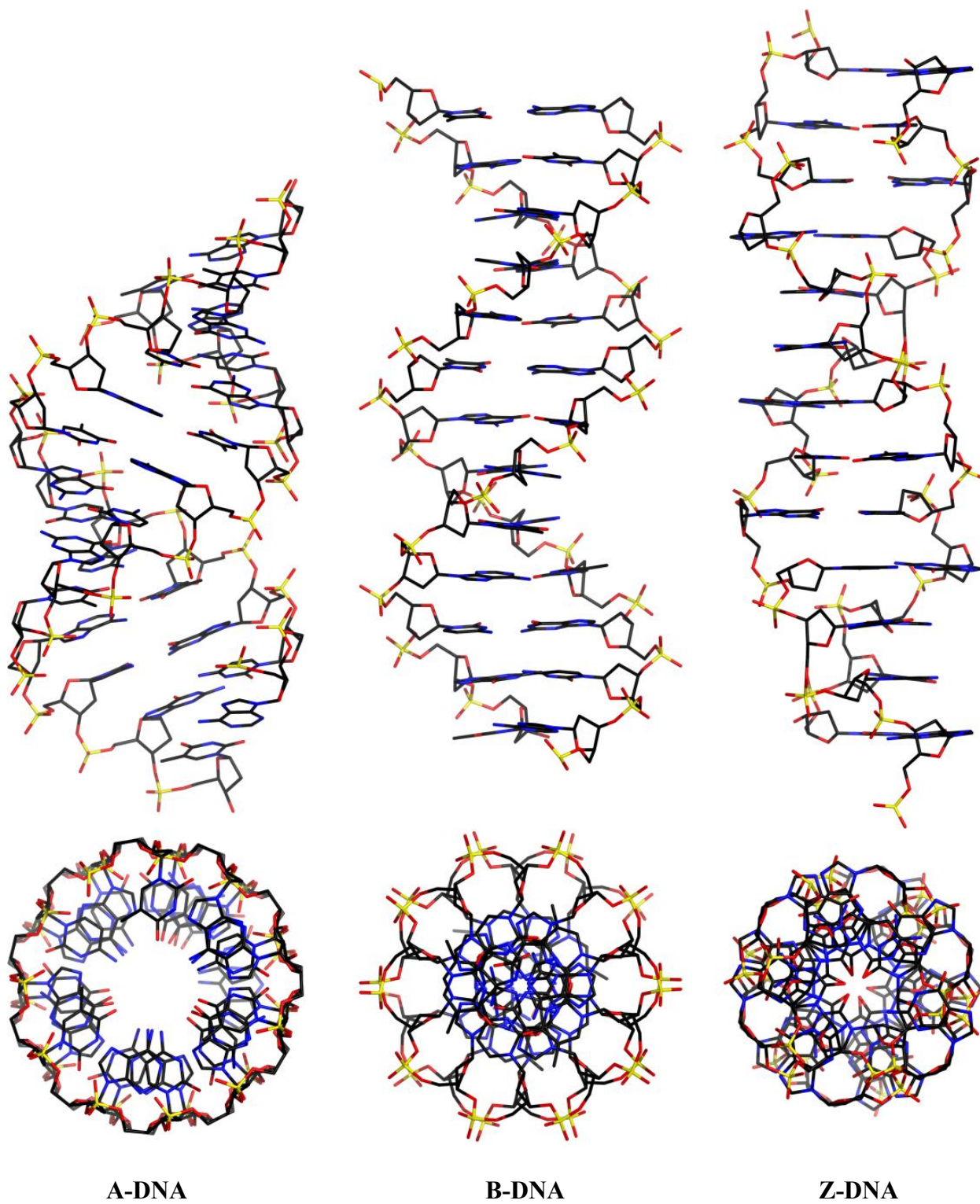
Figure 1-5

Sugar and Base Conformations

A

C3'-endo   C2'-endo

B

anti   syn   anti   syn
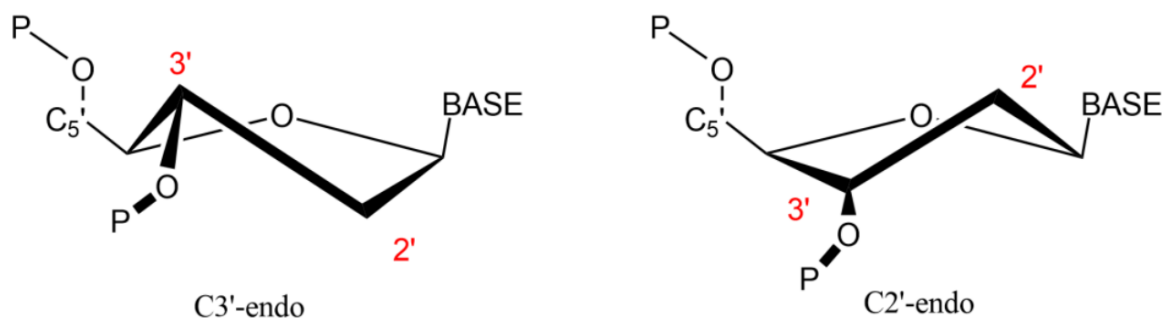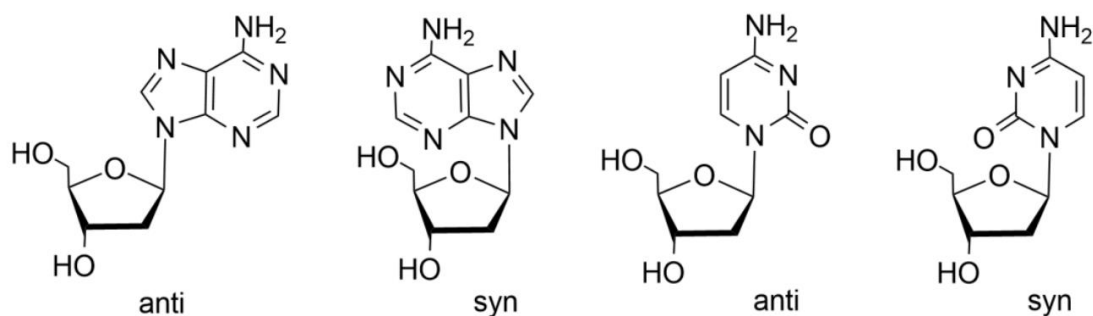
The orientations of (A) 3'-endo and C2'-endo sugar puckers and (B) anti- and syn-purine or pyrimidine bases.[8]

A-DNA has a deep and narrow major groove and a shallow minor groove.[10] This change in grooves is due to the change in the sugar pucker. The ribose sugar in the A-DNA is in 3'-endo conformation which tilts the bases 20° from the helical axis which is dislocated 4.7Å into the major groove. [10] This change results in 11 base pairs per turn and a 2.56Å rise per turn. This right-handed duplex has been used to describe RNA-DNA and RNA-RNA duplexes.

Z-DNA is a vastly different form of DNA. This is a left-handed helical structure resulting in a zig-zag pattern in the phosphodiester backbone. The sugar pucker conformation alternates from 3'-endo, same as A-DNA, for the sugars attached to the purine bases to 2'-endo for those attached to pyrimidine bases. Additionally, purine bases are in syn conformation while the pyrimidine bases stay in anti-conformation.[11] These changes lead to an elongated duplex structure of 19Å per turn and 12 bases per turn.

Table 1-1

Properties of the Three Possible DNA Helixes

Properties	A-DNA	B-DNA	Z-DNA
Helical Direction	Right-handed	Right-handed	Left-handed
Helix Diameter	26Å	20Å	18Å
Base Pair/Turn	11	10	12
Rise/Base Pair	2.56Å	3.4Å	3.8Å
Pitch/Helical Turn	28	34	45.6
Sugar Pucker	C3'-endo	C2-endo	Purines: C3'-endo Pyrimidines: C2'-endo
Glycosyl Angle Conformation	Anti	Anti	Purines: Syn Pyrimidines: Anti
Major Groove	Narrow and Deep	Wide and Deep	Flat
Minor Groove	Wide and Shallow	Narrow and Deep	Narrow and Deep

G-Quadruplex Structure

The G-quadruplex is a tetra-stranded DNA structure more commonly recognized for its ability to regulate telomerase due to the nature of the telomeric sequence $(TTAGGG)_n$. G-Quadruplexes, G4s, form from sequences with tandem repeats of three or more guanine residues which assembly into planar guanine tetrads, or G-quartets via Hoogsteen hydrogen bonds (Figure 1-6). These G-quartets are able to stack on top of each other stabilized by a monovalent cation, like K^+ or Na^+, and give rise to the four-stranded structure. [12,13] G-quartets can stack within a single DNA strand resulting in an intramolecular G4 or they can stack with tetrads from 1 or 3 other strands being a bi- or tetramolecular, intermolecular, quadruplex. [13,14] The topology of the G4 can also differ in the direction of strands which can be termed parallel, antiparallel, or hybrid.[14] Many G-quadruplex forming sequences are found in non-coding regions of DNA, particularly in promoter regions which have made them a target for gene regulation.

i-Motif Structure

Complimentary to the G-quadruplex, cytosine rich strands are able to form an intercalated-motif often called the i-motif. [15] The i-motif was discovered roughly 30 years after the G-quadruplex and has been shown to form under acidic conditions given the requirement of a protonated cytosine to participate in Hoogsteen hydrogen bonding. Similar to the quadruplex, this secondary structure can form intermolecularly from two or four separate strands or intramolecularly within one strand (Figure 1-6). [15,16] The motif is a right-handed helix with a twist angle of about 12-20 Å and a distance between base pairs of 3.1 Å. [16] Due to the sequence locations and pH dependent nature of the i-motif, many researchers have investigated their use as a molecular target to modulate gene expression.

Figure 1-6

G-quadruplex and i-Mofit Structures
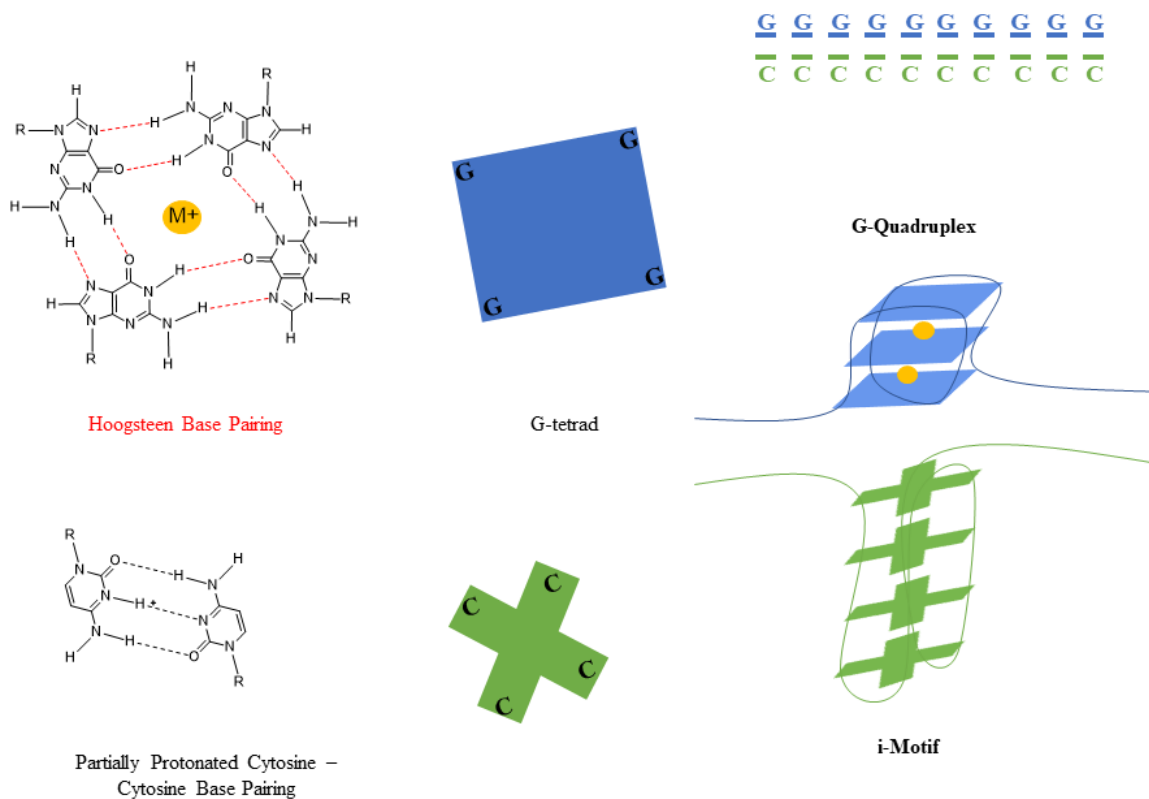
Hydrogen bonding of both the G-quadruplex (top) and i-motif (bottom) and how their secondary structures fold.

Triplex Structure

The first mention of triplex formation was by G. Felsenfeld (1957) in a communication titled "Formation of a Three-Stranded Polynucleotide Molecule." He described the binding of a synthetic polyribonucleotide, polyuridylic acid strand binding into the helical groove of the duplexed polyadenylic * polyuridylic acid strands.[17] He noted this was made possible due to the

hydrogen bonding between the uracil O6 and N1 with the Adenine N10 and N7 (Figure 1-7).

This type of hydrogen bonding would later be coined as Hoogsteen Hydrogen Bonding.[18,19]

Hoogsteen hydrogen bonding refers to the purine position N7 as a hydrogen bond acceptor and either the N10 position for adenine as an H-bond donor or the C6 carbonyl for guanine as an H-bond acceptor.[19] The pyrimidine participating atoms are N3 and either the carbonyl of thymine or the anime group of cytosine located at C4. In order for a cytosine base to participate in triplex formation via the third strand, the environment must be acidic enough to protonate cytosine at the N3 position.[19]

Figure 1-7

Hoogsteen Hydrogen Bonding
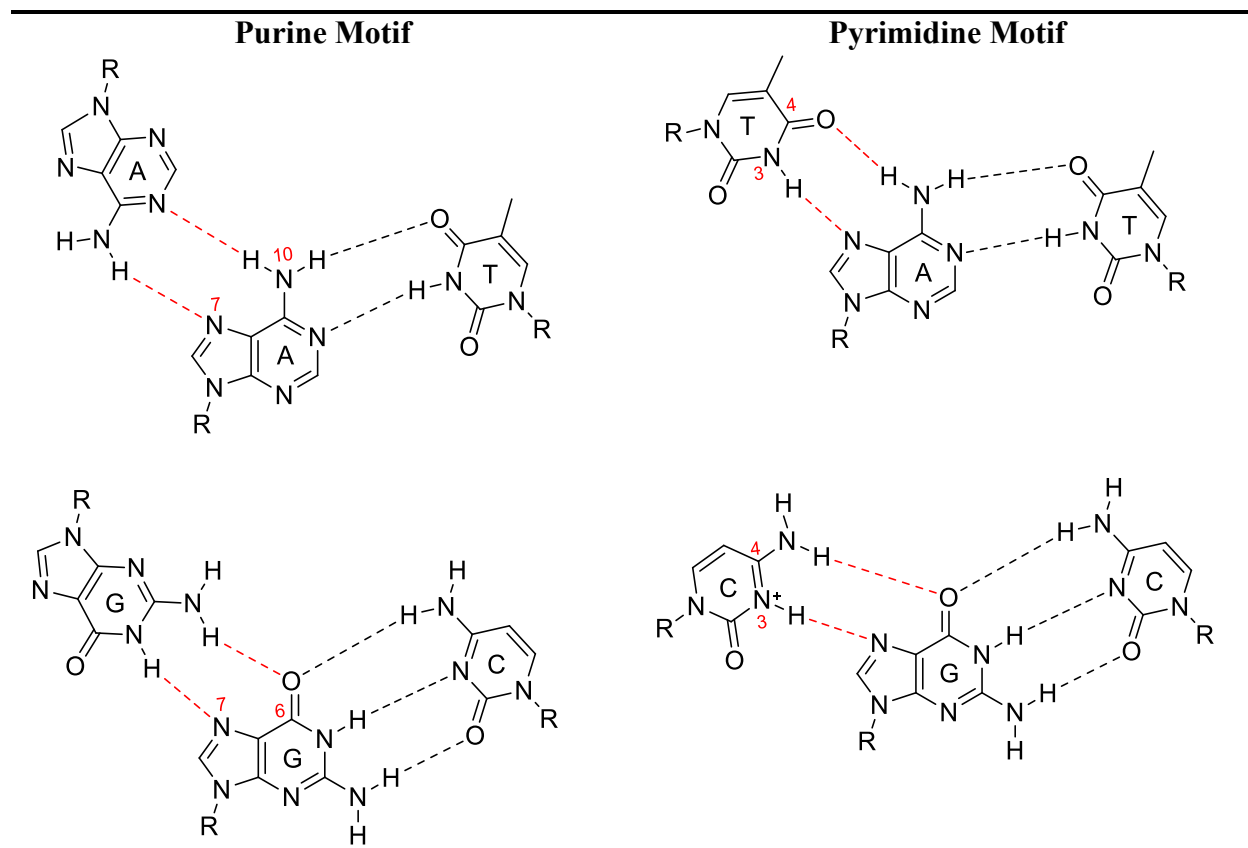
There are two triplex motifs that have been characterized, the purine motif and the pyrimidine motif. The purine motif or purine-purine-pyrimidine (R●R-Y) triplex indicates a purine third strand Hoogsteen hydrogen bonding to another purine strand in an antiparallel manner (G●G-C or A●A-T). [20] The pyrimidine motif or pyrimidine-purine-pyrimidine triplex, represents a pyrimidine third strand that is Hoogsteen hydrogen bonded to a purine strand in a parallel manner (T●A-T or C+●G-C). [21,22]

Upon binding of the third strand, analysis showed structural changes to the B-DNA duplex. Radhakrishnan and Patel (1994) showed a -2 Å displacement into the minor groove as an accommodation for the third strand into the major groove. Additionally, upon binding, there is a slight unwinding of the helix which results in a helical twist of about 31˚. A triplex can result by binding an exogenous third strand separate from the duplex or a third strand that results from an unwinding of the duplex downstream. The two types of formation are referred to as intermolecular and intramolecular triplexes, respectively (Figure 1-8).

Figure 1-8

Intermolecular and Intramolecular Triplex Formation [23-25]

+

Triplex Forming
Oligonucleotide (TFO)

=

Intermolecular Triplex

Intramolecular Triplex

5′   3′
3′   5′
5′   3′

Parallel

Antiparallel

3′   5′
3′   5′
5′   3′
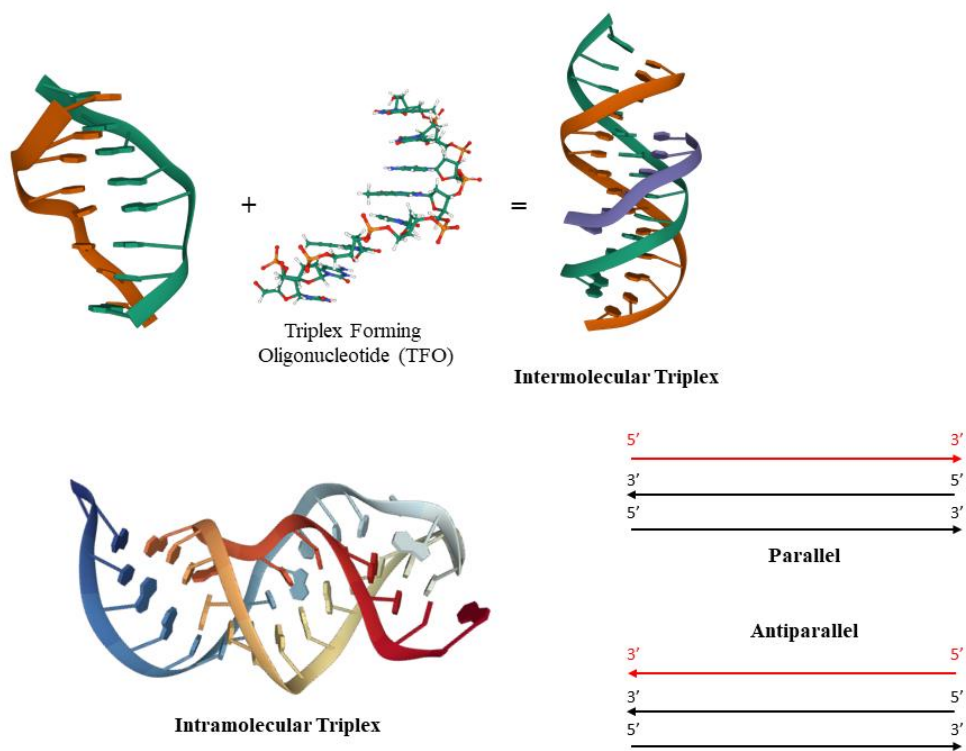
CHAPTER 2: ANTIGENE STRATAGIES

Antigene Therapy

siRNA and miRNA

RNA interference (RNAi) is a biological mechanism to modulate gene expression post-transcriptionally. [26] RNAi was originally identified in plant cells and induces gene silencing by a double-stranded RNA (dsRNA) targeting a complementary mRNA for degradation. [27] RNAi is credited for controlling cell growth, heterochromatin formation, tissue differentiation, and cell proliferation; therefore, a dysfunction involving RNAi can be linked to many cancers, neurological disorders, and cardiovascular diseases. [28] As a promising avenue for new cancer therapeutics, two main categories of RNAi are recognized: short interfering RNA (siRNA) and micro RNAs (miRNA).

The first step in utilizing siRNA involves the processing of a 20-30 nucleotide dsRNA into a siRNA with a 2-nucleotide overhang on the 3' end of each strand by an enzyme called Dicer. [27] miRNAs are generally ~22 nucleotides in length after processing by Dicer. Once formed, either the siRNA or miRNA attaches to a multiprotein complex known as the RNA induced silencing complex or RISC. RISC then separates the strands and the non-coding strand with the more stable 5' end is incorporated into the complex which guides the complex to the target mRNA resulting in cleavage. siRNAs target their fully complementary target for degradation, while miRNAs imperfectly bind to the 3' UTR of their target. [29,30]

Difficulty in developing delivery systems as well as rapid degradation poses a challenge for transferring these systems from bench-top to prescribable therapeutics. Polymer, peptide, and lipid-based delivery systems have been developed, but combinatorial delivery systems have

proven better vehicles. [27] Another issue is their efficacy, only 11-18% of randomly selected siRNAs were shown to have a 90-95% gene silencing effect. [31] This is largely due to their off-target effect having partial sequence homology to off-target mRNAs due to the 3' untranslated region (UTR), and off-target silencing can trigger an immune response and cytokine release. [32,33]

Triplex Formation Antigene Strategy

Oligonucleotides receive a lot of attention for their versatility in research and therapeutic use. One of the most promising uses is inducing triplex formation as a block against transcription. As explained previously, blocking translation by targeting mRNA has been extensively researched as a potential therapeutic, but one downfall is the constant production of the target mRNA. By targeting the DNA sequence and preventing the initiation or elongation of a transcription product [34,35] one prevents the consistent reproduction of the mRNA. The problem with the use of TFOs involves two factors: endonucleases and stability. In order to reduce the amount of degradation by nucleases, researchers have made different modifications to the backbone and anomeric configuration of the glycosidic bond. [36]

It has been shown that changing β-D-deoxyribonucleotides to α-D-deoxyribonucleotides prevents degradation without affecting stabilization. [37,38] With a similar effect, the modifications to the backbone include a change from a phosphodiester linkage to a phosphorothioate, phosphoramidate, or methylphosphonate (Figure 2-1). [36] Another tactic is to do away with the negatively charged DNA backbone completely and replace it with an uncharged, achiral backbone using the structure of N-(2-amino-ethyl) glycine (Figure 2-1). These oligonucleotides are referred to as peptide nucleic acids (PNAs).

A pyrimidine PNA will bind with a 2:1 ratio to its target single or double-stranded sequence leading to a displacement of the original DNA pyrimidine strand of a duplex target. Likewise, a purine PNA can also cause strand displacement but binds with a 1:1 ratio.[36]

Figure 2-1

TFO Modifications

Backbone Modifications

Phosphodiester (original)   Phosphorothioate   Phosphoramidate   Methylphosphonate

Peptide Nucleic Acids
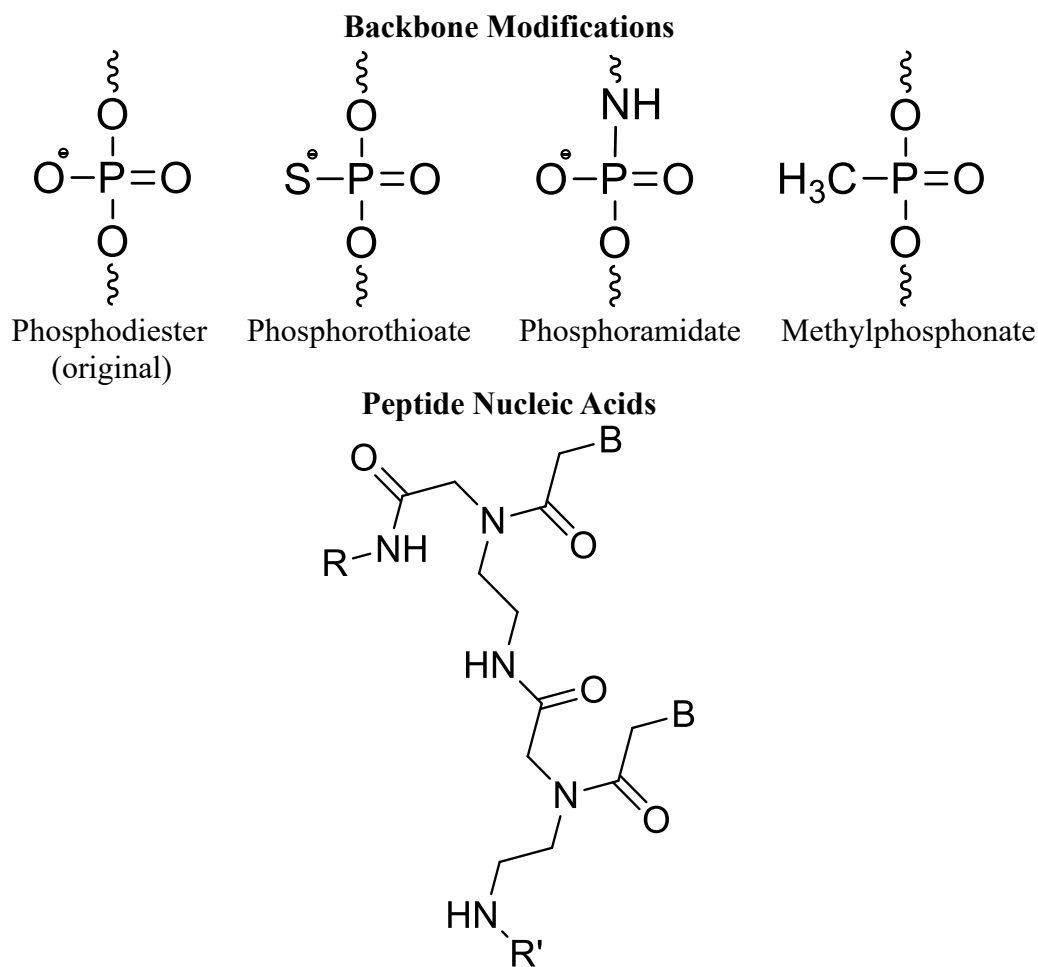
(Top) Structural differences of the backbone modifications can be made to prevent nuclease degradation. (Bottom) A generic structure of a PNA where "B" represents a base.

A TFO is weakly associated upon binding; therefore, when encountered by transcription factors or RNA polymerases it can easily dissociate which has proven to be the case in multiple publications. [36,39,40] In order to solve this problem researchers have taken many different approaches. For TFOs targeting a sequence with G-C base pairs the binding is greatly dependent on the pH of the environment. An acidic pH is needed to protonate the cytosines of the TFO which then allows for Hoogsteen binding to take place. To evade this requirement and induce binding at a neutral pH, researchers have incorporated modified 5-methylcytosines instead. [39,41] Other groups have tried to improve stability by creating entirely new base analogs such as W-shaped nucleic acids (WNAs), which have been shown to form stable triplexes with a high selectivity to the AT site. [40,42] Additionally, some other non-natural nucleobases include 6-amino-5-nitropyridine-2-one, 2-aminopyridine, and 5-methyl-pyrimidin-2-(1H)-one. [43,44] Another way to improve the stability of the triple helix has been to use antigene enhancers (Figure 2-2). Antigene enhancers are generally small molecules that bind to the triplex either by a groove binding or by intercalation. [36] For example, it has been shown that by conjugating acridine, an intercalator, to a TFO, the transcription elongation of an HIV proviral sequence can be blocked *in vitro*. [39] Groove binding molecules, generally have the ability to be partially positively charged in order to interact with the negatively charged backbone and target T●A-T base triplets because of the less crowded minor groove. Selective triplex groove binders include polyamines like Neomycin [45] and aromatic molecules like 4',6-diamidino-2-phenylindole (DAPI), Berenil, and Netropsin. [36,46] Intercalators also target mostly T●A-T base triplets because of the availability of the minor groove. In this case the aromatic moieties are able to participate in pi-pi stacking with the base triplets and stabilize the structure. Examples of intercalators include benzo[e]pyridoindole (B[e]PI), Quinoline, and Benzophenazine. [36,47]

Figure 2-2

Well Known Triplex Binders

Groove binders

Berenil

DAPI

Neomycin B

Netropsin

Intercalators

(B[*e*]PI)

Quinoline

Benzophenazine
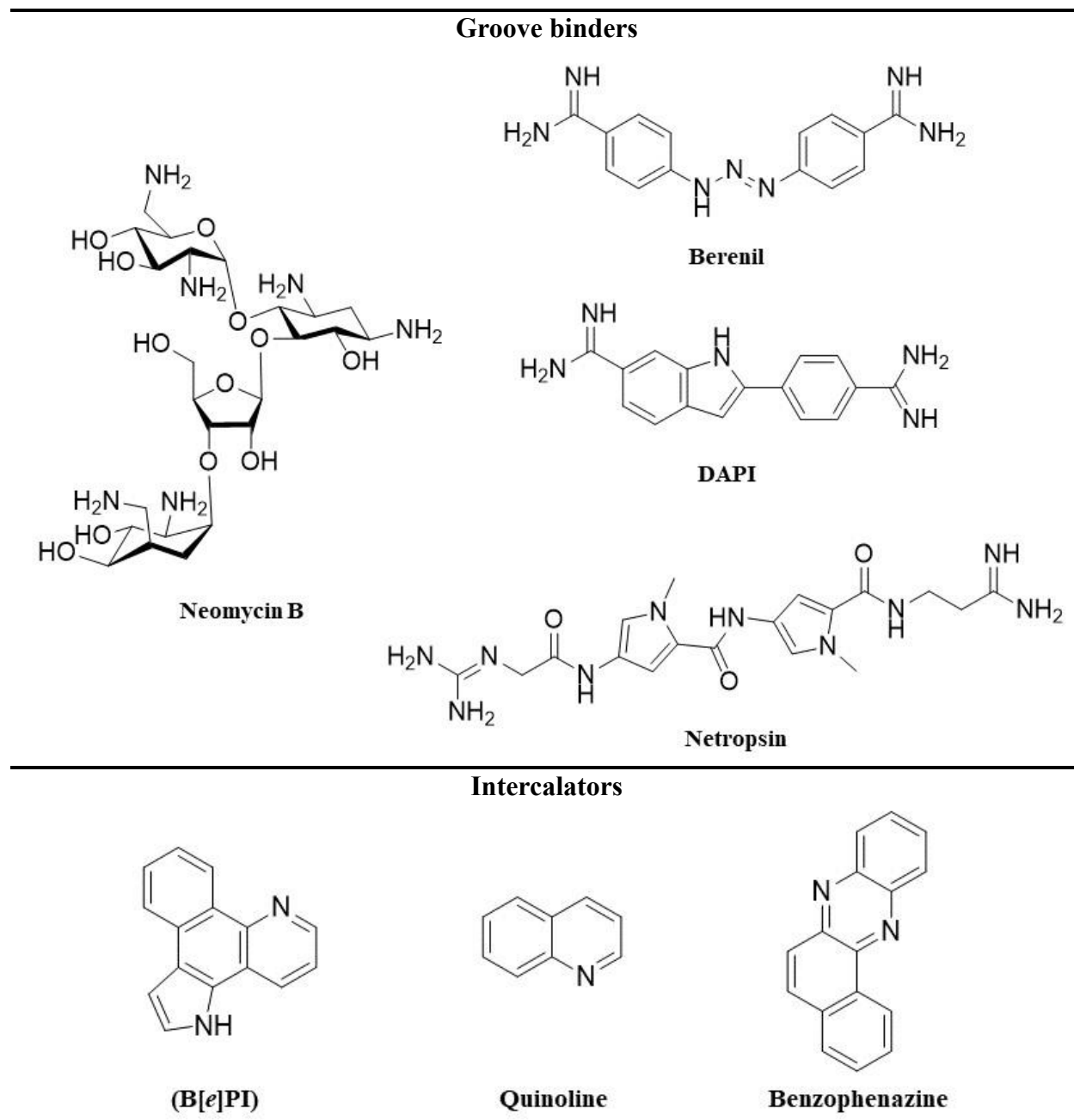
Flavonoids

Anti-oxidants known as polyphenols are important for prosperous health. An important group of phenolic compounds are Flavonoids, which are natural products found in fruits, grains, bark, vegetables, medicinal plants, teas, and wine that exhibit beneficial properties such as anti-inflammatory, anti-carcinogenic, and enzyme modulation. Due to their ability to promote health, they have been significantly researched and used for medicinal, cosmetic, and pharmaceutical applications. One study showed (-)-epigallocatechin-3-gallate could be useful against the progression of neuroinflammation associated with Alzheimer's disease. [48] Within the Flavonoid class of compounds, there are six subclasses characterized by their variation on the basic flavonoid structure (Figure 2-3).

The flavonol subclass is characterized by the hydroxyl group at the third position. Flavonols can be diversified further by methylation and or hydroxylation; therefore, this is the largest subclass of flavonoids. One of the most common and highly researched flavonols is quercetin (3, 3', 4', 5, 7-pentahydroxyflavone), and it's calculated that we ingest about 50 mg daily from our diet (Figure 3-1). [49] Quercetin glycosides, where a sugar replaces a hydroxyl group normally at the third position, are ingested through many foods we eat, and the gut microflora or endogenous biotransformation enzymes cleave the glycosidic bond making quercetin an aglycone more soluble in lipids. [50,51] Quercetin glycosides have been found in apples, berries, capers, grapes, onions, shallots, tea, tomatoes, many seeds, nuts, flowers, barks, and leaves. Interestingly, a study found that an organically grown tomato had 79% more quercetin than one chemically grown. [52]

Figure 2-3

Basic Backbone Structures of Flavonoids
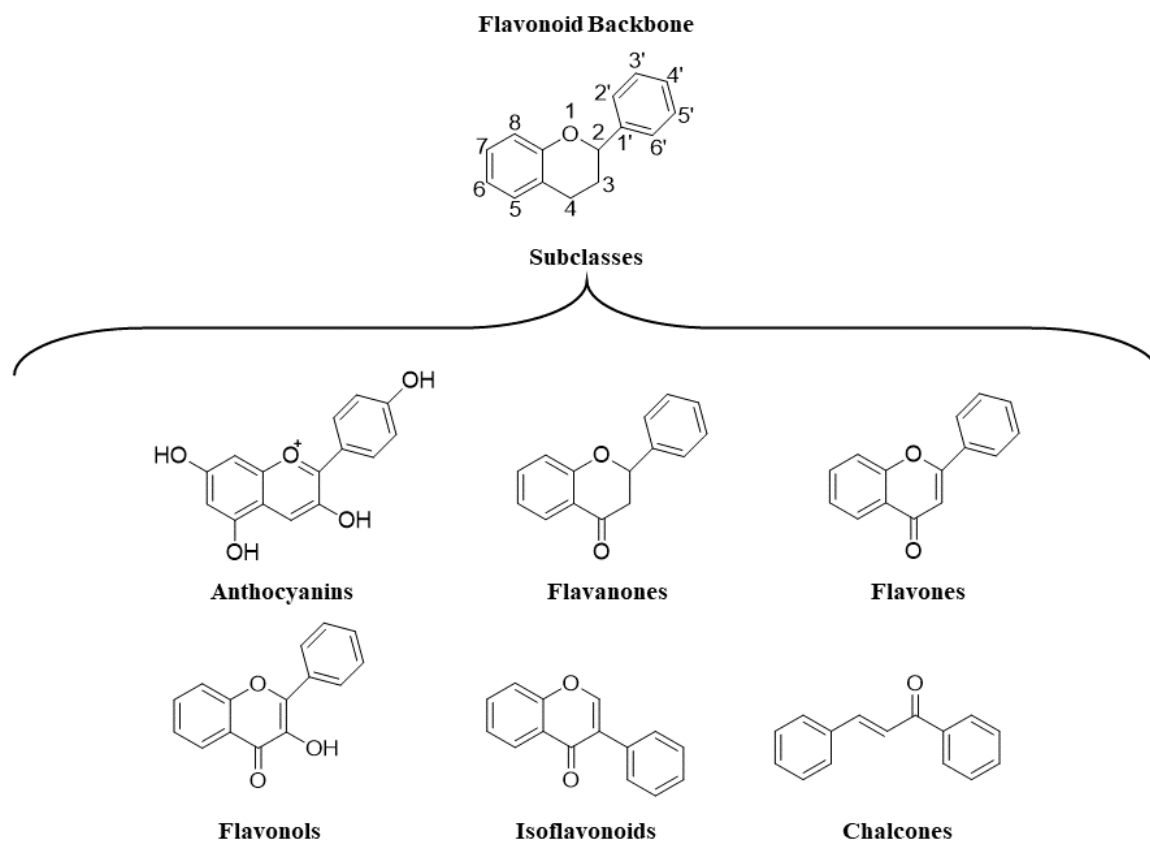
Due to quercetin being readily bioavailable and historical use in natural medicine, it has been greatly researched for its wide range of biological significance including antioxidative, anti-inflammatory, antiviral, and anti-carcinogenic activity. It has been shown that quercetin can increase the body's antioxidative capability by inducing glutathione synthesis[53,54] and increase acetylcholinesterase activity [55]. Rat studies reported an improved motor function recovery after an acute spinal cord injury to be highly dependent on the dosage of quercetin. [56,57] More recently, there was a report of the synergistic effect of vitamin C and quercetin as a prophylactic measure and treatment in conjunction with another pharmacological agent for SARS-CoV-2

(COVID-19).[58] The antiviral activity of quercetin is due to its ability to inhibit polymerases, proteases, reverse transcriptase, bind capsid proteins, and suppress DNA gyrase. [59-63] Quercetin has also been shown to exhibit antiproliferative effects on cancer cells by causing cell cycle arrest in the G1 phase and therefore inducing apoptosis. [64,65]

The shape of quercetin is complementary to both a DNA duplex base pair and a triplex base triplet, indicating its potential use as a DNA binder. However, it has been reported that only at concentrations over 250 μM were interactions between quercetin and the DNA duplex observed. [66] There are no quercetin-triplex DNA complexations detected using ESI mass spectrometry which would imply a weak interaction. [67] However, the quercetin structure has three sites available for metal chelation, the 3-hydroxy-4-keto group, 5-hydroxy-4-keto group, and the catechol groups. [68] As a metal ion complex, quercetin has been shown to have improved DNA binding activity. [68-71] Cell viability assays have shown that a quercetin-zinc (II) complex decreases the IC_{50} values to about half of quercetin alone. The viability of HepG2, SMMC7721, and A549 cells were 9.2%, 17.6%, and 23.8%, respectively, after 100 μM treatment of $Zn(Que)_2(H_2O)_2$ complex for 48. [70] The cytotoxicity of quercetin-metal ion complexes has been attributed to an intercalation binding mode. [70,72]

One of the quercetin metabolites formed from glycosidic bond cleavage is methylated at the third position. [50] Interestingly, by modifying the quercetin structure from 3, 3', 4', 5, 7-pentahydroxyflavone to 3, 3',4',7-tetramethoxyflavonoid and adding an amino containing sidechain at the fifth position drastically increases its specific binding affinity for the DNA triplex.[73]

CHAPTER 3: THE DISCOVERY OF NEW TRIPLEX BINDING LIGANDS BASED ON THE

QUERCETIN STRUCTURE

Quercetin is a highly researched molecule for its ability to modulate key cellular enzymes and influence cellular processes. In this project a series of 5-substituted 3, 3', 4', 7-tetramethoxyflavonoid compounds were investigated for their ability to bind and stabilize the triplex DNA structure. Biophysical studies include UV-Vis thermal denaturation, Circular Dichroism (CD) titration, Differential Scanning Calorimetry (DSC), and Isothermal Titration Calorimetry (ITC). Characterization using these techniques confirms the discovery of potent and selective triplex binding intercalators.

Introduction

The second leading cause of death in the United States is cancer. There is an estimated over 1.9 million new cases in the year 2022 alone and over 600,000 cancer related deaths. [74] Breast cancer is the leading cancer in women and prostate cancer for men with a combined estimate of over 500,000 new cases.

There are six hallmark characteristics of cancer cells: sustained proliferation, evasion of growth suppressors, avoidance of apoptosis, endless replication, angiogenesis, and an invasion or metastasis framework. [75] There can be a myriad of reasons why cells may become cancerous. Some bacteria and viruses can interfere with these cellular functions, for example, the human papillomaviruses (HPVs) which are mainly associated with cervical cancer. [75] Cancer can also be caused by DNA damage and mutagenesis. Two of the pathways DNA damage can lead to cancer are damaged DNA replication leading to a gene mutation and consequently a mutated protein or mutations in a tumor suppressor gene leading to oncogenesis. [76]

Triplex formation antigene therapy is a strategy that has been widely researched with great promise to show the downregulation of oncogene transcription. Potential triplex forming regions are found in locations of the genome essential for meiotic segregation and recombination, i.e., pseudoautosomal region (PAR1) of the sex chromosomes, and for cell communication, particularly in the brain. [77] Unfortunately, free TFOs lack the ability to cross the blood-brain barrier (BBB) limiting the antigene treatment option to exclude brain tumors. [78-80] However, in recent years, with the development of nanoscale delivery systems that have proved to cross the BBB, there is increasing the potential for the antigene strategy to be successful against brain tumors.[81] Nanoparticle-conjugated TFOs have also exhibited better resistance to endogenous DNase enzymes and have been reported at lower therapeutic concentrations for the downregulation of c-myc transcription. [82]

A large quantity of the male-specific region of the Y-chromosome is comprised of large inverted repeats with the triplex-forming ability. Located in this region are gene families essential to spermatogenesis. [83] So it is with logical understanding that much of the TFO antigene research has been conducted using prostate cancer cell lines. Ets is a family of transcription factors, among them, many have been associated with various cancers' development. Ets2 overexpression is associated with prostate and breast cancer. By targeting a sequence 40 bp upstream of the transcription initiation site that overlaps with the Sp1 transcription factor binding site, a TFO can effectively reduce prostate cancer cell viability by over 90%. [84] However, keeping in mind the dynamic nature of the nucleus and unwinding of triplexes by other protein complexes or helicases, to improve triplex stability there is a need for an enhancer. [85]

Daunomycin is an anticancer agent with the ability to inhibit the growth of both cancer cells and normal human fibroblast cells. It also stabilizes the triplex structure, making it an antigene enhancer. By conjugating a TFO with daunomycin there is assurance that the proliferation inhibition is limited to the cancerous cells. To compare, a study was done on two daunomycin-TFO conjugates targeting sequences directly up- and downstream of the c-myc promoter in prostate cancer cells and normal human fibroblast cells. At concentrations that inhibit the growth of the cancerous cells and cause apoptosis, the normal cell growth was not affected. [86] Importantly noted, is the ability to selectively direct cytotoxic effects to the cancer cells which has led to the conjugation and incorporation of TFOs with other anticancer agents with different modes of cytotoxicity.

Gemcitabine is another anticancer agent, which is structurally a cytosine analog, and works by incorporation into the DNA blocking the progression of DNA replication and causing apoptosis. Notably, incorporation of gemcitabine into DNA is cell-cycle dependent, but within a TFO sequence this dependency can be overcome. Nucleotide incorporation as a result of TFO binding is thought to be the result of nucleotide excision repair. It has been reported that a TFO containing gemcitabine had a 10-fold increase of gemcitabine DNA incorporation than the mixture of TFO and gemcitabine or gemcitabine alone. [87]

Many chemotherapeutic agents on the market are extremely cytotoxic due to their ability to cause interstrand cross-linkage of DNA; however, these agents are not specific to oncogene and therefore can cause secondary malignancies. [88] Psoralen is a DNA intercalator that causes crosslinks when exposed to UV-A irradiation and has been used as a treatment for psoriasis and skin cancer. Psoralen-conjugated TFOs can direct psoralen to the desired sequence and cause

crosslink DNA damage. Then, the TFO can be unconjugated utilizing the disulfide bridge between the TFO and psoralen, leaving behind psoralen crosslinked to the DNA. [89]

Quercetin suppresses the cell proliferation of prostate cancer cells by mechanism of cell cycle regulation, apoptosis, and androgen receptor. [90] Quercetin derivatives 3, 3',4' ,7-tetramethoxyflavonoids (Figure 3-1) have been previously studied for their antiproliferative effect against prostate cancer cells. [91] It was identified that 5-O-(N, N-dibutylamino) propyl-3,3',4',7-O-tetramethylquercetin (compound 4 in Figure 3-1) was 35-182 times more potent than quercetin. Herein we will investigate their ability to be potential antigene enhancers by selectively stabilizing triplex DNA. As seen in Figure 3-1, the structures of quercetin (9) and 3, 3', 4', 7-tetramethoxyquercetin (8) are shown as control molecules given the missing substitution at position five with a nitrogen-containing group. Nitrogen substituents have the ability to be partially protonated under physiological conditions which, as seen in the data, significantly improves DNA binding. This is achieved by the electrostatic attraction of the negatively charged DNA backbone to counter the positively charged sidechain.

Figure 3-1

5 Substituted 3, 3', 4', 7 Tetramethoxyquercetin Derivatives

3, 3', 4', 7-tetramethoxyquercetin
8

Quercetin
9

R =

1

2

3

4

7

5

6
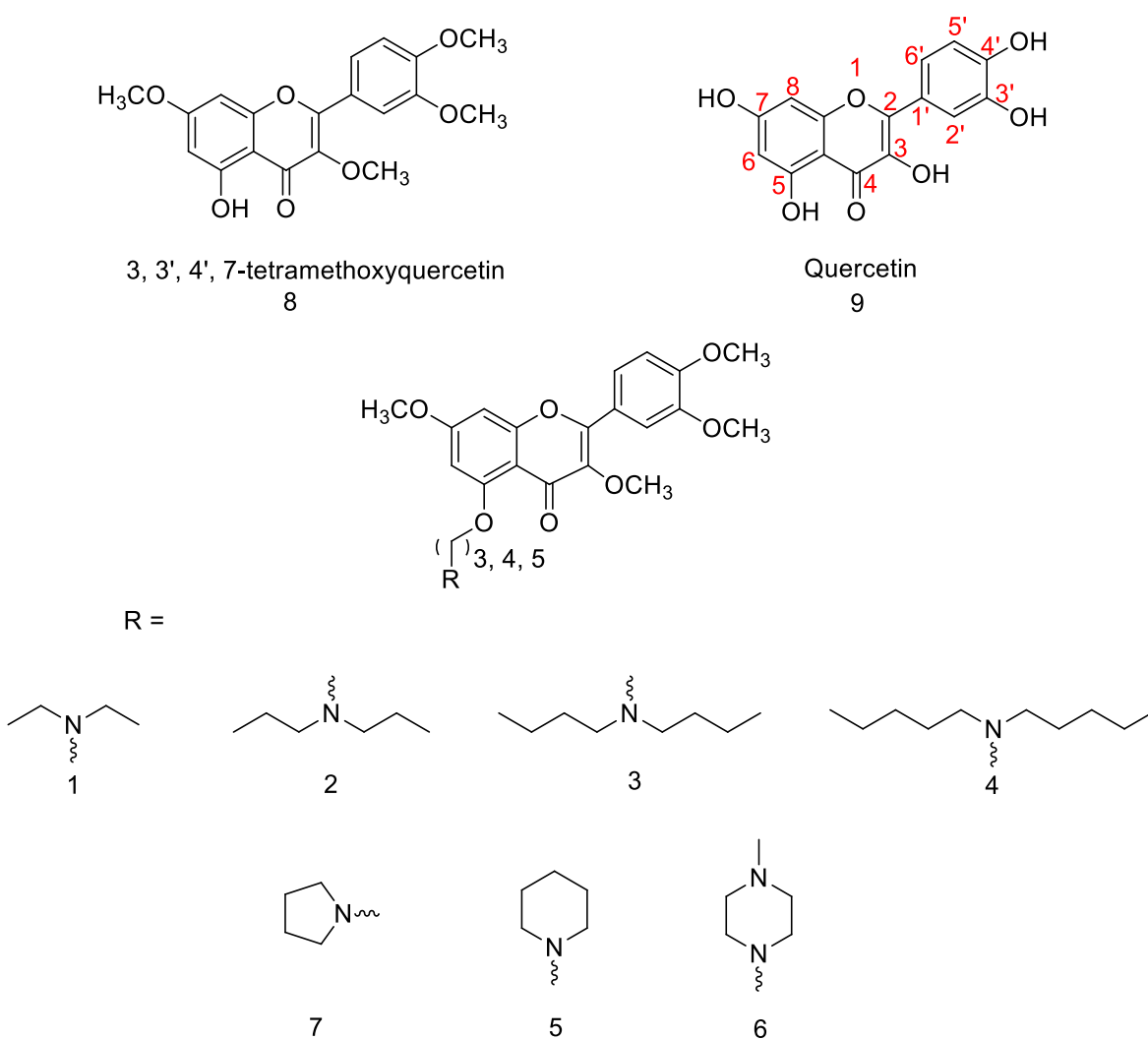
Structures of compounds 1-9 containing a 3, 4, or 5-carbon alkyl linker.

Experimental

Materials and General Methods

All the chemicals were purchased from MilliporeSigma or Fisher Scientific and used without further purification. DNA oligonucleotides were purchased from Fisher Scientific. Polynucleotides were purchased from MilliporeSigma. The concentrations of polynucleotide solutions were determined spectrophotometrically using the following extinction coefficients (in units of mol of nucleotide/L-1 cm-1): $\varepsilon 265 = 9,000$ for poly(dT) and $\varepsilon 260 = 6,000$ for poly(dA)●poly(dT). The concentrations of DNA solutions were determined spectrophotometrically, using the molar extinction coefficients (in units of mol of strand/L-1 cm-1) obtained from OligoAnalyzer (www.idtdna.com). $\varepsilon 260 = 483,700$ for 15GC-T (5'-GAAAAAAAA AAAAAGTTTTCTTTTTTTTTTTTTCTTTTCTTTTTTTTTTTTTC-3'); $\varepsilon 260 = 342,700$ for 10GC-T (5'- GAAAAAAAAGTTTTCTTTTTTTTCTTTTCTTTTTTTTC-3'); $\varepsilon 260 = 331,600$ for 15GC-Td (5'-GAAAAAAAAAAAAAAGTTTTCTTTTTTTTTTTTTC-3'); $\varepsilon 260 = 482,300$ for 15AT-C (5'-AAAAAAAAAAAAAAACCCCTTTTTTTTTTTTTTTCCCCTTTTTTTTTTTTTTT-3'); $\varepsilon 260 = 470000$ for 15GC-2AT (5'- GAGAGGAAGAAGAAGTTTTCTCTCCTTCTTCTTCTTT TCTCTCCTTCTTCTTC-3'); $\varepsilon 260 = 457500$ for 15GC-3AT (5'-GAGAGAAAGAAGAAGTTTCTCTCTTTCTTCTTCTTTCTCTCTTTCTTCTTC-3'); $\varepsilon 260 = 472500$ for 15GC-4AT (5'-GAGGAAAAGAAGAAGTTTTCTCCTTTTCTTCTTCTTTTCTCCTTTTCTTCTTC-3'); $\varepsilon 260 = 476200$ for 15GC-5AT (5'-GAGAAAAAGAAGAAGTTTTCTCTTTTTCTTCTTCTTTTCTCTTTTTCTTCTTC-3'); $\varepsilon 260 = 334000$ for 10GC-3AT (5'-GAAAGAGGAGTTTTCTCCTCTTTCTTTTCTTTCTCCTC-

3') ; ε260 = 336500 for 10GC-5AT (5'-

GAAAAAGGAGTTTTCTCCTTTTTCTTTTCTTTTTCCTC-3') ; ε260 = 340200 for 10GC-

6AT (5'-GAAAAAAGAGTTTTCTCTTTTTTCTTTTCTTTTTTCTC-3') UV spectra were

recorded on a Varian Cary 100 Bio UV-Vis spectrophotometer equipped with a

thermoelectrically controlled 6 × 6 cell holder. Circular dichroism spectra were recorded on a

JASCO J-810 spectropolarimeter using a quartz cuvette with a 1 mm or 1 cm optical path length.

Isothermal microcalorimetric measurements were performed on a TA Instruments Affinity ITC

LV. DSC thermograms were recorded on a TA Instruments Nano DSC.

Preparation of poly(dA)●2poly(dT) for DSC

Stock solutions of poly(dA)●poly(dT) and poly(dT) were first dialyzed in the same 500

mL buffer solution for 6 h and then further dialyzed in a fresh 500 mL buffer solution overnight

at room temperature. The concentrations of both DNA solutions after dialysis were determined

by UV. Poly(dA)●poly(dT) (100 μM/base triplet) and poly(dT) (100 μM/base triplet) in the

absence and presence of 7 or 8 (10 μM) were mixed in a 10 mM sodium cacodylate buffer and

150 mM KCl at pH 7, heated to 95 °C for 5 min, slowly cooled down to room temperature, and

stored at 4 °C overnight.

Preparation of poly(dA)●2poly(dT) for CD

Poly(dA)●2poly(dT) (15 μM/base triplet) and poly(dT) (15 μM/base triplet) were mixed

in a 10 mM sodium cacodylate buffer and 150 mM KCl at pH 7, heated to 95 °C for 5 min,

slowly cooled down to room temperature, and stored at 4 °C overnight.

Preparation of 15GC-T or 15GC-Td for ITC

Stock solutions of 15GC-T or 15GC-Td were first dialyzed in the same 500 mL buffer

solution for 6 h and then further dialyzed in a fresh 500 mL buffer solution overnight at room

temperature. The concentrations of both DNA solutions after dialysis were determined by UV.

15GC-T (10 µM) or 15GC-Td (10 µM) were mixed in a 10 mM sodium cacodylate buffer and

100 mM NaCl at pH 7, heated to 95 °C for 5 min, slowly cooled down to room temperature, and

stored at 4 °C overnight.

Isothermal Titration Calorimetry (ITC)

In a typical experiment, 5 µL aliquots of a ligand (100 µM, 7, 8, or neomycin) were

injected from a 264 µL rotating syringe into an isothermal sample cell containing 185 µL of

15GC-T (10 µM) or 15GC-Td (10 µM) at 15 °C. The corresponding control experiment was

carried out by injecting 5 µL aliquots of a ligand (100 µM, 7, 8, or neomycin) into a solution of

buffer alone. The syringe rotational speed was 125 rpm. The duration of each injection was 4 s,

and the delay between injections was 300 s. The initial baseline was collected for 100 s before

the first injection. A heat burst curve (microjoules per second vs. seconds) was generated from

each injection. The area under each curve was calculated using the NanoAnalyzer software

(Version 3.8.0) to yield a measure of the heat associated with that injection. The heat of ligand

binding to DNA associated with that injection was obtained by subtracting the heat associated

with each ligand-buffer injection from the corresponding heat associated with each ligand-DNA

injection. The buffer condition used in ITC experiments: 10 mM sodium cacodylate buffer, 100

mM NaCl, pH 7.0.

Differential Scanning Calorimetry (DSC)

Two cells, the sample cell containing 600 µL of 100 µM/base triplet poly(dA)●2poly(dT)

in the absence and presence of a ligand (7 or 8, 10 mM) and the reference cell filled with an

equal volume of the buffer, were heated from 25 °C to 90 °C at a rate of 0.2 °C/min. The buffer

condition used in DSC experiments: 10 mM sodium cacodylate buffer, 150 mM KCl, pH 7.0.

NanoAnalyze software (Version 3.8.0) was used to determine thermodynamic parameters and each transition ($T_{3\rightarrow2}$ and $T_{2\rightarrow1}$) was modeled individually using the Gaussian Model.

Thermal Denaturation of poly(dA)•2poly(dT) Monitored by UV

The UV thermal denaturation samples (1 mL) were prepared by mixing poly(dA)•poly(dT) (15 µM/base triplet), poly dT (15 µM/base triplet) in the presence and absence of a ligand (1-9, 10 µM) in a sodium cacodylate buffer (10 mM), KCl (150 mM), pH 7.0. The UV melting spectra were recorded in 1 cm path length quartz cuvettes at 260 nm, 280 nm, and 284 nm, as a function of temperature (25-90 °C, heating rate: 0.2 °C/min). Melting temperatures (T_ms) were determined using the first derivative method. All experiments were carried out in duplicate.

Thermal Denaturation of Intramolecular Triplex Monitored by UV

The UV thermal denaturation samples (1 mL) were prepared by mixing 15GC-T, 10GC-T, or 15AT-C (1 µM) in the presence and absence of a ligand (1-9, 10 µM) in a sodium cacodylate buffer (10 mM), NaCl (100 mM) at pH 7.0. The UV melting spectra were recorded in 1 cm path length quartz cuvettes at 260 nm, 280 nm, and 284 nm, as a function of temperature (5-90 °C, heating rate: 0.2 °C/min). Melting temperatures (T_ms) were determined using the first derivative method. All experiments were carried out in duplicate.

Sequence Selectivity Study

The UV thermal denaturation samples (1 mL) were prepared by mixing 15GC-2AT, 15GC-3AT, 15GC-4AT, 15GC-5AT, 15GC-T, 10GC-3AT, 10GC-5AT, 10GC-6AT, or 10GC-T (1 µM) in the presence and absence of a ligand (5 or 7, 10 µM) in a sodium cacodylate buffer (10 mM), NaCl (100 mM) at pH 7.0. The UV melting spectra were recorded in 1 cm path length quartz cuvettes at 260 nm, 280 nm, and 284 nm, as a function of temperature (5-90 °C, heating

rate: 0.2 °C/min). Melting temperatures (T_ms) were determined using the first derivative method. All experiments were carried out in duplicate.

Viscosity Experiments

Calf thymus DNA and poly(dA)•2poly(dT) were prepared in a mixture of sodium cacodylate buffer (10 mM, pH 7) and KCl (150 mM). The concentration of calf thymus DNA was determined by UV spectroscopy, using a molar extinction coefficient at 260 nm (12,800 M^{-1} cm^{-1} bp^{-1}). Small aliquots of a concentrated stock solution of ethidium bromide or compound 7 were added into a 2 mL of DNA solution (0.5 mM) in an Ostwald-type viscometer at room temperature to obtain the desired ligand/DNA ratios. After each addition, the time for the level of the liquid to pass between two marks on the viscometer was recorded using a stopwatch. The relative viscosities were calculated based on the published equations. [92]

CD Titration

Aliquots of a stock solution containing compound 7 or 8 were gradually added into a solution (2.0 ml) of poly(dA)•2poly(dT) (15 µM/base triplet) in a 10 mM sodium cacodylate and 150 mM KCl at pH 7.0. The final molar ratios of ligand to DNA were varied from 0 to 1.67. After each addition, the solution was gently mixed and incubated for 5 min for equilibrium before collecting the spectrum at room temperature. The overall volume change during the titration was kept at less than 1% of the initial volume. CD spectra were recorded as a function of wavelength (200-700 nm) using a 1-cm pathlength quartz cuvette. The scan speed was 100 nm/min and the data pitch was 0.5 nm. Each spectrum was an average of 3 scans.

Statistical Analysis

Excel software was used to determine the statistical significance. Two-tailed unpaired t-test was performed to show statistically significant ($P < 0.05$) and insignificant ($P > 0.05$) data.

Results and Discussion

5 Substituted 3, 3',4' ,7-tetramethoxyflavonoids are DNA Triplex Selective

Looking at Figure 3-1, two variables must be compared, the R-group and linker length. To begin, we first compared the derivatives containing a 4-carbon linker. Thermal denaturation of poly(dA)●2poly(dT) (15 µM/base triplet) in the presence of compounds 1-9 (10 µM) were monitored by UV at 260 nm as a function of temperature. The results are shown in Figure 3-2. The melting profiles are biphasic. The first transition represents the dissociation of DNA triplex [poly(dA)●2poly(dT)] into DNA duplex [poly(dA)●poly(dT)] and single stand [poly(dT)]. The second transition represents the dissociation of DNA duplex [poly(dA)●poly(dT)] into two single strands [poly(dA) and poly(dT)]. We define the dissociation temperature of the first and second transitions as $T_{m3 \to 2}$ and $T_{m2 \to 1}$, respectively. In the absence of any ligand, the $T_{m3 \to 2}$ value is (35.3 ± 1) ˚C and $T_{m2 \to 1}$ value is (73.7 ± 0.5) ˚C, which are consistent with previous reports.[93] Compounds 1-9 did not provide any additional stability to the duplex [poly(dA)●poly(dT)]. However, five of the derivatives did provide greater thermal stability for the triplex [poly(dA)●2poly(dT)]. The results are shown in Figure 3-3.

Control compounds 8 and 9 show a $\Delta T_{m\,3 \to 2}$ of 1.2 and 2.8 ˚C, respectively. Due to such a weak stabilization, 9 and 8 were determined to have no effect. Compounds 1, 2, 3, and 4 all have a dialkylamino R-group and increased the melting temperature of the triplex by 15.0, 9.9, 7.7, and 6.8 ˚C, respectively. Based on the T_ms of compounds 1-4, it is noticeable as the

dialkylamino chains get longer the stabilization effect reduces. This indicates large dialkylamino groups do not fit well into the binding pocket due to steric hinderance.

Compounds 5-7 containing the cyclic amino R-group show significant stabilization of poly(dA)●2poly(dT) that is also size dependent. The rank order of the size of the cyclic amino R-group is $7 > 5 > 6$. Compounds 7, 5, and 6 have $\Delta T_{m3 \to 2}$s of 17.8, 16.7 and 12.7 ˚C, respectively. Compound 6 containing the largest cyclic amino R-group, N-methylpiperazine, was weaker in triplex stabilization than compounds 7 and 5 ($p < 0.05$). Similar to compounds 3 and 4, the larger ring in compound 6 may provide a negative effect when fitting into the binding pocket. For future experiments, compounds 5 and 7 were considered equal and used interchangeably as the lead compounds.

Figure 3-2

Biphasic Melting Profiles of poly(dA)●2poly(dT) with and without Compounds 1-9 Under

Physiological Conditions
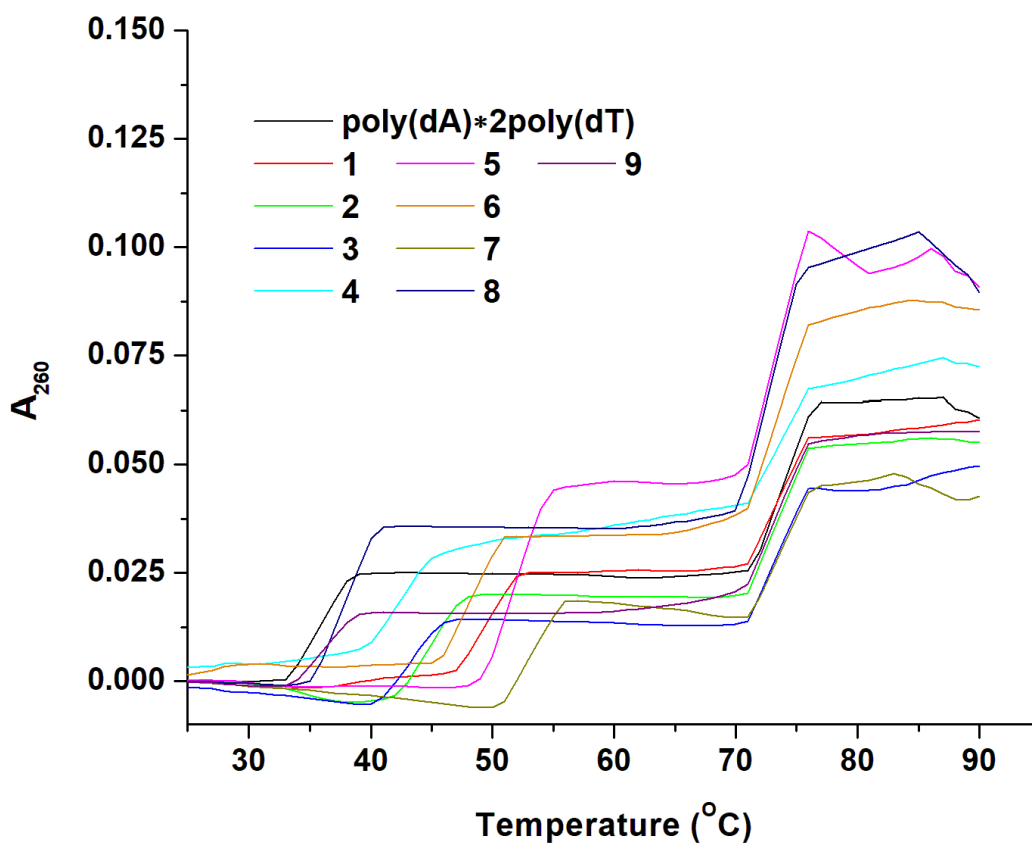
Y-axis adjusted to zero for better presentation and all compounds shown have a C4-linker. Buffer conditions: 10

mM sodium cacodylate and 150 mM KCl, pH 7.

Figure 3-3

Poly(dA)●2poly(dT) Triplex and Duplex Stability Differences in the Presence of Compounds 1-9
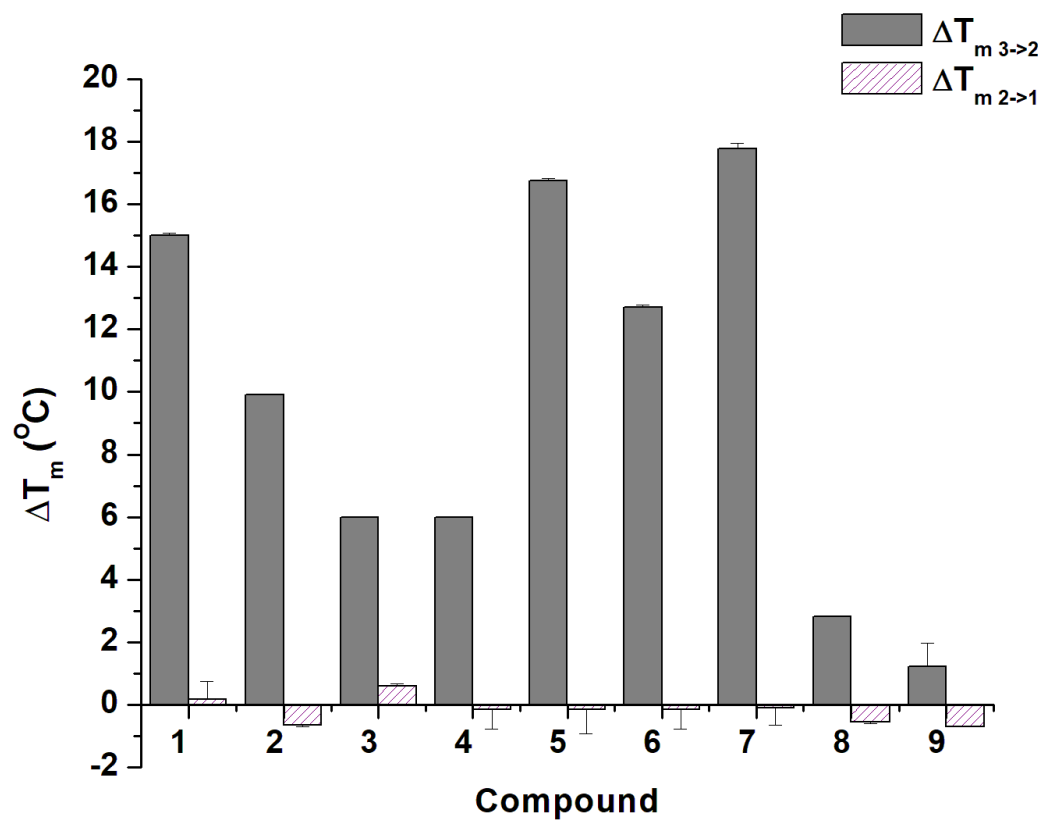
All temperatures and error bars shown are the average of duplicate trials.

The ligand-induced stabilization effect was also investigated using differential scanning calorimetry (DSC). Compounds 7 and 8 were chosen for comparison as representatives of the 5-substituted 3, 3', 4', 7-tetramethoxyflavonoid class of compounds. Two transitions were seen in the DSC thermograms (Figure 3-4), similar to the thermal denaturation profiles from the UV thermal denaturation. The data was analyzed using a two-state model. [94] The 100 μM of poly(dA)●2poly(dT) resulted in a $T_{m\,3\rightarrow2}$ of 32.8 ˚C and a $T_{m\,2\rightarrow1}$ of 72.8 ˚C, agreeing with the temperatures obtained from the UV thermal denaturation. In the presence of 10 μM control compound 8, the melting temperatures of the triplex and duplex did not change. The dissociation temperature of the triplex did increase with 10 μM of 7 by 12.1 ˚C, but dissociation temperature of duplex stayed the same. It is important to note that the stabilization effect is not as significant as the UV data because the ratio of DNA to ligand has increased. However, the thermogram of poly(dA)●2poly(dT) plus 7 showed a broad peak for the dissociation of the triplex to duplex indicating a slower dissociation process. Thermodynamic parameters, ΔH and ΔS were extracted from the DSC thermograms and suggested that the interaction between the triplex and compound 7 is enthalpically driven. As expected, compound 8 did not exhibit a change in ΔH or ΔS. The change in enthalpy for compound 7 was increased by 3.5 kJ/mol and there was a 0.01 kJ/mol change in entropy. A change in entropy upon binding is uniquely due to the displacement of water from the DNA backbone. However, a change in enthalpy may be due to the hydrophobic pi-pi stacking interaction between the base triplets and ligand, suggesting a possible intercalation mode.

Figure 3-4

DSC Thermograms of poly(dA)●2poly(dT) in the Presence and Absence of 7 and 8

Ligand	N/A	8	7
T_m (°C)	36.8	38.5	48.9
ΔH (KJ/mol)	5.19	5.20	8.70
ΔS (KJ/(mol·K)	0.0167	0.0167	0.0271
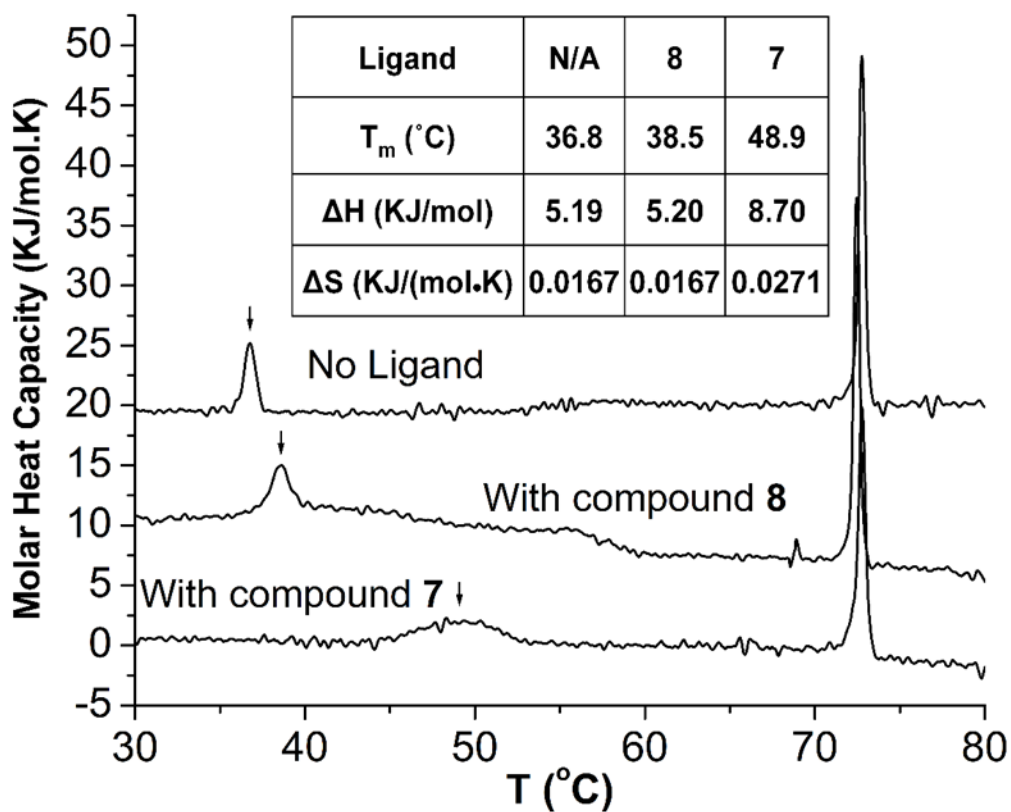
[DNA] = 100 μM /base triplet. Buffer: 10 mM sodium cacodylate, 150 mM KCl, pH 7. The $T_{m3 \to 2}$, ΔH, and ΔS values are shown in the table. The arrows indicate the dissociation of triplex to duplex DNA.

Binding Mode of 5 Substituted 3, 3',4',7-tetramethoxyflavonoids

To further understand the binding-induced changes of poly(dA)•2poly(dT) upon binding compound 7, circular dichroism (CD) was utilized. CD spectra of nucleic acids and ligands can be used to determine the binding stoichiometry. [93,95] Figure 3-5 shows the CD spectra obtained by an incremental titration of 7 or 8 into poly(dA)•2poly(dT) under physiological conditions from 230nm to 300 nm. B-form DNA is characterized by a positive band ~280 nm and a negative band at 245 nm. [96] CD spectrum of poly(dA)•2poly(dT) confirms the triplex to be B-form like and shows the addition of a shoulder band at 259 nm. Addition of compound 7 altered the spectrum indicative of the interaction between the ligand and triplex. While the positive band ~280 nm remained unchanged, the intensity of the negative band ~245 nm greatly reduced, and the shoulder region gradually disappeared. The titration of compound 8 did not change the CD spectrum of the triplex even at high concentrations of the ligand (>20 μM). Combined with the UV data, it can be concluded that 8 does not affect the structure of the triplex DNA.

To determine the ligand-DNA binding stoichiometry, CD values at 247 nm and plotting them against the ligand to DNA ratio the stoichiometry can be determined (Figure 3-5). Wavelength 247 nm was used because each titration clearly diminished the negative intensity. An inflection point at 0.33 base triplet ratio (r_{db}) by reciprocal indicates compound 7 has a binding site of 3 base triplets. Based on the neighbor-exclusion principle, one ligand per three base triplets indicates a possible intercalation binding mode. [97]

Figure 3-5

Circular Dichroism and Job Plot Analysis of Compound 7
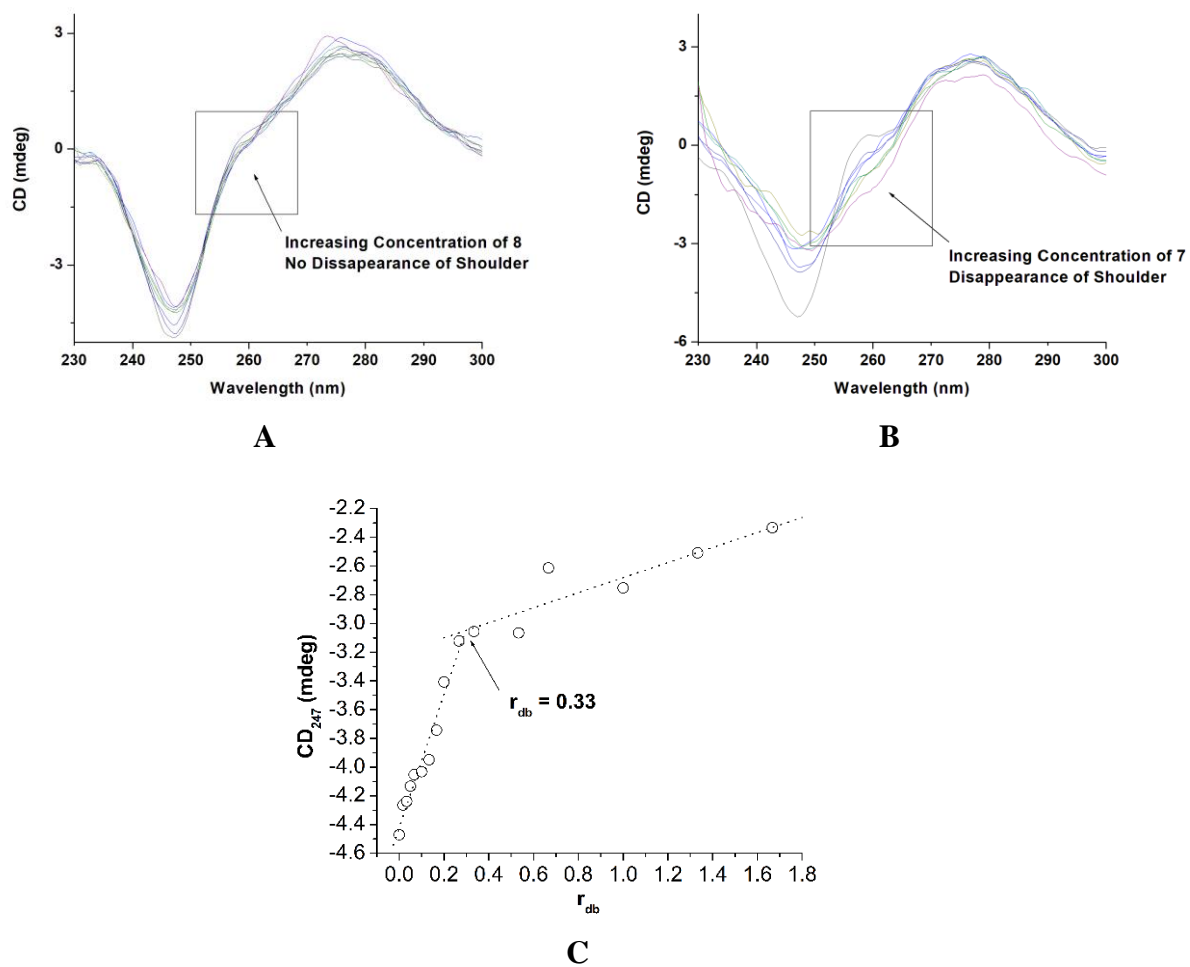
(A) CD spectra of Poly(dA)•2poly(dT) from 230 to 300 nm in the presence of 8 at various concentrations (0-25 µM). (B) CD spectra of poly(dA)•2poly(dT) from 230 to 300 nm in the presence of 7 (C4-linker) at various concentrations (0-25 µM).   (C) A plot of normalized CD value at 247 nm vs rdb extrapolated from the CD spectra in Figure 9B. rdb = ratio of the ligand/base triplet. The continuous lines reflect the linear least-squares fits of each apparent linear domain of the experimental data (o) before and after the apparent inflection point.

To establish the exact binding mode of the quercetin derivatives, the viscosity measurement was used. [92,98] If we assume, based on the neighbor-exclusion principle, that the ligands are intercalators, we would expect an increase in the viscosity proportional to the DNA to ligand ratio. In order for the DNA to accommodate a molecule between the bases pairs or base triplets, the helix must unwind and lengthen. Ethidium Bromide is a commonly used nucleic acid stain that is an intercalating agent. Figure 3-6 demonstrates how the cubed root of the relative viscosity, $(\eta/\eta_0)^{1/3}$, linearly increases as a function of moles of ligand per base pair of calf thymus. A plateau was observed at a ratio of 0.5, consistent with previous reports. [98] This indicated that a maximum of one ethidium bromide can intercalate every two base pairs. The use of ethidium bromide was a benchmark for this study.

Repeating the experiment by titrating our representative compound 7 into poly(dA)●2poly(dT), we noticed the same trend. The viscosity increased as a function of the ligand to DNA ratio and a clear plateau was observed at 0.3. This was consistent with the neighbor-exclusion principle and the CD titration data confirming an intercalation binding mode. Saturation past a ratio of 0.3 clearly indicated one ligand intercalates every three base triplets.

Figure 3-6

Viscosity Changes of poly(dA)●2poly(dT) with Increasing Concentration of 7
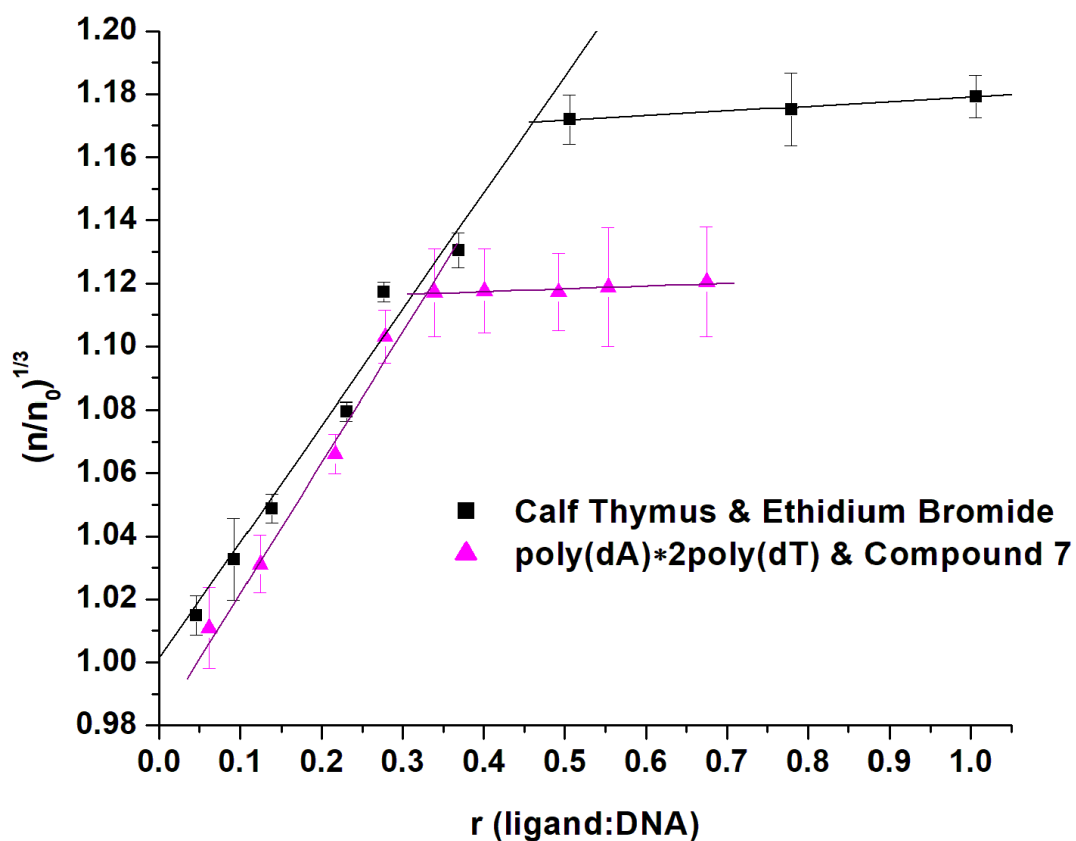
Calf thymus DNA and poly(dA)●2poly(dT) (1 mM) with increasing concentration (0.03 mM to 1 mM) of ethidium bromide and compound 7, respectively. Experimental conditions: 10 mM Sodium Cacodylate pH 7 and 150 mM KCl at room temperature.

5 Substituted 3, 3',4' ,7-tetramethoxyflavonoids Bind to Intramolecular Triplexes

To investigate the derivate's ability to be more biologically relevant, it was of interest to analyze the ability to stabilize shorter intramolecular DNA triplex sequences. Using the same fixed ligand concentration (10 µM), thermal denaturation studies were carried out and monitored by UV at 260 nm for both 15GC-T and 10GC-T (Figure 3-7 and Figure 3-8). 15GC-T contains a 15 nucleotide-long triplex forming region linked by two four-thymidine loops. The middle 13 nucleotides form T●A-T triplets which are flanked by C^+●G-C triplets on both ends. 10GC-T contains a 10-nucleotide triplex forming region consisting of 8 T●A-T triplets flanked by C^+●G-C on both ends, linked by two four-thymidine loops. All melting profiles for both sequences are biphasic.

In the absence of compounds 1-9 under physiological conditions (100 mM NaCl, pH 7), the $T_{m\,3\to2}$ was (20.9 ± 0.4) ˚C and $T_{m\,2\to1}$ (62.9 ± 0.17) ˚C for 15GC-T. Quercetin (9) increased the stabilization of the triplex by (0.7 ± 0.4) ˚C and tetramethylquercetin (8) increased the stability by (3.1 ± 0.4) ˚C. This shows the methoxy groups slightly stabilized the short intramolecular triplex as compared to the polynucleotide intermolecular triplex, but still had no effect on the corresponding duplex. Similar to the structural pattern observed in the thermal denaturation of poly(dA)●2poly(dT), the rank of triplex stabilization for 15GC-T is $1 = 2 > 3 > 4$ for the dialkyamino R-groups and $5 = 7 > 6$ for the cyclic amino R-groups. The melting temperatures of the dialkyamino compounds were (32.2 ± 0.3) ˚C for 1; (32.0 ± 0.1) ˚C for 2; (29.5 ± 0.2) ˚C for 3; (26.4 ± 0.6) ˚C for 4. Notice here the smallest dialkylamino group, diethylamine, provided an equal triplex stabilization as dipropylamine. This is possible because the size and shape of the binding pocket have changed, comparing a long intermolecular triplex to a short intramolecular triplex. Reverse from the polynucleotide triplex data, compound 5

stabilized 15GC-T one degree higher than compound 7, $\Delta T_{m\,3\rightarrow2}$ (13.5 ± 0.0) ˚C and $\Delta T_{m\,3\rightarrow2}$ (12.5 ± 0.6) ˚C, respectively. However, they are still considered to have similar triplex stabilization effects.

Figure 3-7

Thermal Denaturation of Intramolecular Triplex 15GC-T with Compounds 1-9
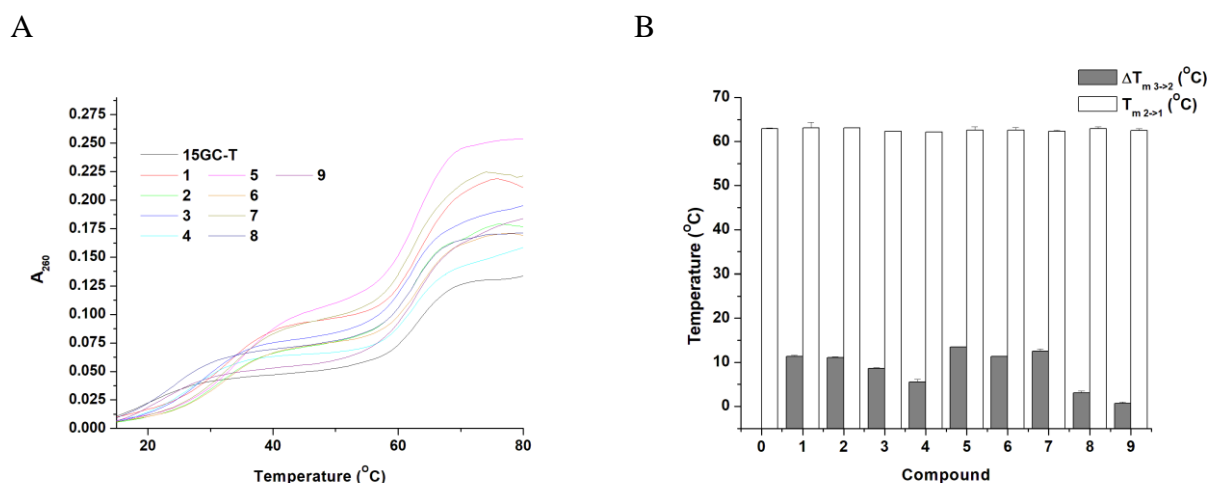
 (A) UV-thermal denaturation profiles of 15GC-T (1 µM) in the absence and presence of compounds 1-9 (10 µM). Absorbance adjusted to zero for better presentation. (B) 15GC-T stabilization difference in 10 mM sodium cacodylate and 100 mM NaCl, pH 7.

Under physiological conditions, 10GC-T exhibited a $T_{m\,3\rightarrow2}$ of (19.5 ± 0.4) ˚C and a $T_{m\,2\rightarrow1}$ of (58.1 ± 1.0) ˚C. The ligands followed the same stabilization pattern as previously described for poly(dA)●2poly(dT) and 15GC-T. The cyclic amino R-groups show the strongest ligand-induced triplex stabilization effect with no effect on the duplex. The triplex melting temperatures were (29.7 ± 0.0) ˚C for 5; (28.7 ± 0.4) ˚C for 7; (27.1 ± 0.1) ˚C for 6. The dialkylamino groups stabilized the triplex by 8.2 ˚C, 7.0 ˚C, 6.2 ˚C, and 4.6 ˚C for compounds 1,

2, 3, and 4, respectively, with no effect on the duplex stability. It can be confirmed that the 5-substituted 3, 3',4' ,7-tetramethoxyquercetin derivatives are relevant for biological applications to target both short triplex sequences and intramolecular sequences.

Figure 3-8

Thermal Denaturation of Intramolecular Triplex 10GC-T with Compounds 1-9
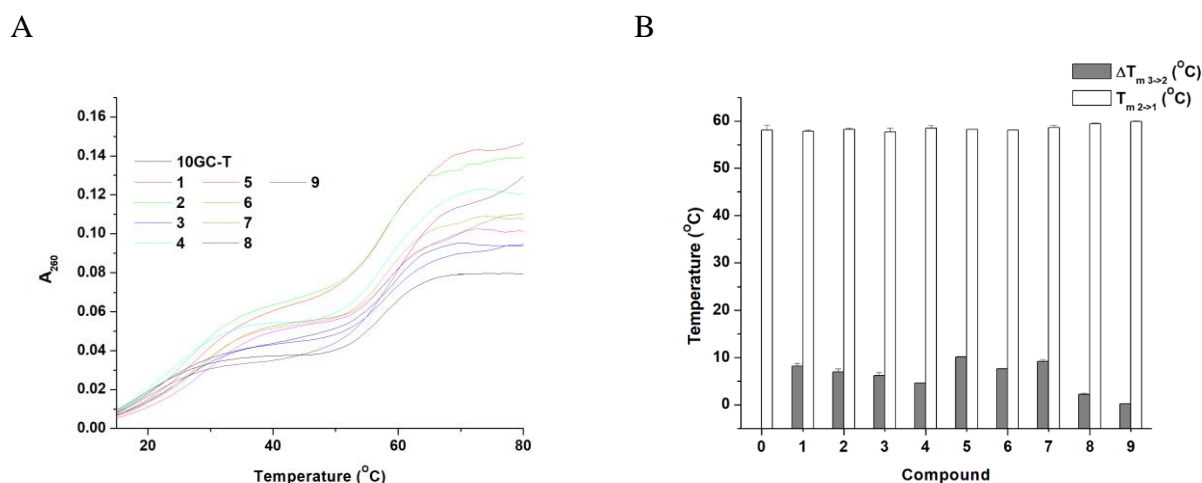
(A) UV-thermal denaturation profiles of 10GC-T (1 µM) in the absence and presence of compounds 1-9 (10 µM). Absorbance adjusted to zero for better presentation. (B) 10GC-T stabilization difference in 10 mM sodium cacodylate and 100 mM NaCl, pH 7.

Comparing 5 Substituted 3, 3',4' ,7-tetramethoxyflavoid Derivatives with Neomycin a Known Triplex Binding Molecule

Neomycin is a well-known selective triplex groove binder used for the purpose of accurately evaluating the derivatives stabilization effect. [93,99] UV thermal denaturation experiments of poly(dA)●2poly(dT) were conducted in the presence of compound 5 or neomycin with varying concentrations 0-20 µM. Both compounds increased the stability of the triplex as a

function of increasing concentration and did not show any effect of the duplex stability (Figure 3-9). At 20 μM the stabilization effect of both compounds was about equal with a $\Delta T_{m\,3\to2}$ of ~24 ˚C. It is noteworthy to mention compound 5 at concentrations lower than 20 μM resulted in better triplex stability than that of neomycin. As a comparison, 1 μM of 5 increased the $T_{m\,3\to2}$ of the triplex by 6 ˚C whereas neomycin barely changed it ($p < 0.05$).

Additionally, the same experiment was performed using shorter intramolecular triplex sequences. Sequences 15GC-T and 10GC-Tdid not show the same degree of triplex stabilization. In fact, at lower concentrations from 1-5 μM the two ligands are comparable in strength. It is interesting; however, when using 15AT-C, a 15 nucleotide T●A-T triplex with two C connecting loops, the result shows a similar trend as poly(dA)●2poly(dT). This suggested that that the two C^+●G-C flanking triplets of 15GC-T and 10GC-T are blocking 5 from effectively binding. Referring back to Figure 1-2, this may be due to the openness of the AT minor groove as opposed to the GC minor groove. However, the data from the concentration-dependent study confirms that compound 5 is a potent and specific triplex binding ligand, and its triplex stabilizing effect is comparable to the well-known effect that neomycin has at the low drug-to-DNA ratios.

Figure 3-9

Triplex Stabilization Comparison of Compound 5 and Neomycin

A

B

C

D
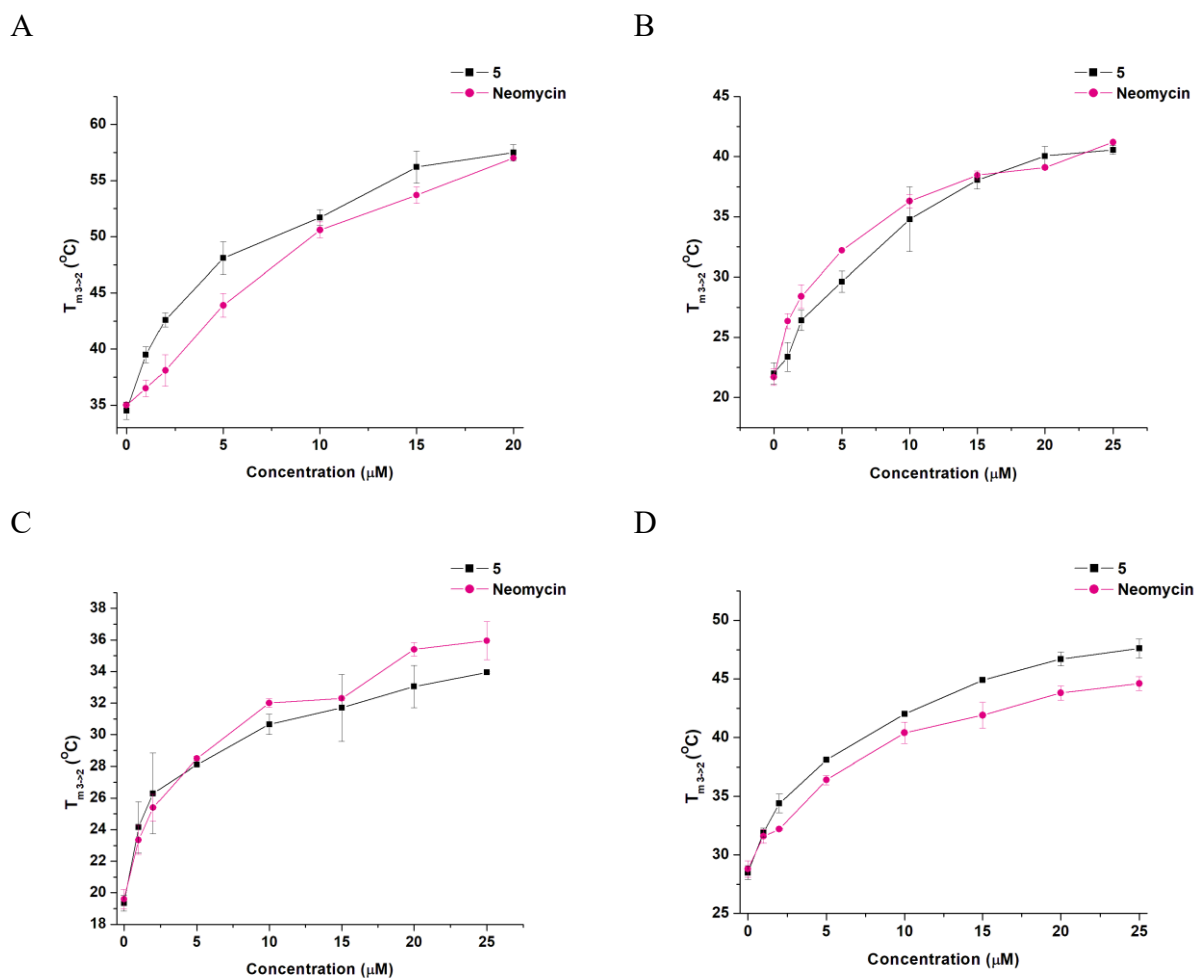
Poly(dA)●2poly(dT) (A), 15GC-T (B), 10GC-T (C), and 15AT-C (D). [Polynucleotide triplex] = 15 μM/base triplet, [intramolecular triplex] = 1 μM, ligand concentration 0, 1, 2, 5, 10, 15, 20, and 25 μM. Buffer conditions: 10 mM sodium cacodylate, 150 mM KCl, pH7 for polynucleotide triplex; 10 mM sodium cacodylate, 100 mM NaCl, pH 7 for intramolecular triplex.

The binding affinity and specificity of a ligand to an oligonucleotide can be quantified using isothermal titration calorimetry (ITC). [100,101] Thermodynamics of compounds 7, 8, and neomycin binding to either 15GC-T or the intramolecular duplex 15GC-Td were determined. The ITC profiles were obtained from a series of injections of a ligand (100 μM) into a 10 μM solution of either 15GC-T or 15GC-Td in cacodylate buffer at pH7 and 110 Na$^+$ at 15 ˚C. The temperature was chosen to be below room temperature to ensure the presence of the intramolecular triplex before addition of the ligand. Figure 3-10 shows a representative ITC profile of compound 7 titrated into a solution of either 15GC-T and 15GC-Td and the resulting corrected injection heats plotted as a function of the ligand:DNA molar ratio. Corrected injection heats are obtained by subtracting the blank data (titrations of ligand into an oligonucleotide free buffer solution) to account for the dilution effect. It is revealed that 7 binds with an exothermic single binding process and was best fit by the independent model using the NanoAnalyze software by TA Instruments. With a 90% confidence level, the data yielded a dissociation constant (K_d) of $(3.1 \pm 1.1) \times 10^{-5}$ M. Agreeing with previous DSC data, the binding of 7 with 15GC-T is primarily enthalpically driven with a ΔH value of $-(32.4 \pm 4.5)$ kJ/mol and a TΔS of -7.6 kJ/mol. This was another piece of supporting evidence based on Chaires suggestion that intercalators have unfavorable entropic and favorable enthalpic changes.[102] The overall stoichiometry for binding of 7 to 15GC-T was determined to be approximately six ligands per triplex DNA. Considering 15GC-T contains a 15 nucleotide-long triplex sequence, the binding stoichiometry suggests about three base triplets per bound molecule 7, which is in agreement with data obtained from the CD titration and the viscosity measurement. Notice in column B, no meaningful titration curve from the binding isotherm of compound 7 to 15GC-Td which prohibited the extraction of thermodynamic parameters. 15GC-Td is an intramolecular duplex

containing a 15 nucleotide-long duplex forming region linked by a four-thymidine loop. This indicates only the heat of dilution is observed and no interaction between 15GC-Td and 7, expected from thermal denaturation experiments where no change in duplex stability was observed.

Represented in the upper panels of Figure 3-11 are the isotherms of a series titration of compound 8 into 15GC-T (A) and the corrected injection heats (B). Notice the similar titration trend as compound 7 and 15GC-Td. Due to there being no meaningful curve and just the heat of dilution, no thermodynamic parameters for 8 into 15GC-T were extrapolated. This is in agreement with previous data and confirms that an amino side chain at the fifth position of these 3, 3', 4', 7-tetramethoxyquercetin derivatives is necessary for binding.

To compare, neomycin titrated into 15GC-T was performed under the same conditions at 15 ˚C. This yielded a K_d of $(1.6 \pm 0.6) \times 10^{-5}$ M (Figure 3-10 lower panels). Neomycin's K_d and the K_d of 7 $((3.1 \pm 1.1) \times 10^{-5}$ M) are comparable, confirming that compound 7 is a strong triplex binder.

Figure 3-10

Isothermal Titration Calorimetry of Pyrrolidine Derivative into 15GC-T and 15GC-Td
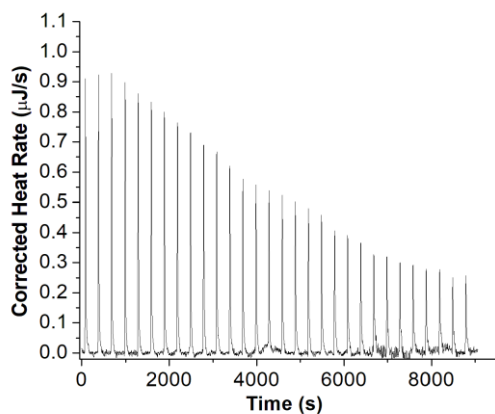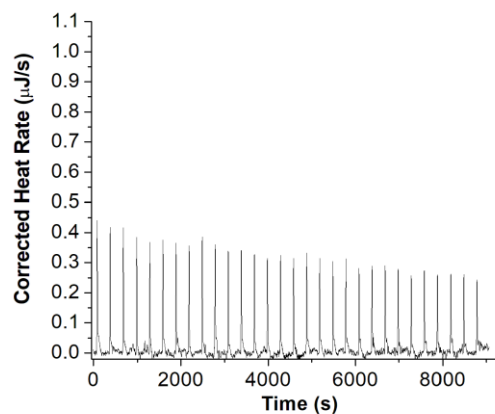
A (upper panel)
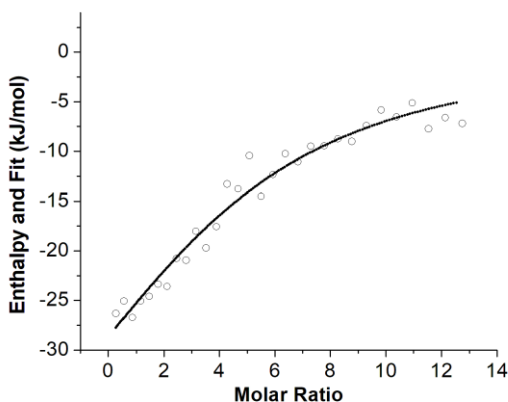
B (upper panel)
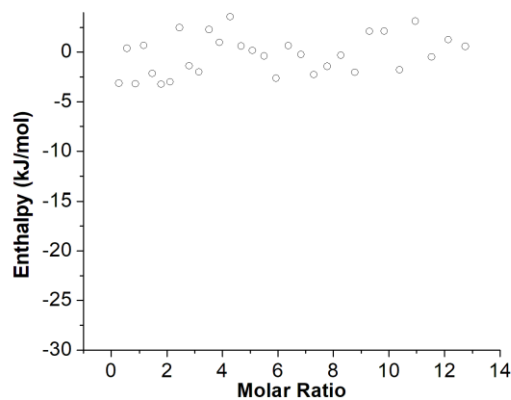
A (lower panel)

B (lower panel)

Upper panel: ITC profile of 15GC-T (10 µM) (A) and 15GCT-d (10 µM) (B) titrated with 100 µM 7 (C4-linker).

Lower panel: The dotted line represents the corrected injection heats plotted as a function of the [7]/[DNA] molar ratio. The smooth solid line reflects the calculated fit of the data using the independent model from the software NanoAnalyze. Upward peaks represent an exothermic event.

Figure 3-11

Isothermal Titration Calorimetry of Neomycin into 15GC-T and 15GC-Td
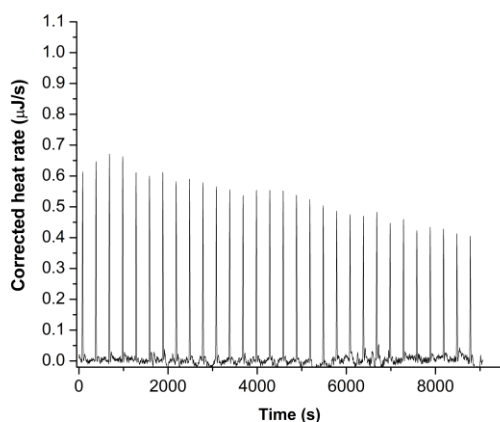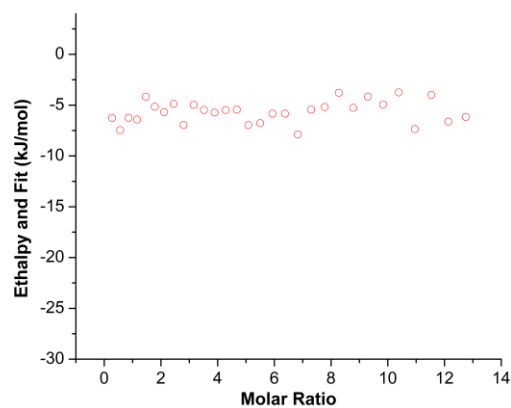
A (upper panel)   B (upper panel)
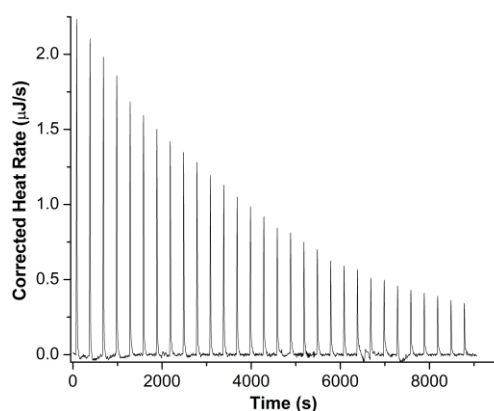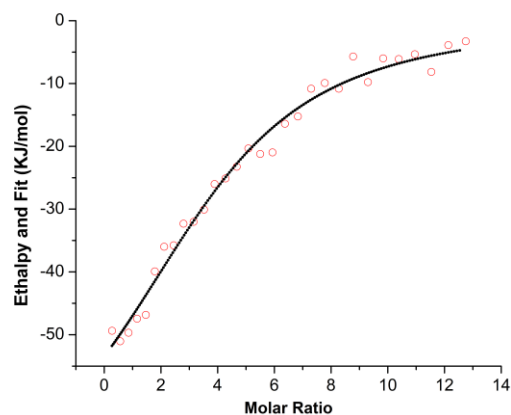
A (lower panel)   B (lower panel)

A (upper panel) and A (lower panel): ITC profile of 15GC-T (10 µM) titrated with 8 and neomycin (100 µM), respectively, in a 10 mM sodium cacodylate buffer with 100 mM NaCl, pH 7.0 at 15 °C. B upper and lower panel: The dotted line represents the corrected injection heats plotted as a function of the ligand to DNA molar ratio. The smooth solid line reflects the calculated fit of the data using the independent model from the software NanoAnalyze.

Sequence Specificity

Intramolecular triplex sequences with varying T●A-T lengths were used to examine the necessary amount of T●A-T tracts for ligand binding. The stoichiometry was determined to be 3 base triplets per 1 ligand using CD titration and ITC. The sequences in Table 3-1 were used to determine the minimum T●A-T length for ligand-induces stabilization of the triplex. The triplex sequences (1 µM) were prepared with and without compounds 5 and 7 (10 µM) under physiological conditions. As expected, there was no stabilization effect on 15GC-2AT by compounds 5 or 7. 15GC-2AT does not contain three sequentially placed T●A-T tracts to allow for ligand binding. However, 15GC-3AT also does not indicate a ligand-induced stabilization effect of the triplex. This can be explained because upon ligand binding there is a localized change in conformation (i.e., bend or stretch) and having a minimum of three T●A-T triplets does not provide enough flexibility. The results of 10GC-T sequence variations confirm the results determined from 15GC-T variation. Table 3-2 shows more than five T●A-T triplets are necessary for significant ligand-induced stabilization. Although the stoichiometry is 1 ligand per three base triplets, three T●A-T triplets do not provide enough flexibility for proper ligand binding. Additionally, with an increase of 3 ˚C for 10GC-5AT upon binding both compound 5 and 7, it confirmed five T●A-T triplets are needed for ligand binding.

Table 3-1

Sequence Specificity Sequences

Name	# T•A-T	Sequence 5'→ 3'
15GC-2AT	2	GAGAGG**AAG**A**AG**A**AG**GTTTTC**TT**C**TT**C**TT**CCTCTCTTTT-CTCTCC**TT**C**TT**C**TT**C
15GC-3AT	3	GAGAG**AAA**GAAGAAGTTTTCTTCTTC**TTT**CTCTCTTTT-CTCTC**TTT**CTTCTTC
15GC-4AT	4	GAGG**AAAA**GAAGAAGTTTTCTTCTTC**TTTT**CCTCTTTT-CTCC**TTTT**CTTCTTC
15GC-5AT	5	GAG**AAAAA**GAAGAAGTTTTCTTCTTC**TTTTT**CTCTTTT-CTC**TTTTTCTT**CTTC
15GC-T	13	G**AAAAAAAAAAAAA**GTTTTC**TTTTTTTTTTTTT**CTTTT-C**TTTTTTTTTTTTT**C
10GC-3AT	3	G**AAA**GAGGAGTTTCTCCTC**TTT**CTTTTC**TTT**CTCCTC
10GC-5AT	5	G**AAAAA**GGAGTTTCTCC**TTTTT**CTTTTC**TTTTT**CCTC
10GC-6AT	6	G**AAAAAA**GAGTTTCTC**TTTTTT**CTTTTC**TTTTTT**CTC
10GC-T	8	G**AAAAAAAA**GTTTTC**TTTTTTTT**CTTTTC**TTTTTTTT**C

Table 3-2

15GC-T and 10GC-T AT base-pair Sequence Variation Effects

Compound		5	7
15GC-2AT	**$\Delta T_{m\ 3->2}$ (˚C)**	0.6	0.1
	St.Dev.	0.57	0.00
15GC-3AT	**$\Delta T_{m\ 3->2}$ (˚C)**	0.1	0
	St.Dev.	0.00	0.00
15GC-4AT	**$\Delta T_{m\ 3->2}$ (˚C)**	1.75	-0.15
	St.Dev.	0.07	0.35
15GC-5AT	**$\Delta T_{m\ 3->2}$ (˚C)**	1.4	0.35
	St.Dev.	0.00	0.07
15GC-T (13AT)	**$\Delta T_{m\ 3->2}$ (˚C)**	13.5	12.5
	St.Dev.	0.00	0.57
10GC-3AT	**$\Delta T_{m\ 3->2}$ (˚C)**	0.1	-0.35
	St.Dev.	1.34	0.71
10GC-5AT	**$\Delta T_{m\ 3->2}$ (˚C)**	3.2	3.25
	St.Dev.	0.07	0.00
10GC-6AT	**$\Delta T_{m\ 3->2}$ (˚C)**	4.2	2.6
	St.Dev.	1.41	0.71
10GC-T (8AT)	**$\Delta T_{m\ 3->2}$ (˚C)**	10.2	9.2
	St.Dev.	0.00	0.42

Triplex (1 µM) thermal dissociation difference upon binding compound 5 or 7 (10 µM) in 10

mM sodium cacodylate pH7 and 100 mM NaCl.

Conclusion

We have confirmed the discovery of a novel class of triplex binding ligands based on the

natural product quercetin. This is significant because, alone, quercetin cannot provide triplex

stabilization under physiological conditions and pH 7. Thermal denaturation studies show that

this class of compounds selectively bind to the triplex structure with no change in duplex

stability. This shows the potential to be an antigene enhancer *in vivo*. Additionally, the size of

the R-group affects the potency of the ligands. Shorter dialkylamino side chains are more

favorable to fit the binding pocket than longer chains. However, cyclic amino R-groups provide

the strongest stabilization effect, particularly in the order of pyrrolidine = piperidine >

piperazine. The binding affinity of the lead compounds 7 and 5 was shown to be comparable to

the known potent triplex binding ligand, neomycin. Based on the stoichiometry of 3 base triplets

per ligand and viscosity test, the binding mode of these ligands is intercalation and shares similar

binding elements as naphthyquinolines, another class of triplex binding ligands. [103] The

elements are: (1) compounds have sufficient aromatic surface areas to stack with the crescent-

shaped base triplet; (2) compounds contain cations (amino groups) to neutralize the negative

density of the triplex backbones. (3) compounds have an unfused aromatic system that is

flexible enough to maximize the stacking efficiency to the propeller-twisted base triplet. In

addition, the attaching point of side chains to the aromatic system in our ligands is an oxygen

atom, which lowers the energy barrier for rotation of side chains [104] facilitating their reorientation

within a triplex groove. Finally, more than five sequential TAT triplets are necessary for

sufficient ligand binding and triplex stabilization.

CHAPTER 4: THE BINDING OF 5-SUBSTITUTED 3, 3', 4', 7-

TETRAMETHOXYQUERCETIN COMPOUNDS UNDER VARYING SOLUTION

CONDITIONS

Intracellular conditions can vary based on disease and extracellular factors. It was of interest to vary the conditions of the triplex solution to gain a greater understanding of the ligand-DNA interaction. UV-Vis thermal denaturation was used to investigate the effect of changing pHs, salinity, and cell crowding. The results concluded the nitrogen contained in the R-group competes with K^+ and Na^+ ions for the DNA backbone and an increased pH provided for a stronger ionic attraction. Additionally, mimicking increased cell crowding resulted in a more stable triplex structure.

Introduction

The cell cycle is a process by which genetic information is duplicated and transmitted from a parent to two daughter cells. The cell cycle is divided into five distinct phases G_1, S, G_2, M and G_0 phase. [105] During G_1 phase, the cell is subject to extracellular stimulation and growth factors before leading into S phase which involves DNA replication. G_2 phase consists of preparing the cell for mitosis and formation of the necessary structural components. Mitosis, or M Phase, is characterized by the generation of bipolar mitotic spindles, segregation of sister chromatids, and cellular division. Following division, the two daughter cells move into G_0 Phase which is a temporary state of rest from the replicative cell cycle.

Figure 4-1

The Cellular Cycle
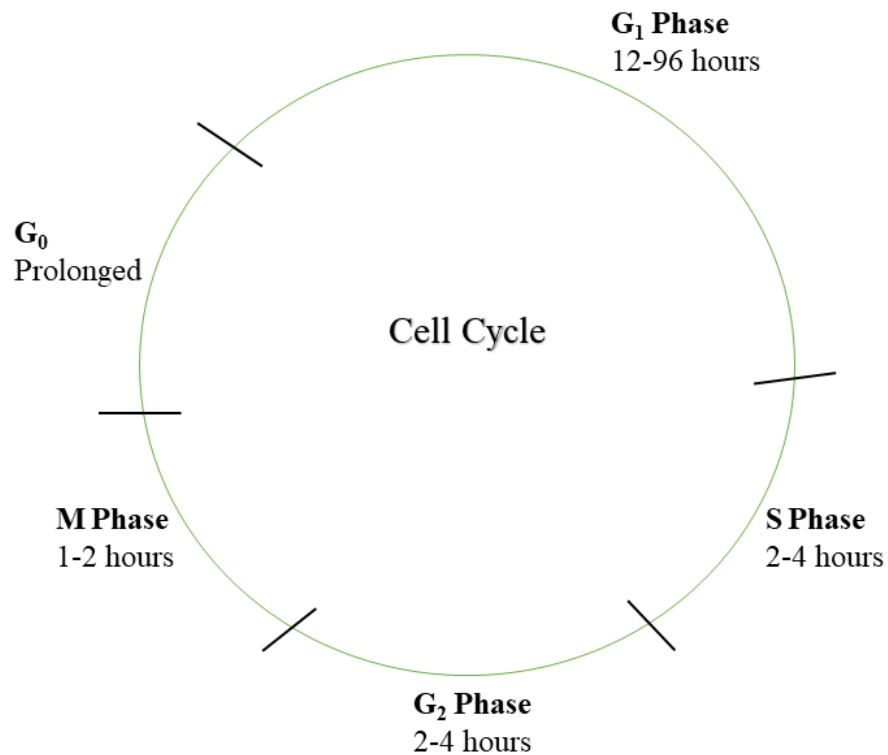
Changes between cell cycle phases influence the local levels of ionic concentration. High ionic concentrations are found during the initial phase of mitosis, prophase, to aid the condensation of the chromatin. [106] However, salt concentration must lower to normal ionic levels during S and G_2 phase to allow for DNA replication and flexibility of DNA. [106,107] If high ionic levels were present during these phases, the replication of DNA would be halted and signal apoptosis.

Another variable of cellular condition is pH. Suborganelles within a cell can be inherently pH sensitive for normal function. Cytochromes within the mitochondria create a proton gradient used to form ATP, cellular energy. Whereas, other organelles use ATP and pump protons into the lumen and increase pH for the process of breakdown and recycling of endocytosed material. [108] However, the physiological pH of an overall cell is 7.4 and intracellular acidification has been associated DNA cleavage and apoptosis. [109-111] Interestingly, the pH of cancer tissue has been found to be lower than the pH of normal tissue. [112] This has led researchers to try to develop pH-sensitive chemotherapeutics. The environmental conditions of a cell can fluctuate based on many factors. It has even been shown that normally prescribed pharmaceuticals, like chloroquine and dexamethasone, can alter intracellular pH. [113] For this reason, it was of interest to investigate the binding of compounds 1-9 in a variety of solution conditions.

Experimental

Materials and General Methods

All the chemicals were purchased from MilliporeSigma or Fisher Scientific and used without further purification. DNA oligonucleotides were purchased from Fisher Scientific. Polynucleotides were purchased from MilliporeSigma. The concentrations of polynucleotide solutions were determined spectrophotometrically using the following extinction coefficients (in units of mol of nucleotide/L-1 cm-1): $\varepsilon 265 = 9,000$ for poly(dT) and $\varepsilon 260 = 6,000$ for poly(dA)•poly(dT). The concentrations of DNA solutions were determined spectrophotometrically, using the molar extinction coefficients (in units of mol of strand/L-1 cm-1) obtained from OligoAnalyzer (www.idtdna.com). $\varepsilon 260 = 483,700$ for 15GC-T (5'-GAAAAAAAA AAAAAGTTTTCTTTTTTTTTTTTTCTTTTCTTTTTTTTTTTTC-3'); $\varepsilon 260$

= 342,700 for 10GC-T (5'- GAAAAAAAAGTTTTCTTTTTTTTCTTTTCTTTTTTTTC-3');

UV spectra were recorded on a Varian Cary 100 Bio UV-Vis spectrophotometer equipped with a

thermoelectrically controlled 6 × 6 cell holder.

Thermal Denaturation of poly(dA)●2poly(dT) Monitored by UV

The UV thermal denaturation samples (1 mL) were prepared by mixing

poly(dA)●poly(dT) (15 µM/base triplet), poly(dT) (15 µM/base triplet) in the presence and

absence of a ligand (1-9, 10 µM) in a sodium cacodylate buffer (10 mM), KCl (50, 150, or 250

mM), pH 6.0, 7.0, or 8.0. The UV melting spectra were recorded in 1 cm path length quartz

cuvettes at 260 nm, 280 nm, and 284 nm, as a function of temperature (25-90 °C, heating rate:

0.2 °C/min). Melting temperatures (T_ms) were determined using the first derivative method. All

experiments were carried out in duplicate.

Thermal Denaturation of Intramolecular Triplex Monitored by UV

The UV thermal denaturation samples (1 mL) were prepared by mixing 15GC-T or

10GC-T (1 µM) in the presence and absence of a ligand (1-9, 10 µM) in a sodium cacodylate

buffer (10 mM), NaCl (25, 100, or 200 mM) at pH 6.0, 7.0, or 8.0. The UV melting spectra were

recorded in 1 cm path length quartz cuvettes at 260 nm, 280 nm, and 284 nm, as a function of

temperature (5-90 °C, heating rate: 0.2 °C/min). Melting temperatures (T_ms) were determined

using the first derivative method. All experiments were carried out in duplicate.

 PEG Studies

The UV thermal denaturation samples (1 mL) were prepared by mixing

poly(dA)●poly(dT) (15 µM/base triplet), poly(dT) (15 µM/base triplet) in the presence and

absence of a ligand (1-9, 10 µM) in a sodium cacodylate buffer (10 mM, pH 7.0), KCl (150

mM), EDTA (100 M), and either PEG200 or PEG400 at various percentages: 0, 1, 5, 10, 15, and

20%. The UV melting spectra were recorded in 1 cm path length quartz cuvettes at 260 nm, 280

nm, and 284 nm, as a function of temperature (25-90 °C, heating rate: 0.2 °C/min). Melting

temperatures (T_ms) were determined using the first derivative method. All experiments were

carried out in duplicate.

Results and Discussion

Varying pH

Cellular and extracellular pH can vary depending on multiple conditions. Table 4-1

compares the poly(dA)•2poly(dT) triplex stability upon binding compounds 1-9 (C4-linker) at

pH 6, 7, and 8. The thermal stability of the triplex and duplex without any ligand stayed

consistent regardless of pH variation. Also consistent with previous data, compounds 1-9 do not

have a ligand-induced stabilization effect on the duplex regardless of pH changes. The

stabilization effect of the derivatives 1-4, 5, and 6 on the triplex stayed consistent at pH 7 and 8.

However, at pH 6 the stabilization effect on the triplex increased for all compounds, except

compound 7 which stayed the same. This inverse relationship between pH and triplex stability is

the result of a partial protonation of the amino containing R-group at lower pH. This partial

positive charge provides a stronger electrostatic attraction between the R-group and the

negatively charged backbone of the DNA.

Table 4-1

pH Effect on the Ligand-Induced Stabilization Effect for poly(dA)●2poly(dT)

Compound	pH	$T_{m\,3\text{-}>2}$ (°C)	$\Delta T_{m\,3\text{-}>2}$ (°C)	St.Dev.	$T_{m\,2\text{-}>1}$ (°C)	$\Delta T_{m\,2\text{-}>1}$ (°C)	St.Dev.
poly(dA)●2poly(dT)	6	34.0	-	0.00	73.0	-	0.00
	7	35.3	-	1.00	73.7	-	0.50
	8	34.6	-	0.47	73.0	-	0.00
9	6	54.7	19.6	0.55	73.1	0.1	0.05
	7	36.5	1.2	0.74	73.0	-0.7	0.00
	8	37.2	2.6	0.07	73.2	0.1	0.07
8	6	39.2	4.2	0.07	72.9	-0.2	0.35
	7	38.2	2.8	0.03	73.2	-0.6	0.07
	8	38.9	4.3	0.28	72.7	-0.4	0.64
1	6	50.2	16.2	0.07	72.9	-0.1	0.42
	7	41.2	15.0	0.00	73.9	0.2	0.58
	8	40.2	14.2	0.07	73.1	0.1	0.00
2	6	47.0	13.0	0.00	73.3	0.3	0.35
	7	45.2	9.9	0.00	73.1	-0.7	0.07
	8	44.2	9.6	0.00	73.1	0.1	0.14
3	6	45.0	11.0	0.00	73.0	0.0	0.00
	7	43.0	7.7	0.00	73.0	-0.6	0.07
	8	42.5	7.9	0.64	73.1	0.1	0.10
4	6	41.2	7.2	0.00	73.0	0.0	0.35
	7	42.1	6.8	0.00	73.6	-0.2	0.64
	8	41.2	6.7	0.07	72.9	-0.1	0.21
7	6	51.0	17.0	0.00	73.0	0.0	0.00
	7	53.1	17.8	0.18	73.6	-0.1	0.57
	8	49.1	14.5	0.07	73.0	0.0	0.00
5	6	52.1	18.1	0.00	73.1	0.1	0.00
	7	52.1	16.7	0.07	73.6	-0.2	0.78
	8	51.5	16.9	0.75	73.6	0.5	0.64
6	6	50.6	16.6	0.71	73.2	0.1	0.07
	7	48.0	12.7	0.07	73.6	-0.2	0.64
	8	47.2	12.6	0.07	73.2	0.1	0.07

pH changes effect on the interaction between poly(dA)●2poly(dT) (15 µM/ Base triplet) and compounds 1-9 (10 µM) in 10 mM sodium cacodylate and 150 mM KCl.

Comparing the stabilization effect of the dialkylamino compounds 1-4 across the pH range, a shorter alkyl chain provides a more significant stabilization effect for the polynucleotide triplex. At pH 6 the increased positive charge holds the smaller diethylamine R-group into the binding pocket and provides the best stabilization of this group. Comparing the cyclic amino R-groups, 5-7, the ability to stabilize the triplex at pH 6 is comparable being $\Delta T_{m3\to2}$ of 18.1 °C for 5; 17.0 °C for 7; 16.6 °C for 6. It is at pH 8 where one compound keeps its stabilization potency, proving to be a lead compound under all three conditions. Compound 5, though equal to 7 at pH

7 and 6, provides better stabilization at pH 8. It is possible that as the nitrogen becomes less positive at a higher pH, a larger ring is needed to better fit into the binding pocket. Compound 7 at pH 8 increased the triplex stability by 14.5 ˚C compared to 17.8 ˚C and 17.0 ˚C at pH 7 and 6. It is lower, indicating the reduced positive charge on the nitrogen of the pyrrolidine group is not strong enough to properly hold the smaller ring in the binding pocket. Compound 7 did not increase the triplex stability as the pH decreased, suggesting ~ 52 ˚C is the maximum stability of its DNA-ligand complex. It should be noted that control compound 8 did not provide significant stabilization of the triplex; however, quercetin did stabilize the triplex by 19 ˚C at pH 6 which is currently under investigation by our group.

Next, to investigate if the same is true for intramolecular triplexes, the same experiments were conducted with 15GC-T (Table 4-2) and 10GC-T (Table 4-3). The melting temperature of 15GC-T varied with the change in pH, increasing with pH. This is accounted for by the flanking $C^+{\bullet}G$-C base triplets of the triplex. The cytosine of the third strand must be protonated to participate in Hoogsteen hydrogen bonding. Therefore, as the pH decreases, the level of protonation increases providing more triplex stability. Watson-Crick hydrogen bonding is not reliant on cytosine protonation; therefore, the stability of the corresponding duplex does not vary. Tetramethoxyquercetin (8) did not provide significant triplex stability, but quercetin (9) selectively increased the 15GC-T triplex stability by 10.6 ˚C. Examining the $\Delta T_{m3\to2}$ of compounds 1-7, it is evident that the change was not as significant at pH 6 as at pH 7 or 8. This is due to the increased stability of the triplex alone. The amino R-groups provide the best stabilization for 15GC-T despite changes in pH. Compound 5 with the piperidine R-group provided the best stabilization of 15GC-T with $T_{m3\to2}$s of (29.5 ± 0.4) ˚C, (34.4 ± 0.0) ˚C, and

(43.0 ± 0.1) ˚C; compared to (13.9 ± 1.7) ˚C, (20.9 ± 0.4) ˚C, and (32.0 ± 0.1) ˚C of 15GC-T at

pH 8, 7, and 6 respectively. Overall, the rank order of these compounds is 5 > 7 > 6.

Comparing the dialkylchain compounds (1-4) the stabilization effect ranked in the order

of 1 > 2 > 3 > 4 for pH 7 and 6. However, at pH 8 the stabilization shifts to 2 > 3 > 4 > 1.

Although the same general trend of smaller alkyl chain is better is still being followed, we can

explain this lost effectiveness by considering the nitrogen's charge at pH 8. It can be assumed

that as the nitrogen becomes less positively charged and has a weakened interaction with the

DNA backbone a larger chain is necessary to fit snuggly into the binding pocket. This will need

to be confirmed by molecular modeling in future experiments.

Table 4-2

pH Effect on the Ligand-Induced Stabilization Effect for 15GC-T

Compound	pH	$T_{m\,3\to2}$ (°C)	$\Delta T_{m\,3\to2}$ (°C)	St.Dev.	$T_{m\,2\to1}$ (°C)	$\Delta T_{m\,2\to1}$ (°C)	St.Dev.
15GC-T	6	32.0	-	0.10	62.3	-	0.44
	7	20.9	-	0.40	62.9	-	0.17
	8	13.9	-	1.66	62.9	-	0.26
9	6	42.6	10.6	0.57	62.2	-0.1	0.14
	7	21.6	0.7	0.35	62.5	-0.4	0.42
	8	15.8	1.9	0.99	62.6	-0.4	0.78
8	6	34.1	2.1	0.07	62.4	0.1	0.85
	7	24.0	3.1	0.35	62.9	0.0	0.42
	8	18.4	4.5	0.28	63.1	0.1	0.07
1	6	41.5	9.5	0.71	62.6	0.3	0.71
	7	32.2	11.3	0.28	63.1	0.2	1.34
	8	20.4	6.5	0.75	61.8	-1.1	1.14
2	6	40.1	8.1	0.21	62.5	0.2	0.42
	7	32.0	11.1	0.14	63.1	0.2	0.00
	8	25.1	11.2	0.00	63.2	0.3	0.07
3	6	38.7	6.7	0.07	63.1	0.8	0.07
	7	29.5	8.6	0.21	62.3	-0.6	0.14
	8	24.3	10.4	0.14	62.7	-0.2	0.57
4	6	37.1	5.1	0.07	63.1	0.8	0.14
	7	26.4	5.5	0.64	62.2	-0.7	0.07
	8	23.8	9.9	0.57	62.7	-0.3	0.49
7	6	41.8	9.8	0.42	62.6	0.3	0.85
	7	33.4	12.5	0.57	62.4	-0.5	0.21
	8	28.5	14.6	0.71	63.0	0.1	1.41
5	6	43.0	11.0	0.14	62.8	0.5	1.70
	7	34.4	13.5	0.00	62.6	-0.3	0.71
	8	29.5	15.6	0.35	63.2	0.3	0.07
6	6	41.9	9.9	0.14	62.8	0.5	0.07
	7	32.2	11.3	0.14	62.6	-0.3	0.64
	8	20.3	6.4	1.22	62.7	-0.2	0.50

15GC-T (1 μM) with and without the presence of compounds 1-9 (10 μM) in 10 mM sodium cacodylate and 100 mM NaCl.

Similar to 15GC-T, as pH increased, so did the stability of the 10GC-T triplex with no change in duplex stability. Tetramethoxyquercetin (8) did not stabilize the intramolecular triplex; however, quercetin (9) did provide a 6.7 °C stabilization at pH 6. Compounds 1-4 stabilized the triplex with less significance at pH 6 than pH 7 and 8. This is because 10GC-T, in the absence of ligand, had a higher degree of stability from the two flanking protonated $C^+\bullet G\text{-}C$ triplets. The

dipropylamino group (2) was the optimal dialkylchain length, striking the right balance between size and charge.

Consistent with previous data, the cyclic amino R-groups provided better triplex stabilization. At pH 7 and 8 the piperidine (5) and pyrrolidine (7) were equivalent in their ability to stabilize the short 10GC-T intramolecular triplex. However, keeping with the findings from the polynucleotide intermolecular triplex and the longer intramolecular triplex, compound 5 provided a more significant stabilization of 10GC-T at pH 6 than compound 7. Due to the size of the piperazine (6) R-group, it was unable to stabilize the triplex to the same degree as 5.

Varying the pH confirmed that cyclic amino R-groups provide a better triplex stabilization effect than dialkylamines. Although both groups contain nitrogen available for protonation, the surface area of the rings in compounds 5-7 proved to be of significance. An interesting detail was that the additional nitrogen in piperazine (6) did not provide additional stabilization as the pH increased. This can be attributed to potential steric hindrance preventing a proper fit into the binding pocket, outweighing possible electrostatic attraction. The smaller rings provided by 5 and 7 stabilize the triplex DNA structure equally at pH 7 and 8; however, at pH 6 compound 5 provided an increased stability.

Table 4-3

pH Effect on the Ligand-Induced Stabilization Effect for 10GC-T

Compound	pH	$T_{m\,3\text{->}2}$ (°C)	$\Delta T_{m\,3\text{->}2}$ (°C)	St.Dev.	$T_{m\,2\text{->}1}$ (°C)	$\Delta T_{m\,2\text{->}1}$ (°C)	St.Dev.
10GC-T	6	33.9	-	0.21	59.6	-	0.64
	7	19.5	-	0.35	58.1	-	1.00
	8	13.9	-	0.71	58.6	-	0.64
9	6	40.6	6.7	0.57	57.7	-2.0	0.49
	7	19.7	0.2	0.07	59.9	1.8	0.14
	8	14.1	0.1	1.34	58.7	0.1	0.14
8	6	34.1	0.2	0.00	59.0	-0.6	0.00
	7	21.7	2.2	0.21	59.4	1.3	0.21
	8	16.0	2.1	1.13	58.7	0.1	0.78
1	6	36.7	2.8	0.35	59.1	-0.5	0.14
	7	27.7	8.2	0.64	57.8	-0.3	0.28
	8	19.3	5.4	0.21	58.9	0.3	0.49
2	6	38.1	4.2	0.00	60.2	0.6	1.48
	7	26.5	7.0	0.64	58.2	0.1	0.28
	8	21.7	7.8	0.49	58.6	-0.1	0.64
3	6	37.7	3.8	0.71	58.2	-1.5	0.07
	7	25.7	6.2	0.64	57.7	-0.4	0.78
	8	18.4	4.5	1.91	58.4	-0.3	0.07
4	6	36.3	2.4	0.28	58.1	-1.6	0.07
	7	24.1	4.6	0.00	58.5	0.3	0.49
	8	19.9	6.0	0.07	58.6	0.0	0.71
7	6	38.0	4.1	1.20	57.6	-2.0	0.71
	7	28.7	9.2	0.42	58.6	0.4	0.49
	8	24.2	10.3	0.14	58.7	0.1	0.42
5	6	40.0	6.1	1.27	58.2	-1.4	0.85
	7	29.7	10.2	0.00	58.2	0.1	0.07
	8	23.4	9.5	0.21	58.6	-0.1	0.49
6	6	38.8	4.9	0.35	58.6	-1.1	0.78
	7	27.1	7.6	0.07	58.1	-0.1	0.07
	8	19.2	5.3	1.34	57.6	-1.0	0.71

10GC-T (1 μM) with and without the presence of compounds 1-9 (10 μM) in 10 mM sodium cacodylate and 100 mM NaCl.

Varying Salt Competition

In addition to variations in pHs, cells can vary in their salt concentration. Positive metal ions like K^+ and Na^+ bind the backbone of DNA to counteract its negative charge. In this section we will compare the derivatives' ability to bind the triplex when there is more or less salt competition.

Using the polynucleotide DNA triplex, salt concentrations were varied from 50 mM to 250 mM of KCl (Figure 4-2). Linearly related, as the concentration of K^+ increased so did the triplex stability. At 50 mM KCl, poly(dA)●2poly(dT) denatured below room temperature at 7.5 ˚C, represented in Figure 4-1. Using 150 mM KCl and 250 mM KCl the $T_{m\ 3 \to 2}$s were (35.3 ± 1.0) ˚C and (48.0 ± 0.0) ˚C, respectively. With the addition of 8 and 9, the stability stayed consistent with the host triplex except in low salt conditions. At 50 mM KCl, compounds 8 and 9 stabilized the triplex by 15.1 and 9.1 ˚C, respectively, indicating the flavonoid backbone and tetra methoxy groups play a role in the ligand-DNA binding. When complexed with compounds 1-4 at K^+ concentrations of 150 and 250 mM the stability trend was $1 > 2 > 3 > 4$, following our previously determined trend. Note, the degree of triplex stabilization was smaller at higher salt concentration (250 mM) because of the increased competition between the K^+ and the R-group. When there is less competition with the salt the trend resulted as $2 > 3 = 4 > 1$. When there is less crowding around the binding pocket from the salt, the diethylamino (1) R-group is too small and cannot efficiently pack into the pocket.

Examining compounds 5, 6, and 7, it can be concluded that 5 and 7 have a better stabilization effect for the polynucleotide triplex regardless of changes in salt concentration. However, similar to compound 1, compound 7 lost potency at low salt concertation compared to 5. This can be explained similarly that under reduced crowding conditions the pyrrolidine (7) R-

group cannot effectively fill the binding pocket. Additionally, as previously stated, it can be
assumed the piperazine (6) R-group provides too much steric hindrance for an effective fit into
the binding pocket and therefore was weaker compared to 5 and 7.

**Figure 4-2**

The Effect of Salinity on Triplex Stabilization
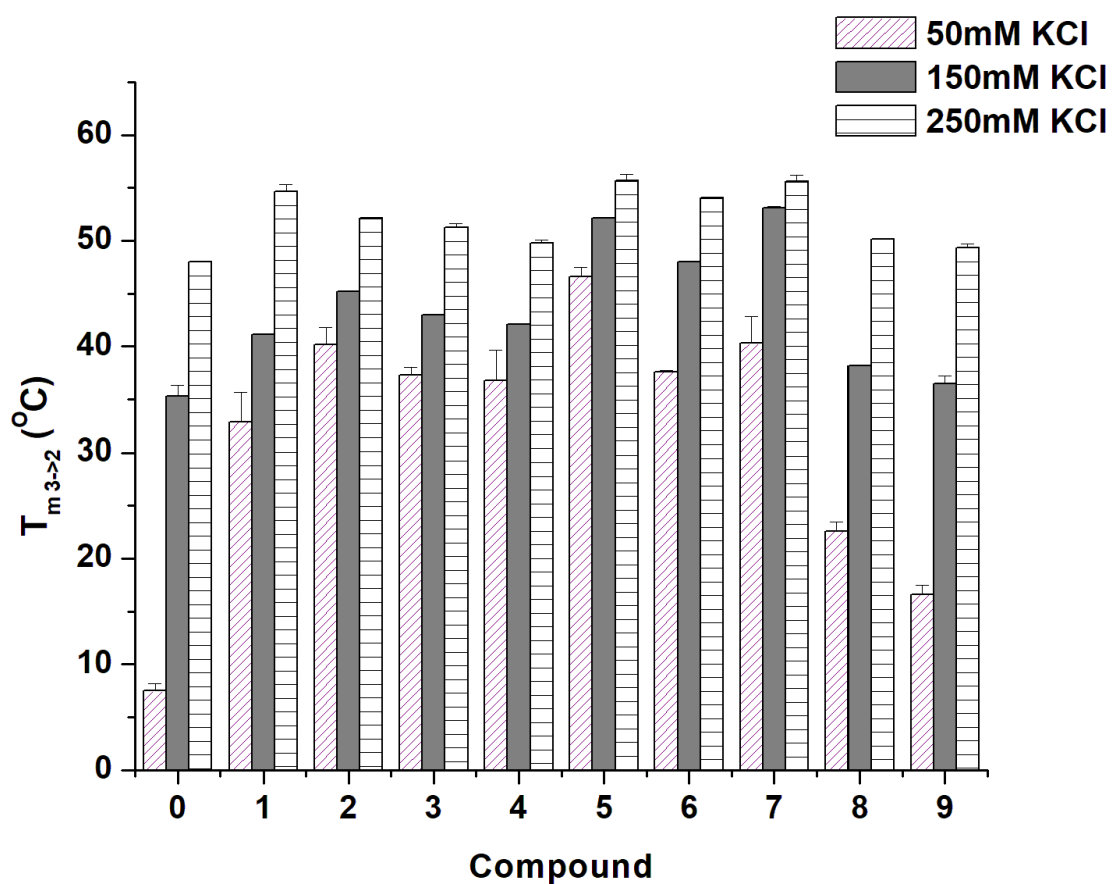
[15 µM/ base triplet] of poly(dA)•2poly(dT) triplex (0) and compounds 1-9 (10 µM) under different KCl
concentrations. Error bars obtained by the average of duplicate trials.

Figure 4-3 shows the change in melting temperature upon complexation of compounds 1-9 with 15GC-T at 25, 100, and 200 mM NaCl. Similar to the polynucleotide triplex, the stability of 15GC-T increased as the concentration of Na^+ increased. Therefore, due to more competition, the degree of stabilization upon ligand binding decreased. At 25 mM NaCl, the strongest stabilization effect came from binding compound 5 followed by 7 then 2. This is consistent with the data from $poly(dA) \bullet 2poly(dT)$. Also consistent was the trend of $2 > 3 > 4 > 1$ for the dialkylamines and $5 > 7 > 6$ for the cyclic amines for all salinity conditions. Tetramethoxyquercetin (8) provided a 5.6 ˚C stabilization and quercetin (9) provided a nominal 1.7 ˚C stabilization. Compounds 8 and 9 provided even less stabilization at 100- and 200-mM Na^+ and were considered to have no effect. In the presence of 200 mM NaCl, the stabilization effect of compounds 1, 2, 3, 4, and 6 diminished to less than 5 ˚C. They increase the triplex stabilization by 1.6 ˚C, 2.7 ˚C, 1.7 ˚C, 2.5 ˚C, and 2.7 ˚C, respectively, and were determined to have no effect. Under high salt competition, 5 and 7 had equal strength improving the melting temperature by 5 ˚C.

Figure 4-3

15GC-T Stability Changes as a Result of Ligand-Ion Competition
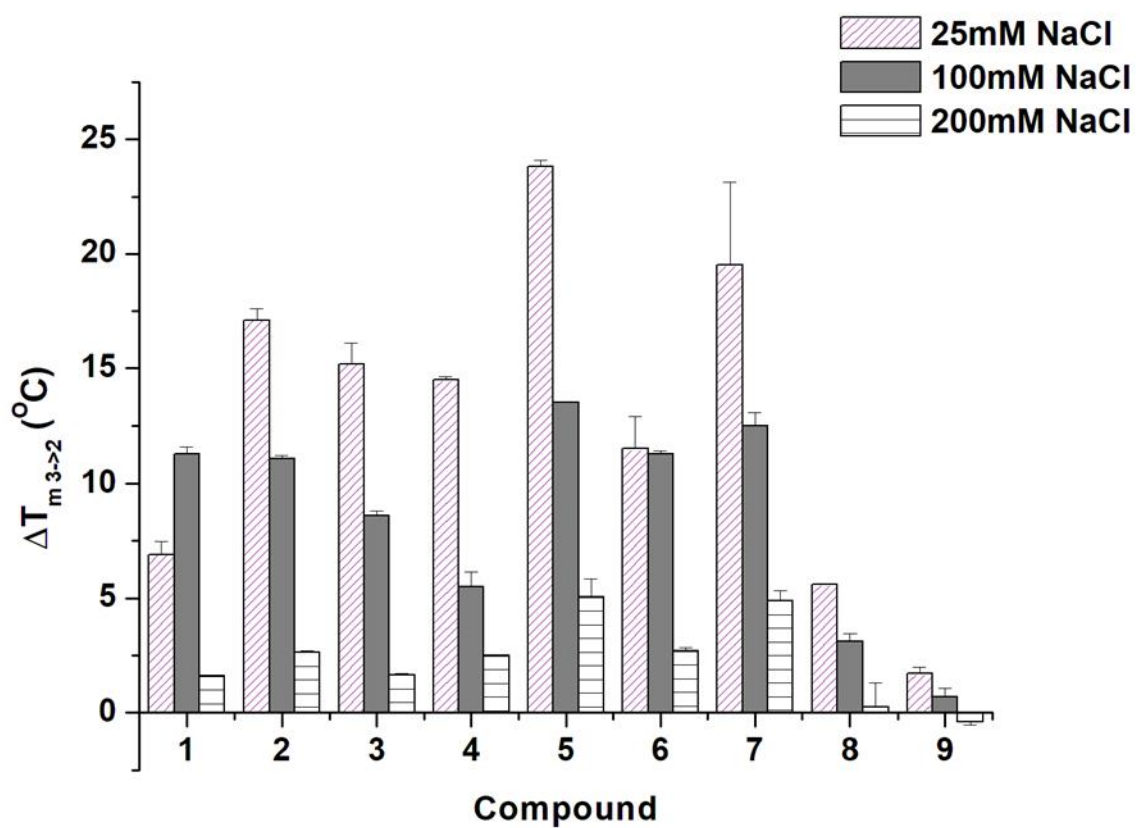
The difference in melting temperature as a result of ligands 1-9 (10 μM) binding 15GC-T (1 μM) under different

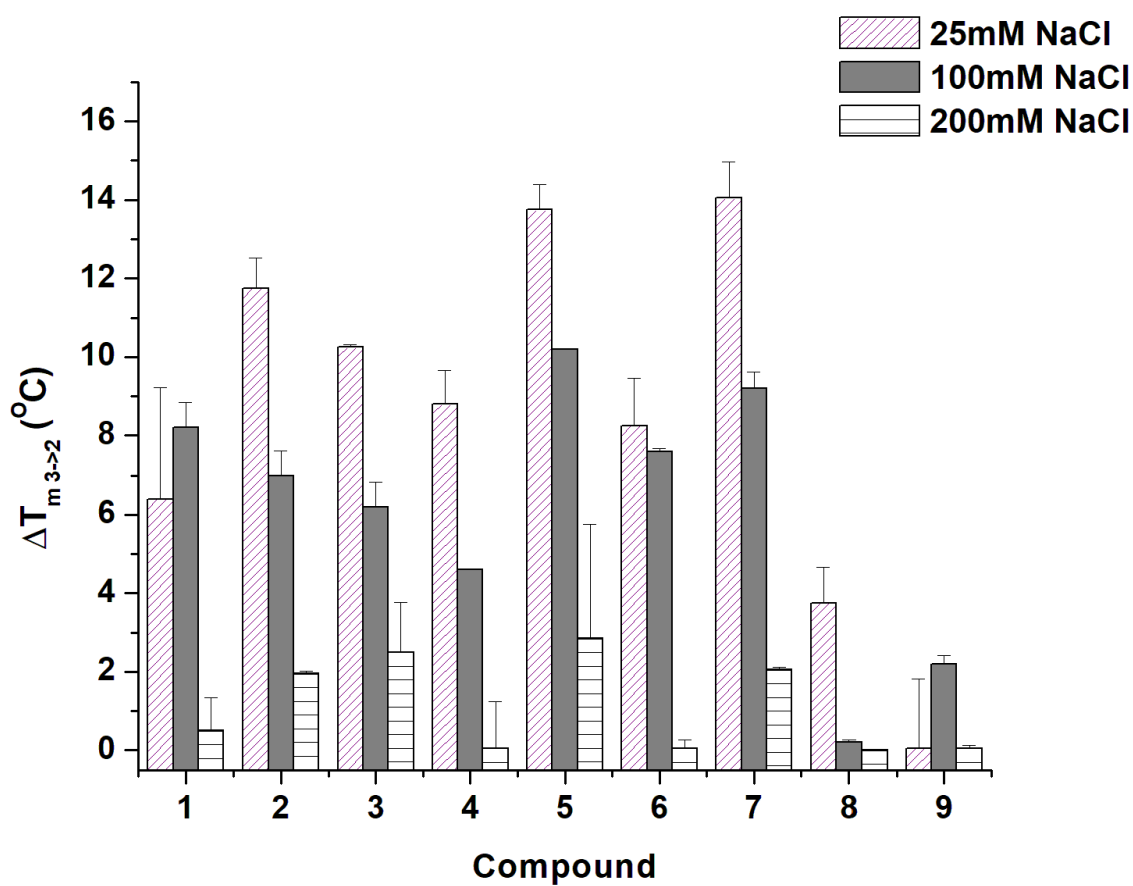NaCl concentrations. Error bars obtained by the average of duplicate trials.

Compound 7 was used as a representative ligand to investigate its ability to bind 15GC-T without the presence of salt. First, the triplex was formed in two ways. Way one was mixing 0 or 10 µM of ligand in 1 µM of DNA, 10 mM sodium cacodylate pH 7, and water (no salt) then completely denaturing the solution by holding the solution temperature at 95 ˚C and allowing it to slowly cool to room temp before storage at 4 ˚C. The second way was considered "no heat." The DNA was first denatured and cooled in water alone before preparing the UV solution. The two solution preparations were to determine if the ligand can promote and stabilize the triplex structure. As seen in Table 4-4, compound 7 can promote triplex formation and stabilize the structure to 13.6 ˚C. This result showed the introduction of the ligand induces triplex formation, even in unfavorable conditions.

Table 4-4

A Representative Look at the Salt and Ligand Competition

Compound	NaCl (mM)	Heat	$T_{m\,3\text{-}>2}$ (˚C)	St.Dev.
15GC-T	0	No	0.0	0.00
	0	Yes	9.4	0.49
	25	Yes	9.1	0.14
	100	Yes	21.0	0.35
	200	Yes	31.1	1.48
7	0	No	13.6	0.42
	0	Yes	19.4	0.14
	25	Yes	30.1	3.65
	100	Yes	33.4	0.42
	200	Yes	37.4	0.42

Furthermore, investigation using 10GC-T was conducted using 25, 100, and 200 mM NaCl. Under 200 mM NaCl conditions, all compounds had less than a 5 ˚C increase in triplex stability. It can be assumed that for smaller intramolecular triplexes, high salt competition blocks access to the binding pocket. Opposingly, low Na^+ conditions (25 mM) allowed best for the cyclic amino compounds 5 and 7 to effectively stabilize the triplex, followed by the dipropylamnio compound 2. Similar to the previous dialkylamino stabilization order, the effective stabilization order was 2 > 3 > 4 > 1 in low salinity conditions. This confirmed compound 1 is too small to snugly fit into the binding pocket on its own. The cyclic amino tertiary groups are effective in the order of 5 = 7 > 6. Keeping in mind the binding pocket is smaller because of 10GC-T being a shorter sequence, 6 is too bulky to provide as significant stabilization as compounds 5 and 7 under any ion conditions.

Figure 4-4

Ionic and Ligand Competition for the 10GC-T Backbone

The change of 10GC-T (1 μM) stability in the presence of compounds 1-9 (10 μM) under different NaCl

concentrations. Error bars obtained by the average of duplicate trials.

Mimic Cell Crowding

Polyethylene glycol (PEG) is a polymer often used to study solution crowding effects. The stability of the poly(dA)●2poly(dT) triplex with and without the presence of compounds 1-9 was tested in the presence of 1-20% PEG200. The results are shown in Figure 4-4. Based on the excluded-volume contributions, the denaturation of the initial state (triplex) would result in a volume increase (random coil) which in the presence of PEG will exclude significant volume. Therefore, the initial state would be stabilized in the presence of molecules which occupy significant volume (PEG). [114] It was then expected and shown for poly(dA)●2poly(dT) to have an increased stabilization in the presence of PEG with a linear relation to PEG concentration. In the presence of compounds with little to no effect (8, 9, 3, and 4) the stability of the polynucleotide tripled at pH 7. However, compounds with significant effects on triplex stability lost potency in the presence of PEG200. Compounds 1, 5, 6, and 7 were dramatically affected by the addition of 1% PEG, but compounds 5 and 7 still had the most significant stabilization effect with $\Delta T_{m\,3 \to 2}$ of 11.6 ˚C and 10.9 ˚C. As the percentage of PEG200 increased, the significance of the stabilization effect of all derivatives decreased for two reasons. One, the stability of poly(dA)●2poly(dT) increases and two, there is increased crowding and competition possibly getting in the way of ligand binding. One report noted that low-molecular mass PEGs may weaken ligand affinity but high molecular mass PEGs may increase ligand affinity. [115]

Figure 4-5 shows the results of using a high molecular weight polyethylene glycol, PEG4000. Upon adding 1% PEG4000, the $\Delta T_{m\,3 \to 2}$ did decrease for compounds 5 and 7, but not to the same degree as PEG200. The $\Delta T_{m\,3 \to 2}$s of 5 and 7 in the presence of 1% PEG4000 were 13.1 ˚C and 15.1 ˚C, respectively. Using the higher molecular weight PEG allowed for a greater degree of stabilization than the lower molecular weight PEG. However, similar to the PEG200,

as the percentage of PEG4000 increased, the $\Delta T_{m\,3\rightarrow2}$s decreased because the stability of

poly(dA)•2poly(dT) alone improved. At 20% PEG4000 there was no difference in stability

upon adding any derivative. The $T_{m\,3\rightarrow2}$s ranged from 54.0 ˚C to 55 ˚C with 20% PEG4000. It

can be concluded that PEG exerts a multipart chemical and steric effect within solution.
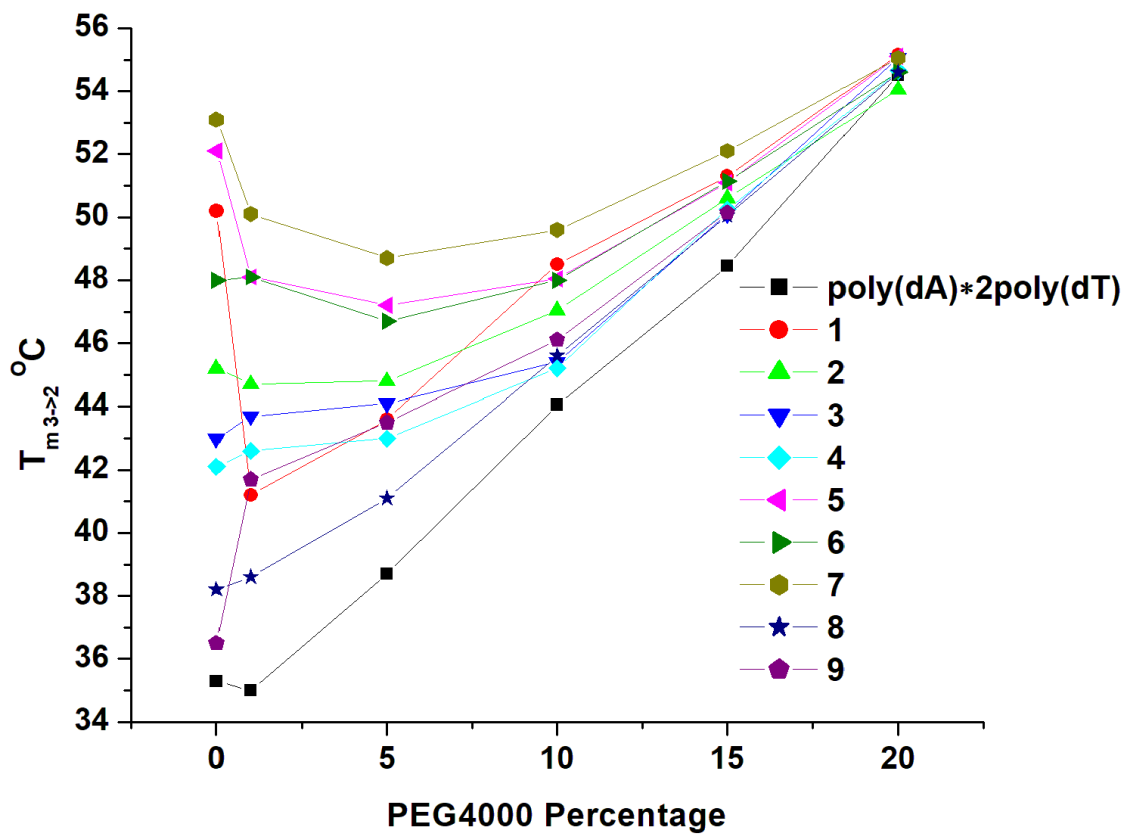
Figure 4-4

Effect of PEG200 on Triplex and Triplex-Ligand Stability
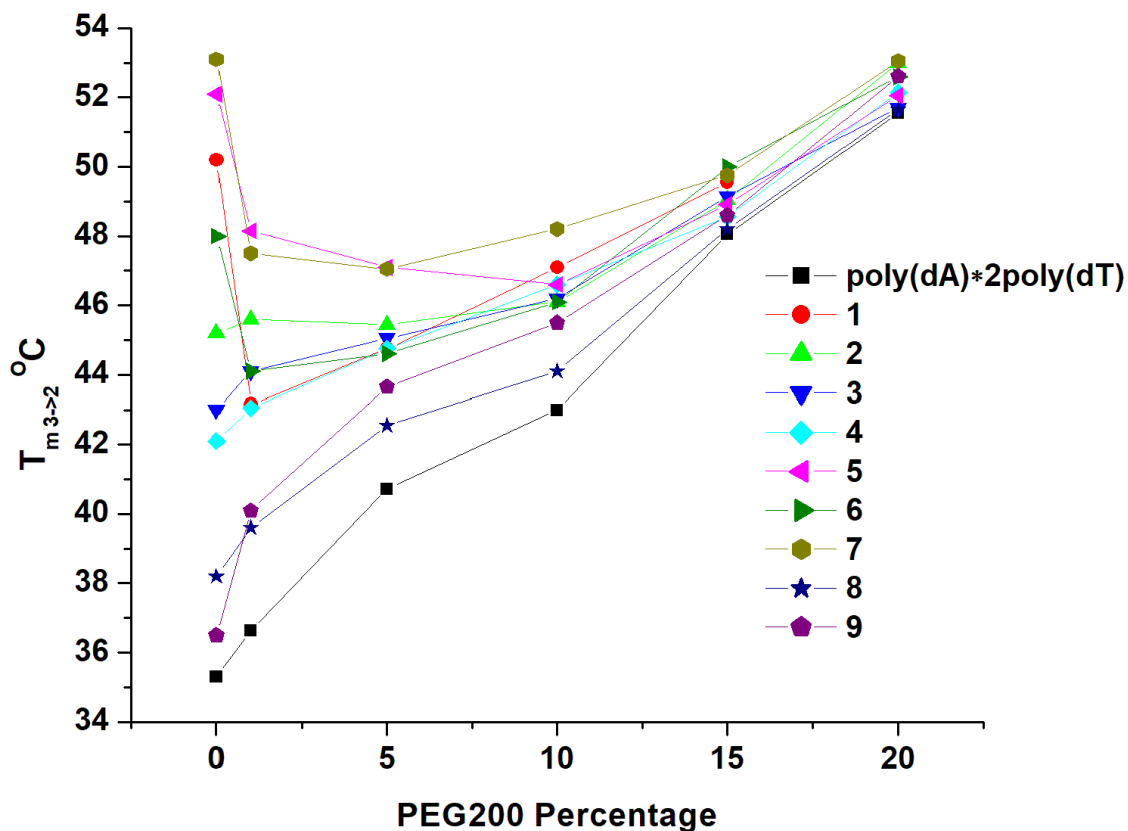
Melting temperatures of poly(dA)•2poly(dT) (15 µM/ base triplet) alone and in the presence of compounds 1-9 (10

µM) as a function of percent polyethylene glycol. Buffer conditions: 10 mM sodium cacodylate pH 7, 150 mM

KCl, and 100 µM EDTA.

Figure 4-5

Effect of PEG4000 on Triplex and Triplex-Ligand Stability

Melting temperatures of poly(dA)●2poly(dT) (15 μM/ base triplet) alone and in the presence of compounds 1-9 (10 μM) as a function of percent polyethylene glycol 4000. Buffer conditions were 10 mM sodium cacodylate pH 7, 150 mM KCl, and 100 μM EDTA.

Conclusion

By varying the ionic concentration of both NaCl and KCl, the results concluded the nitrogen containing R-group competes with the Na^+ and K^+ ions for the negatively charged DNA backbone. These results showed reduced $\Delta T_{m3\rightarrow2}s$ upon binding both the intramolecular and the intermolecular triplex because the stability of the triplex structure increased linearly with ionic concentration due its aid in DNA condensation. [106]

Additionally, the stability of the intramolecular triplexes 15GC-T and 10GC-T increases inversely with pH because of the two flanking $C^+\bullet$G-C triplets. As the pH lowers the amount of cytosine protonation increases allowing for stronger triplex formation. The decrease in pH also increased the partial positive charge on the nitrogen group of compounds 1-7. This increased the attraction for the backbone. The smaller R-groups of the two categories, compounds 1 and 7, demonstrated that as pH increased and the nitrogen charge lessened, the structures were too small to effectively fit into the binding pocket of the intramolecular triplexes. Therefore, compounds 2 and 5 are more optimal structures for their respective groups, dialkylamine or cyclic amine.

PEG crowding studies used to mimic the intracellular space, demonstrated the excluded-volume effect and increased the stability of the polynucleotide triplex. The higher molecular weight PEG did not exhibit as much steric hindrance and interfere with DNA-ligand binding to the same extent as PEG200. Overall, within an intracellular solution mimic, the greatest stability was still provided by the cyclic amine R-group derivatives. The stability order was 7 > 5 > 6, which further concludes a smaller amino ring provides the best stabilization.

CHAPTER 5: THE EFFECTS ON BINDING WHEN VARYING THE 5-SUBSTITUTED 3, 3',

4', 7-TETRAMETHOXYQUERCETIN LINKER LENGTHS

This chapter describes the investigation of varying the linker length of the 3, 3', 4', 7-tetramethoxyquercetin derivatives to understand the effects on binding. Using UV-Vis thermal denaturation, derivatives with either a 3- carbon or 5-carbon linker were examined on their ability to stabilize a polynucleotide intermolecular triplex or two short intramolecular triplexes. It was determined a shorter linker is beneficial for binding. Additionally, despite variation in linker length, cyclic amino R-groups are consistently better at stabilizing the triplex structure. Variation in linker length had no effect on the stability of the duplex DNA. Finally, all compounds were investigated using poly(rA)●2poly(rU) to determine the selectivity of the derivatives. All compounds had no significant stabilization effect in the presence of the RNA indicating the compounds are DNA selective.
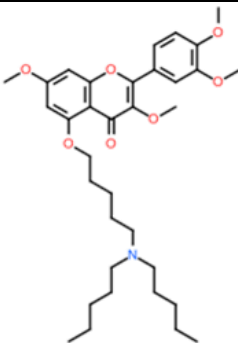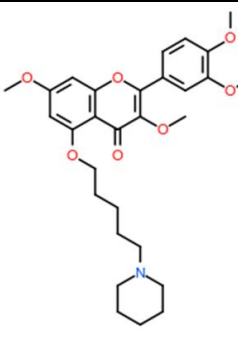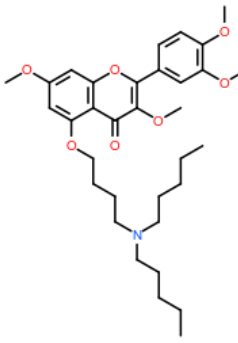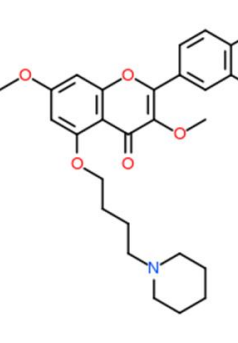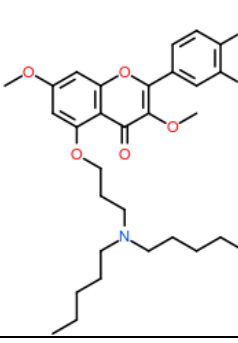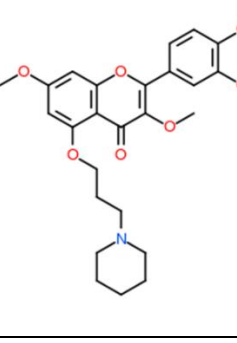
Introduction

There are a number of factors to consider in the field of drug discovery and development. Mainly the "rule of 5" to estimate solubility and permeability of a potential drug and determine its "drug likeness." Most marketed drugs follow the following five rules, molecular weight is under 500, calculated Log P is less than 5, the structure has less than five hydrogen bond donors (HBD), and less than 10 hydrogen bond acceptors (HBA). [116] It is important that a molecule adheres to these rules to allow the necessary solubility for high throughput assays and primary screening. In general, that concentration is 10 μM. [117] Table 5-1 demonstrates how small changes to the structure can drastically change whether or not a compound is considered "drug like." Varying the linker length for compound 4 does not greatly improve the predicted "drug

likeness." This is because the molecular weight and Log P value are too large. However, varying the linker length of compound 5 increased the "drug likeness." In this chapter, we will explore how changing the linker length of the derivatives influences their ability to stabilize the triplex structure.

Table 5-1

"Drug Likeness" of the Weakest (4) and Strongest (5) Derivatives

Compound 4	Rule of 5	Compound 5	Rule of 5
	Molecular formula: $C_{34}H_{49}NO_7$ Molecular weight: 583.35 (> 500) Number of HBA: 8 Number of HBD: 0 LogP: 7.87 (> 5)		Molecular formula: $C_{29}H_{37}NO_7$ Molecular weight: 511.26 (> 500) Number of HBA: 8 Number of HBD: 0 LogP: 4.77
	Molecular formula: $C_{33}H_{47}NO_7$ Molecular weight: 569.34 (> 500) Number of HBA: 8 Number of HBD: 0 LogP: 7.37 (> 5)		Molecular formula: $C_{28}H_{35}NO_7$ Molecular weight: 497.24 Number of HBA: 8 Number of HBD: 0 LogP: 4.27
	Molecular formula: $C_{32}H_{45}NO_7$ Molecular weight: 555.32 (> 500) Number of HBA: 8 Number of HBD: 0 LogP: 7.22 (> 5)		Molecular formula: $C_{27}H_{33}NO_7$ Molecular weight: 483.23 Number of HBA: 8 Number of HBD: 0 LogP: 4.13

Values calculated using Molsoft LLC software.

Experimental

Materials and General Methods

All the chemicals were purchased from MilliporeSigma or Fisher Scientific and used

without further purification. DNA oligonucleotides were purchased from Fisher Scientific.

Polynucleotides were purchased from MilliporeSigma. The concentrations of polynucleotide

solutions were determined spectrophotometrically using the following extinction coefficients (in

units of mol of nucleotide/L-1 cm-1): $\varepsilon 265 = 9,000$ for poly(dT), $\varepsilon 260 = 6,000$ for

poly(dA)●poly(dT), $\varepsilon 260 = 9,350$ for poly(rU), and $\varepsilon 260 = 7,140$ for poly(rA)●poly(rU). The

concentrations of DNA solutions were determined spectrophotometrically, using the molar

extinction coefficients (in units of mol of strand/L-1 cm-1) obtained from OligoAnalyzer

(www.idtdna.com). $\varepsilon 260 = 483,700$ for 15GC-T (5'-GAAAAAAAA

AAAAAGTTTTCTTTTTTTTTTTTTCTTTTCTTTTTTTTTTTTC-3'); $\varepsilon 260 = 342,700$ for

10GC-T (5'- GAAAAAAAAGTTTTCTTTTTTTTTCTTTTCTTTTTTTTC-3'); UV spectra were

recorded on a Varian Cary 100 Bio UV-Vis spectrophotometer equipped with a

thermoelectrically controlled 6×6 cell holder.

Thermal Denaturation of poly(dA)●2poly(dT) Monitored by UV

The UV thermal denaturation samples (1 mL) were prepared by mixing

poly(dA)●poly(dT) (15 µM/base triplet), poly(dT) (15 µM/base triplet) in the presence and

absence of a ligand (1-9, 10 µM) in a sodium cacodylate buffer (10 mM), KCl (50, 150, or 250

mM), pH 6.0, 7.0, or 8.0. The UV melting spectra were recorded in 1 cm path length quartz

cuvettes at 260 nm, 280 nm, and 284 nm, as a function of temperature (25-90 °C, heating rate:

0.2 °C/min). Melting temperatures (T_ms) were determined using the first derivative method. All

experiments were carried out in duplicate.

Thermal Denaturation of poly(rA)●2poly(rU) Monitored by UV

The UV thermal denaturation samples (1 mL) were prepared by mixing poly(rA)●poly(rU) (15 µM/base triplet), poly(rU) (15 µM/base triplet) in the presence and absence of a ligand (1-9, 10 µM) in a sodium cacodylate buffer (10 mM), NaCl (25 mM), 0.1 mM EDTA, pH 6.8. The UV melting spectra were recorded in 1 cm path length quartz cuvettes at 260 nm, 280 nm, 284 nm, and 287 nm as a function of temperature (25-90 °C, heating rate: 0.2 °C/min). Melting temperatures (T_ms) were determined using the first derivative method. All experiments were carried out in duplicate.

Thermal Denaturation of Intramolecular Triplex Monitored by UV

The UV thermal denaturation samples (1 mL) were prepared by mixing 15GC-T or 10GC-T (1 µM) in the presence and absence of a ligand (1-9, 10 µM) in a sodium cacodylate buffer (10 mM), NaCl (25, 100, or 200 mM) at pH 6.0, 7.0, or 8.0. The UV melting spectra were recorded in 1 cm path length quartz cuvettes at 260 nm, 280 nm, and 284 nm, as a function of temperature (5-90 °C, heating rate: 0.2 °C/min). Melting temperatures (T_ms) were determined using the first derivative method. All experiments were carried out in duplicate.

Preparation of 15GC-T for ITC

Stock solution of 15-GCT was first dialyzed in 500 mL buffer solution for 6 h and then further dialyzed in a fresh 500 mL buffer solution overnight at room temperature. The concentrations of both DNA solutions after dialysis were determined by UV. 15GC-T (10 µM) was mixed in a 10 mM sodium cacodylate buffer and 100 mM NaCl at pH 7, heated to 95 °C for 5 min, slowly cooled down to room temperature, and stored at 4 °C overnight.

Isothermal Titration Calorimetry (ITC)

In a typical experiment, 5 µL aliquots of a ligand (100 µM, 7 C3-linker) were injected from a 264 µL rotating syringe into an isothermal sample cell containing 185 µL of 15-GCT (10 µM) at 15 °C. The corresponding control experiment was carried out by injecting 5 µL aliquots of a ligand (100 µM, 7 C3-linker) into a solution of buffer alone. The syringe rotational speed was 125 rpm. The duration of each injection was 4 s, and the delay between injections was 300 s. The initial baseline was collected for 100 s before the first injection. A heat burst curve (microjoules per second vs. seconds) was generated from each injection. The area under each curve was calculated using the NanoAnalyzer software (Version 3.8.0) to yield a measure of the heat associated with that injection. The heat of ligand binding to DNA associated with that injection was obtained by subtracting the heat associated with each ligand-buffer injection from the corresponding heat associated with each ligand-DNA injection. The buffer condition used in ITC experiments: 10 mM sodium cacodylate buffer, 100 mM NaCl, pH 7.0.

Results and Discussion

Polynucleotide Triplex Stabilization

Figure 5-1 shows the structures of the 3, 3', 4', 7-tertamethoxyquercetin derivatives. As previously stated there are two variables that may affect binding, the R-group and linker length. All previously discussed studies were conducted with 4-carbon linker length derivatives in order to individually evaluate the significance of the R-groups. Discussed in this chapter is the effect of linker length on the compounds ability to stabilize the triplex structure. Table 5-1 demonstrates the importance of linker length for poly(dA)●2poly(dT) triplex stabilization. Overall, it can be determined that the shorter the linker, the better the stabilization effect is.

Figure 5-2

*Structures of the 3, 3', 4', 7-tertamethoxyquercetin Derivatives with Varying Linker Lengths*
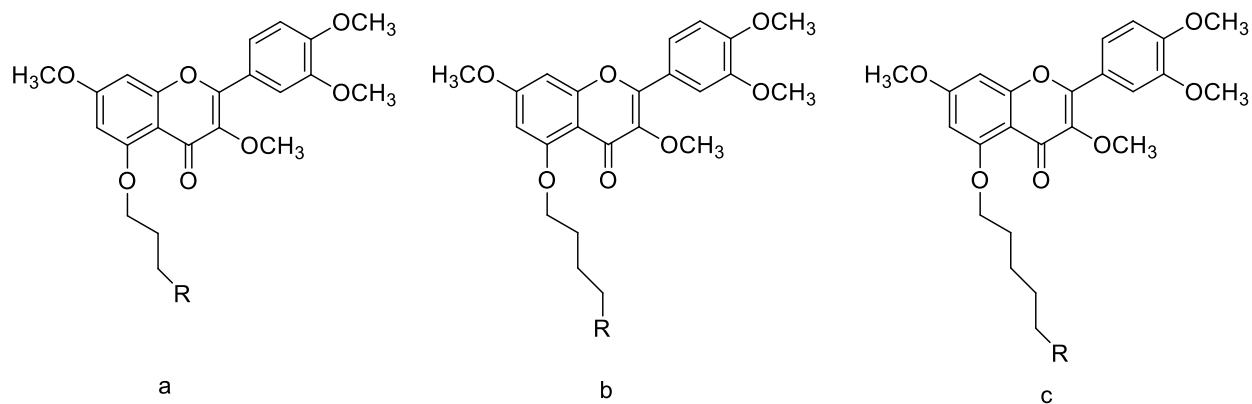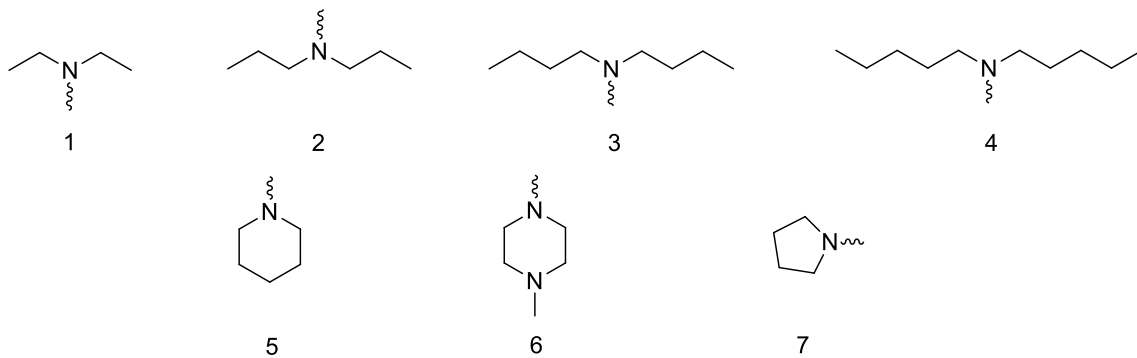
The C3-linker length increased the stabilization effect for all alkyl chain R-group compounds (1-4). The $\Delta T_{m\,3\rightarrow2}$ was significantly increased for 1a and 3a compared to the 1b, 1c, 3b, and 3c derivatives. However, overall, the same general stabilization trend ($1 > 2 > 3 > 4$) was observed ranging from pH 8 to 6. At pH 7, compounds 1a, 1b, and 1c provided an 18.1 ˚C, 15.0 ˚C, and 12.9 ˚C triplex stabilization, respectively. This indicated that a 5-carbon linker is not ideal for the R-group to properly fit into the binding pocket. Across the pH range, the optimal dialkylamine derivative was 1a the 5-diethylamine substituted 3, 3', 4', 7-tetramethoxyquercetin.

Examining the binding of compounds 5-7, the cyclic amino R-groups consistently outperformed the dialkylamines and the C3-linker improved the stabilization effect. At pH 7, the C3-linker did not significantly improve the ligand-induced stabilization effect for 5a ($T_{m\,3\rightarrow2}$ 22.1 ˚C) over compounds 6a and 7a ($T_{m\,3\rightarrow2}$ 20.1 ˚C). At pH 6 however, the stabilization effect order was 6a > 5a > 7a with $\Delta T_{m\,3\text{->}2}$s of 23.4 ˚C, 20.8 ˚C, and 18.9 ˚C, respectively. Interestingly, at pH 6 the piperazine (6a) R-group provided the best stabilization which was not the case for the 6b and 6c derivatives. It can be determined that the shorter linker length allows the two partially positive nitrogen atoms to fit snugly into the binding pocket at pH 6. Despite the results at pH 6, compound 5a, 5- piperidine substituted 3, 3', 4', 7-tetramethoxyquercetin, was the optimal ligand because of its consistency.

Figure 5-2.

*Linker Length Comparison for Stabilizing poly(dA)●2poly(dT)*
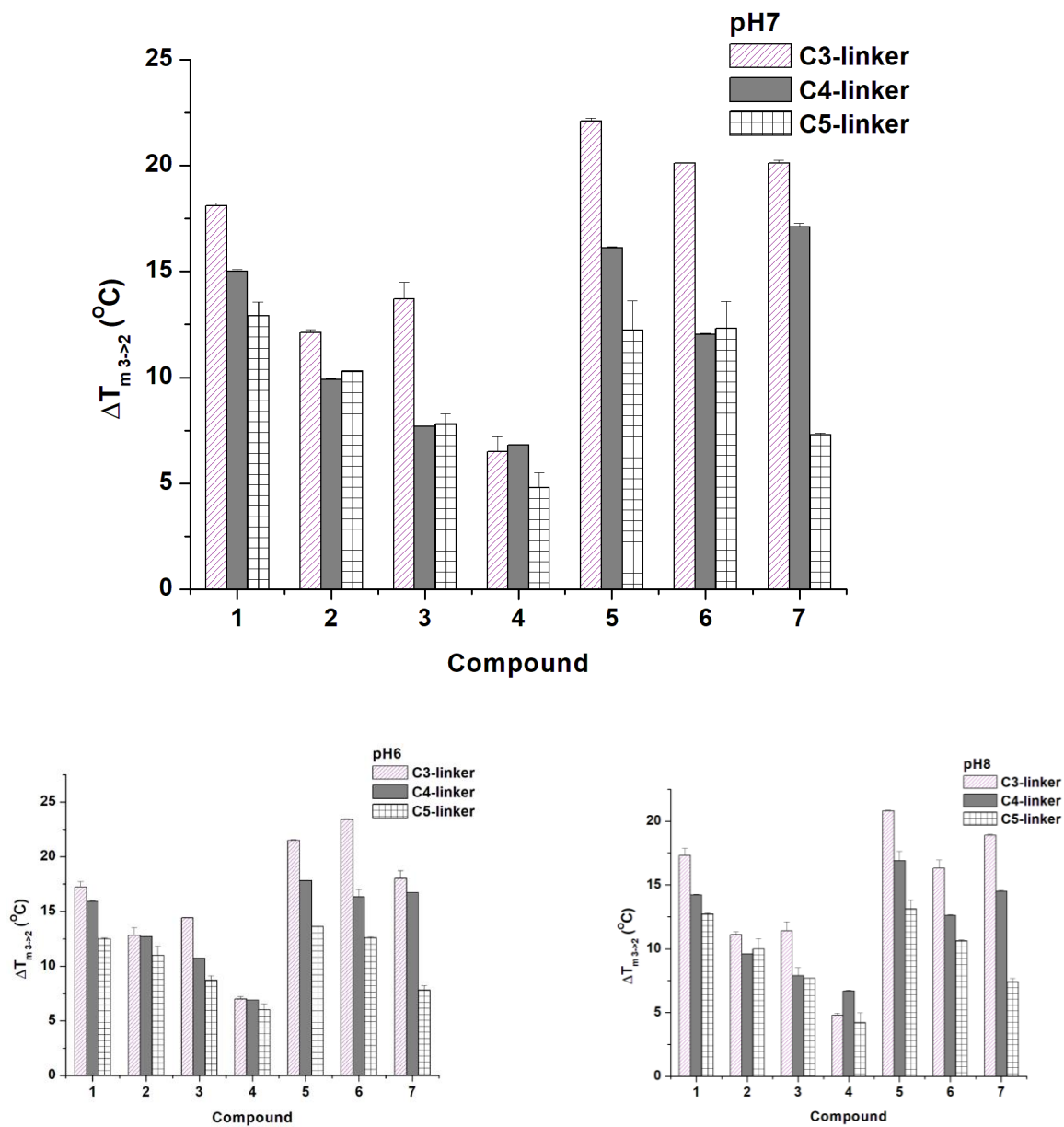
Comparison of linker length as it affects the ligand-induced stabilization of poly(dA)●2poly(dT) (15 μM/base triplet) at different pHs. Experimental conditions: 150 mM KCl, 10 mM sodium cacodylate (pH 6, 7, or 8), and 10 μM ligand.

Figure 5-3 shows representative melting curves for poly(dA)•2poly(dT) in the presence and absence of compounds 5a, 5b, and 5c under three different salt conditions. As shown previously in chapter four, the triplex denatured below room temperature in low salt concentration (50 mM KCl). Poly(dA)•2poly(dT) does form in 150 and 250 mM KCl and dissociates at 35 ˚C and 48 ˚C, respectively. Consistently, the same general trend for the dialkylamine derivatives is the same for all linker variations across the ion concentration range. The smaller the alkyl chain, the better the stabilization effect is. Notice for the diethylamine derivative (1b), the R-group cannot provide a significant stabilization effect for low salt conditions. However, 1a and 1c are able to provide better stabilization. This showed that a four-carbon linker length for the smallest alkyl chain R-group in low salt conditions is unfavorable. The 3-carbon linker improved the potency of all derivatives on stabilizing triplex DNA

The cyclic amine derivatives provided better stabilization across all ionic conditions for the three and four carbon linker derivatives. As the linker lengthened, the significance of containing a cyclic amino group diminished. The extra flexibility prevents the ring from sufficiently packing into the binding pocket. Compound 5a provided the best ligand-induced stabilization effect for 150 mM KCl ($\Delta T_{m\,3\to2}$ 22.1 ˚C) and 250 mM KCl ($\Delta T_{m\,3\to2}$ 11.1 ˚C) concentrations. However, as competition with the ions decreased, the larger piperazine group (6a) was able to efficiently fit into the binding pocket and more effectively stabilize poly(dA)•2poly(dT). Overall, the three carbon linker length derivatives provided the best triplex stabilization in all salinity conditions.

Figure 5-3

Investigation of Linker Length Variation Under Different Ionic Concentrations
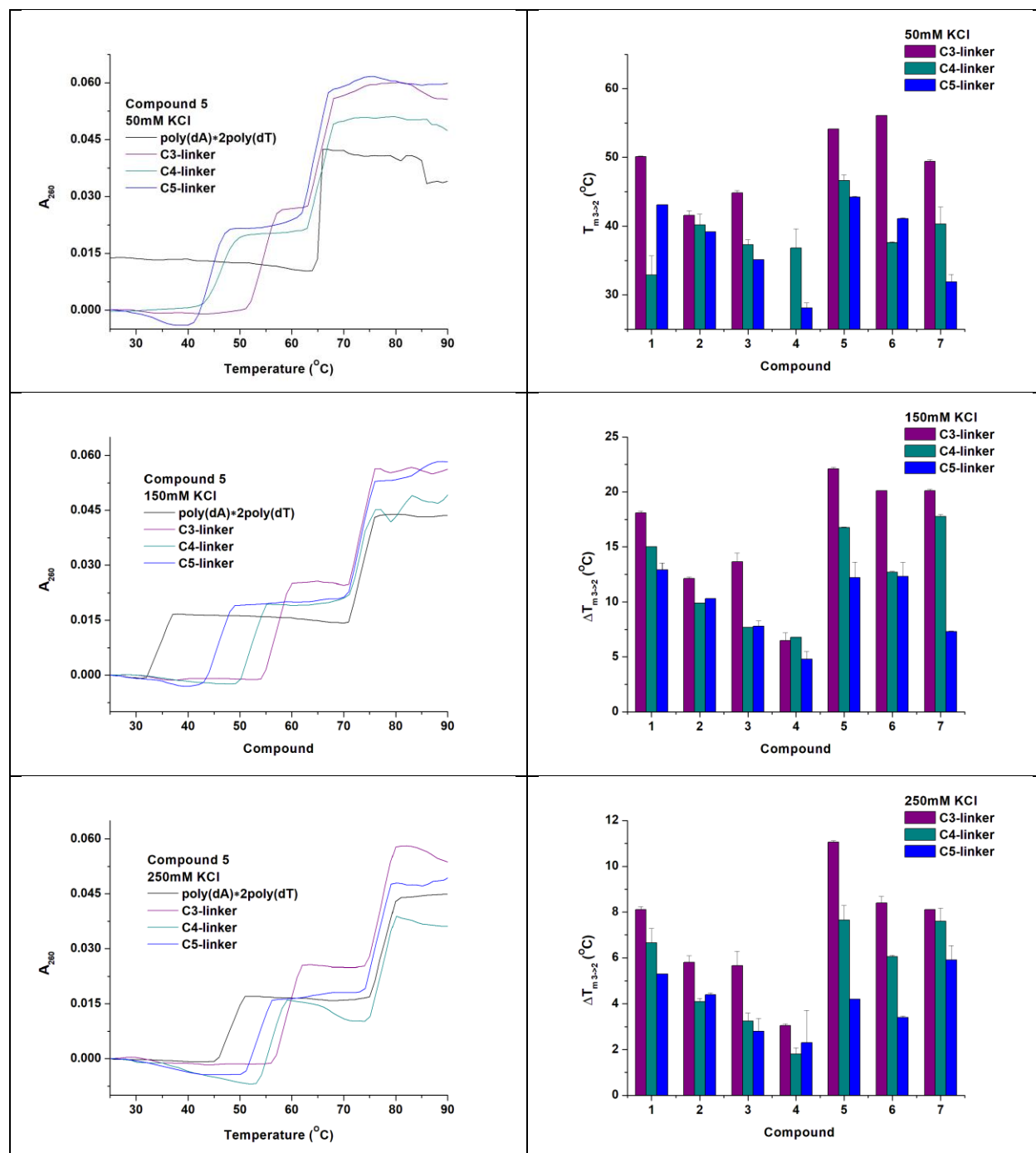
Left: Representative UV-thermal denaturation profiles of poly(dA)•2poly(dT) in 50, 150, or 250 mM KCl. Right: Comparison of $T_{m\,3\to2}$s or $\Delta T_{m\,3\to2}$s in 50, 150, or 250 mM KCl.

Intramolecular Triplex Stabilization

Figure 5-4 compares the stability of the 15GC-T (1 µM) in the presence of compound 1-7 (10 µM) distinguished by their linker length. The data was consistent with the data collected from the polynucleotide intermolecular triplex. However, due to a difference in the size and shape of the binding pocket, compound 6a did not provide the best stabilization under acidic conditions as it did with poly(dA)●2poly(dT). Compound 5a provided the best ligand-induced stabilization effect of all the compounds. It is noteworthy that the thermal stabilization of intramolecular triplex DNA by compounds 5a and 6a is comparable at pH 6.

Figure 5-5 shows the results of comparing all derivatives in 25, 100, and 200 mM NaCl. At 25 mM NaCl, there is very low competition with salt ions and therefore less crowding within the binding pocket. Previously, we have seen compound 1b has a better stabilization effect in a more crowded environment that helps hold the R-group in place. However, with a three or five carbon linker that requirement can be evaded. It can be assumed the C3-linker perfectly aligns the R-group with the binding pocket, whereas, the C5-linker provides the needed flexibility for the diethylamine to properly align with the pocket. Overall, for all linker variations, at 25 mM NaCl the smaller the dialkylamine, the better the stabilization effect is. Interestingly, the three-carbon linker provided a more favorable result for all compounds except for compound 4a, dipentylamine. Different from the polynucleotide triplex, compounds 5, 6, and 7 resulted in a stabilization order of $5 > 6 > 7$ for 15GC-T rather than $6 > 5 > 7$ in low ionic concentration. This can be attributed to the difference in the shape and size of the binding pocket.

For the 100 mM Na^+ concentration, compounds 5a, 6a, 7a, and 1a provided the most significant triplex stabilization upon binding. In general, the C4- and C5-linker derivatives provided similar effects on 15GC-T stabilization; however, compounds 4 and 7 had inverted

trends. The long dipentylamine R-group provided better stabilization as the linker length increased, which directly increased the flexibility. The extra flexibility may allow the larger R-group to more efficiently angle into the binding pocket. Compound 7 inversely benefitted from linker length. The extra flexibility did not allow the smaller pyrrolidine R-group to efficiently pack into the binding pocket.

Finally, with increased ion competition, the overall change in melting temperature lowered because the stability of 15GC-T alone increased. Notice, although the $\Delta T_{m\,3\to2}$ are 5 ˚C and lower, compounds 1c, 2c, and 3c benefit from the extra flexibility when compared to 1b, 2b, and 3b. Still, the C3-linker better positions the R-groups to fit into the binding pocket. The same is shown for compounds 5, 6, and 7. The C3-linker length greatly improved the ligand-induced triplex stabilization. Overall, the piperidine R-group derivative (5a) outperformed all other ligands under all ionic concentrations. The $\Delta T_{m\,3\to2}$s of 5a are 31.2 ˚C, 22.1 ˚C, 12.1 ˚C for 25, 100, and 200 mM NaCl, respectively.

Figure 5-4

Linker Length Comparison for Stabilizing 15GC-T
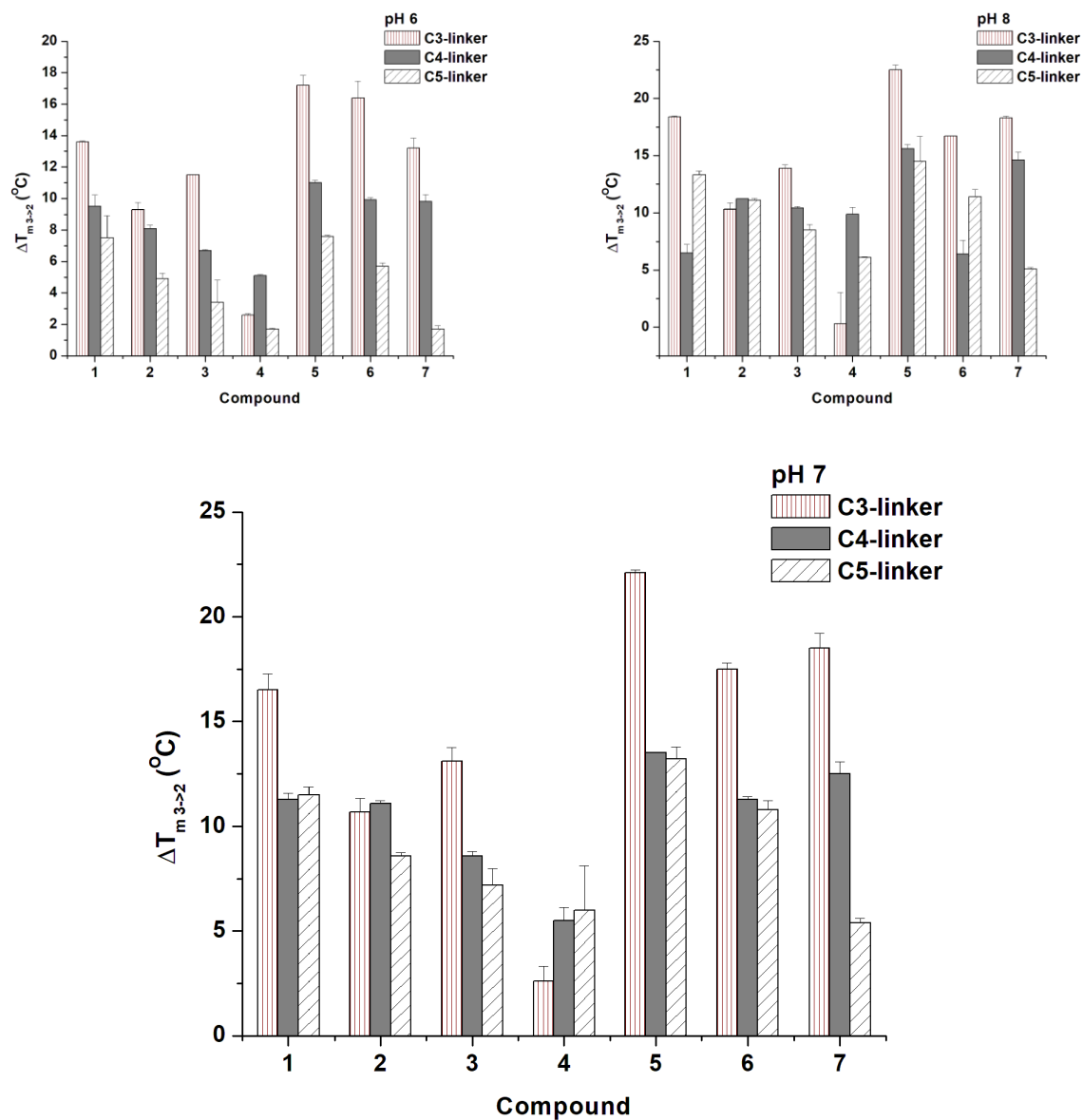
Linker length comparison as it affects the ligand-induced stabilization of 15GC-T in differing pH conditions.

Solution conditions: 100 mM NaCl, 10 mM sodium cacodylate (pH 6, 7, or 8), 1 μM DNA, and 10 μM ligand.

Figure 5-5

Comparing Ligand-Induced Stabilization of 15GC-T While Varying Linker Length and Salinity
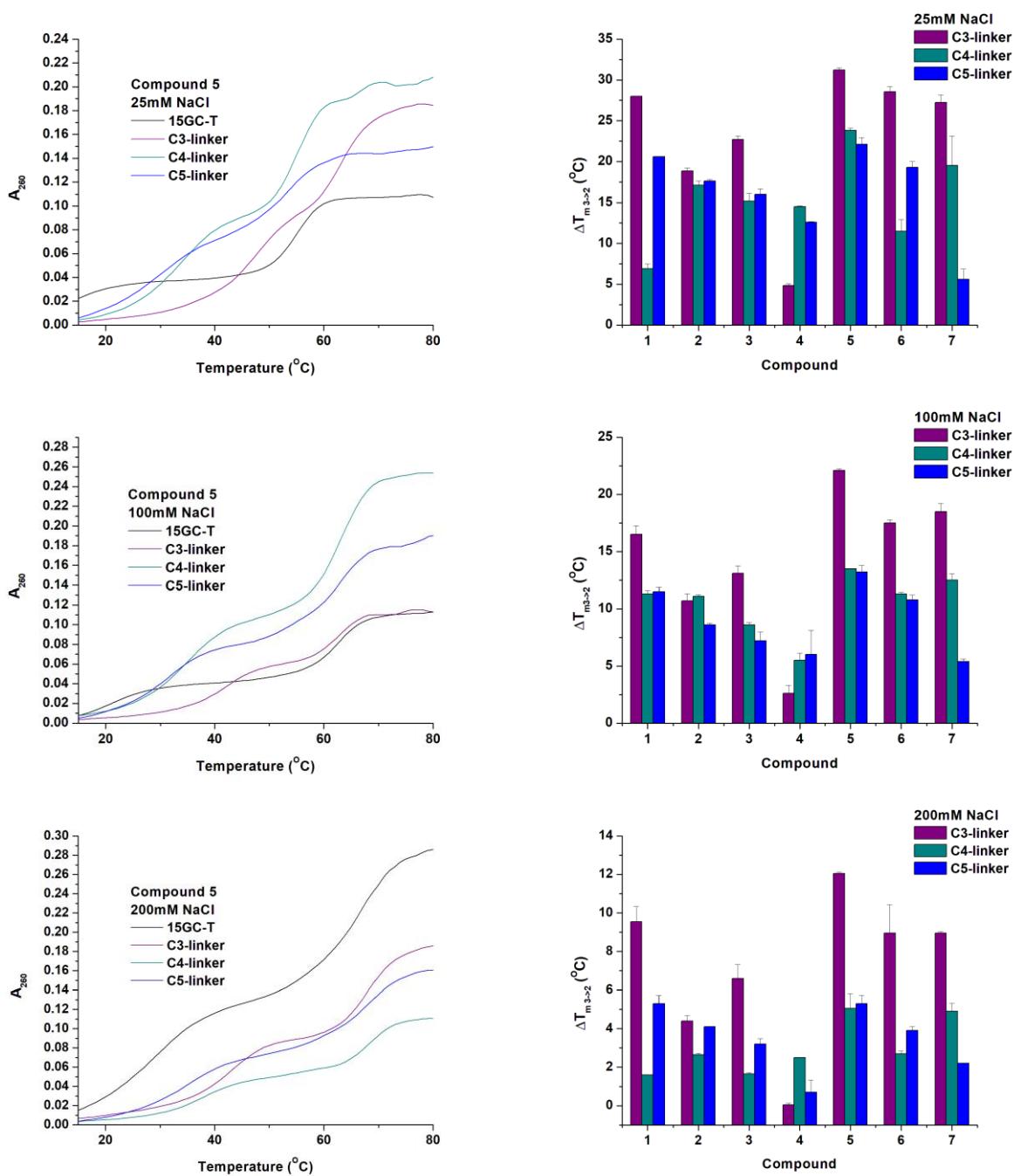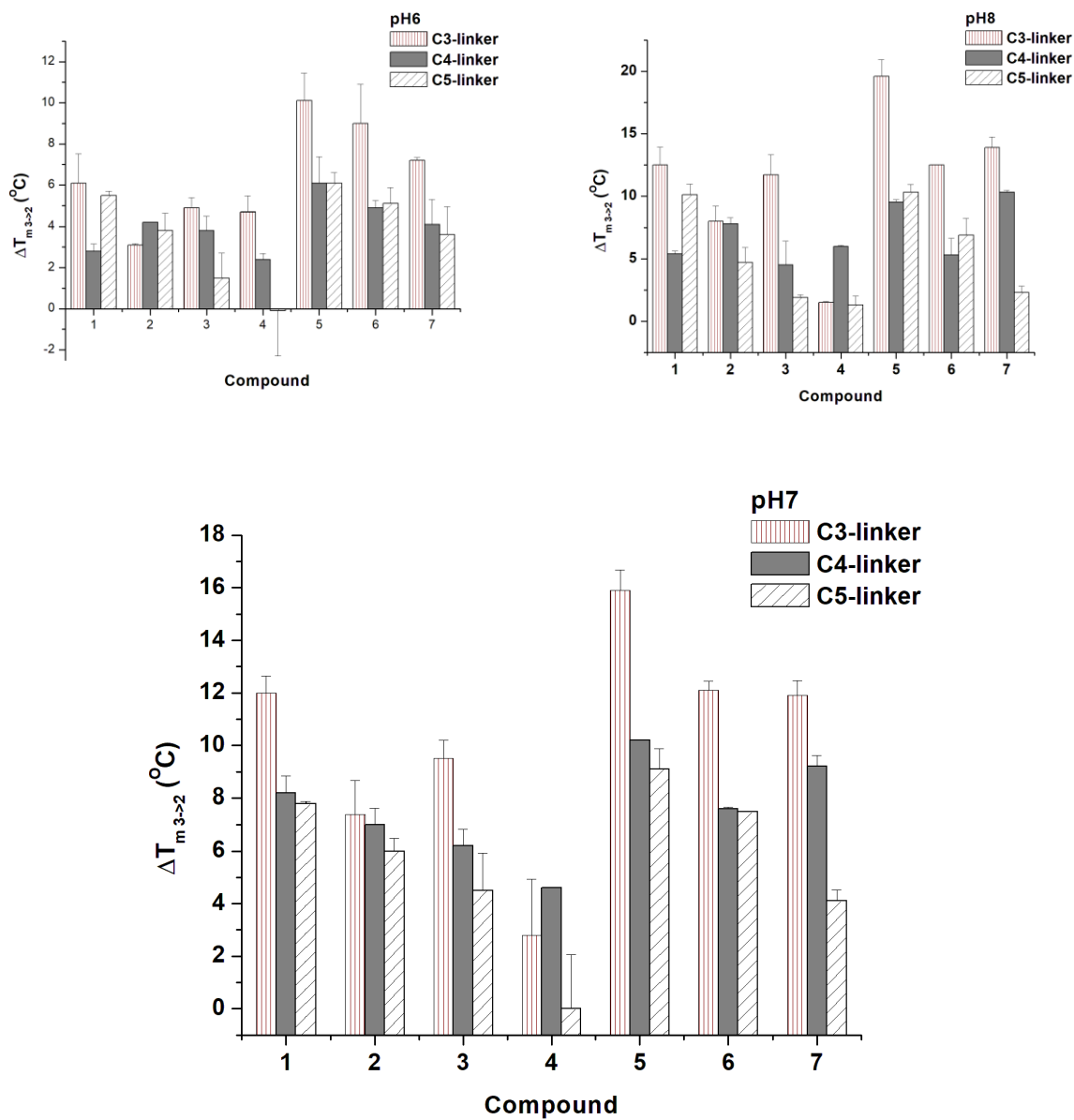

Left: Representative UV-thermal denaturation profiles of 15GC-T in 25, 100, or 200 mM NaCl. Right: Comparison of $\Delta T_{m\ 3\rightarrow2}$s in 25, 100, or 200 mM NaCl.

The thermal dissociation temperatures for 10GC-T at pH 6, 7, and 8 are (35.0 ± 0.0) ˚C, (19.7 ± 0.3) ˚C, and (11.6 ± 0.5) ˚C, respectively. Figure 5-6 shows the change in triplex stability upon binding compounds 1-7 with either a three, four, or five-carbon linker. Cyclic amino R-group derivatives (5a, 6a, and 7a) outperformed the stabilization effect of the four- and five-carbon linker derivatives. Notice, at pH 6 compounds 5b and 5c, 6b and 6c, and 7b, and 7c had relatively the same $\Delta T_{m\,3\to2}s$ 6.1 ˚C for 5; 5.0 ˚C for 6; 4.0 ˚C for 7. Instead, the three-carbon linker improved the ligand-induced triplex stabilization to equal $\Delta T_{m\,3\to2}s$ of (10.1 ± 1.3) ˚C for 5a; (9.0 ± 1.9) ˚C for 6a; (7.2 ± 0.1) ˚C for 7a. At pH6, the piperidine (5a), piperazine (6a), and pyrrolidine (7a) compounds outperform all dialkylchain derivatives. For pH 7 and 8, the compounds that provided the best stabilization were the same as previous data and consisted of only C3-linker derivatives. For pH 8, the order of best stabilization was 5a > 7a > 6a = 1a, which had $\Delta T_{m\,3\to2}s$ equal to (19.6 ± 1.3) ˚C for 5a; (13.9 ± 0.8) ˚C for 7a; (12.5 ± 0.0) ˚C for 6a; (12.5 ± 1.4) ˚C for 1a. At pH 7, the compound order was 5a > 6a = 7a = 1a with $\Delta T_{m\,3\to2}s$ of (15.9 ± 0.8) ˚C, (12.1 ± 0.4) ˚C, (11.9 ± 0.6) ˚C, and (12.0 ± 0.6) ˚C, respectively.

Figure 5-7 displays the results of varying the ion concentration. Consistent with previous data, the piperazine 5-substituted 3, 3', 4', 7-tetramethoxyquercetin (6a) derivative provided an increased stabilization effect under low ionic concentrations (25 mM Na^+). However, continuously the piperidine 5-substituted 3, 3', 4', 7-tetramethoxyquercetin derivative (5a) provided the best stabilization of 10GC-T regardless of ionic concentration. The data presented in Figure 5-6 and Figure 5-7, confirmed that despite changes in triplex length and shape, derivatives with a three-carbon linker provided the best angle for the R-group binding. Compound 5a is the overall lead compound for any future modifications.

Figure 5-6

*Linker Length Comparison for Stabilizing 10GC-T at pH 6, 7, and 8*

Linker length comparison as it affects the ligand-induced stabilization of 10GC-T in differing pH conditions.

Solution conditions: 100 mM NaCl, 10 mM sodium cacodylate (pH 6, 7, or 8), 1 μM DNA, and 10 μM ligand.

Figure 5-7

Comparing Ligand-Induced Stabilization of 10GC-T While Varying Linker Length and Salinity
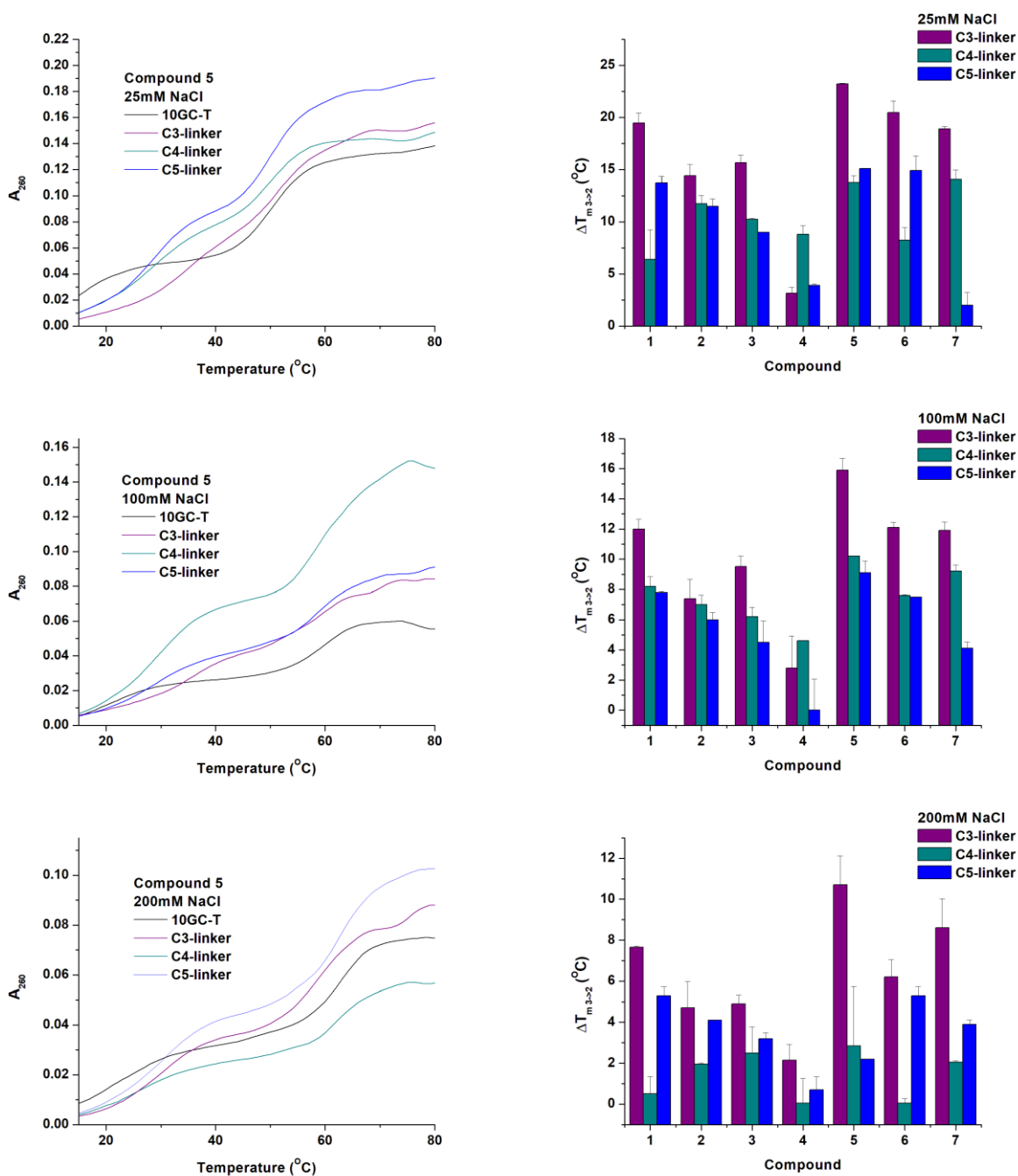
Left: Representative UV-thermal denaturation profiles of 10GC-T in 25, 100, or 200 mM NaCl. Right: Comparison of $\Delta T_{m\,3\rightarrow2}$s in 25, 100, or 200 mM NaCl.

Compound 7a Binds Stronger to Triplex DNA Than Compound 7b Determined by ITC

The isothermal titration calorimetry (ITC) of compound 7a into 15GC-T is shown in

Figure 5-8 and the data is presented in Table 5-2. The binding of 7a is an exothermic event and a

single binding process as seen in the isotherm. The binding stoichiometry obtained suggests

approximately 3 to 4 bound ligands. Table 5-2 also shows the dissociation constant decreased to

about half of 7b's K_d from (31 ± 1.1) μM to (12.1 ± 4.9) μM. The K_d is now equal to that of

neomycin (16 ± 0.6) μM. The increased binding affinity suggests that the 3-carbon linker helps

7a provide a better triplex stabilization effect than compound 7b.

Figure 5-8

ITC of Compound 7a to 15GC-T
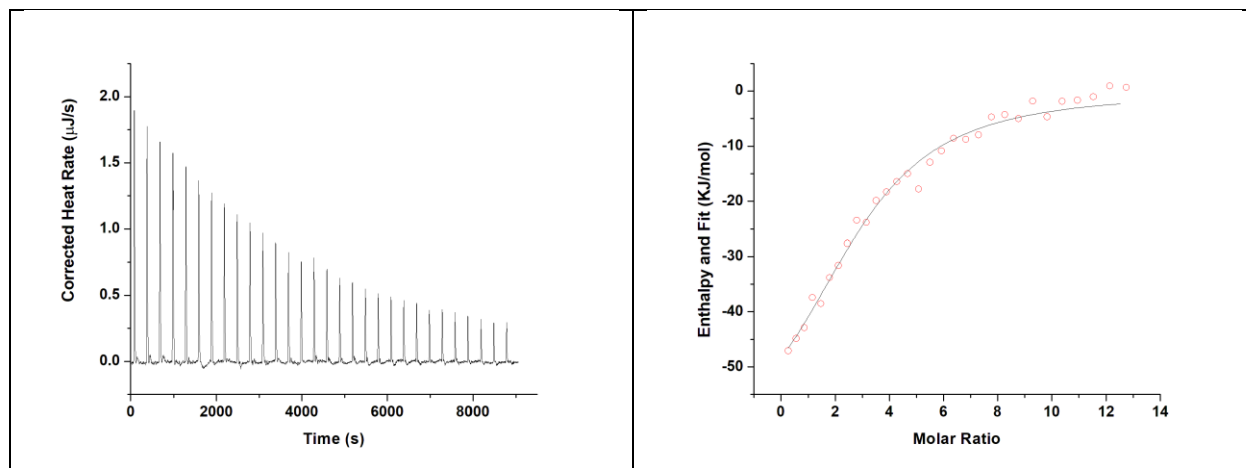
Left: ITC profile of 15GC-T (10 μM) titrated with C3-linker 7 (100 μM) in a 10 mM sodium cacodylate buffer with

100 mM NaCl, pH 7 at 15 ˚C. Right: The dotted line represents the corrected injection heats plotted as a function of

the [7]/[DNA] molar ratio. The smooth solid line reflects the calculated fit of the data using the independent model

from the software NanoAnalyze. Upward peaks represent an exothermic event.

Table 5-2

*Extrapolated ITC Data of Compound 7a to 15GC-T*

Compound	7b	7a
K_d (μM)	31 ± 1.1	12.1 ± 4.9
n	6.0	3.7

Investigation of poly(rA)●2poly(rU) Binding

The change in melting temperature of a polynucleotide RNA triplex, poly(rA)●2poly(rU) (15 μM/base triplet), in the absence and presence of ligands 1-9 (10 μM) at pH 6.8 are shown in Figure 5-9. All melting profiles are biphasic. All compounds showed no effect on the stabilization of the duplex RNA, suggested by the little to no change in melting temperatures of the duplex. The piperazine derivative (6a) had the largest effect on the RNA duplex with an increase of 2.5 ˚C. Compounds 1-7 also did not show a drastic difference in $T_{m\ 3\to2}$ values. At most, compound 5b increased the $T_{m\ 3\to2}$ value by (3.7 ± 1.2) ˚C, indicating a very weak stabilizing effect. Based on these results, it can be determined that compounds 1-9 do not have a stabilization effect on RNA triplex and duplex structures. These derivatives are DNA triplex selective.

Figure 5-9

Poly(rA)●2poly(rU) Triplex $\Delta T_{m\,3\to2}$ and $\Delta T_{m\,2\to1}$ in the Presence of Compounds 1-9
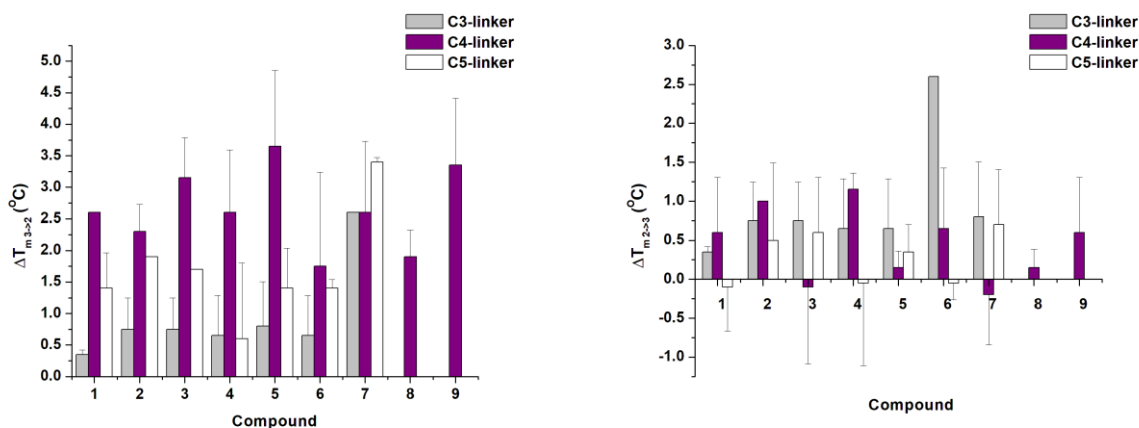
Changes in UV melting temperatures of poly(rA)●2poly(rU) and poly(rA) ●poly(rU) at 260 nm with 10 μM of a ligand (1–9). Each value is an average of duplicated experiments.

Conclusion

In summary, we have discovered a novel class of DNA triplex-specific binding ligands based on the natural product quercetin. The observed enhancement is significant, considering that quercetin alone cannot effectively bind to triplex DNA under experimental conditions. After comparing the effects of the three-, four-, and five-carbon linker lengths, we can conclude the binding affinities of several molecules are comparable (if not better) to the potent triplex binding ligand, neomycin. Two structural trends were observed. First, a smaller nitrogen containing R-group allows for more effective packing into the binding site with a preference for a cyclic amine. Secondly, a shorter linker length allows for better angling of the R-group into the pocket, thereby drastically improving the ligand-induced stabilization effect.

The binding mode of these derivatives was determined to be intercalation, supported by Job's method, ITC, and viscosity measurement. The stoichiometry of the 7a reduced to almost half the amount from the 7b, while having an increased binding affinity. More importantly, this

class of molecules showed to have no effect on duplex DNA, triplex RNA, or duplex RNA. The selectivity for specifically targeting the triplex DNA structure implies the applications for in vivo targeting. The PEG studies in chapter 4 indicate the piperidine and pyrrolidine derivatives can overcome the cell crowding and stabilize the triplex.

The large aromatic surface of quercetin is a promising scaffold for drug development. It is noteworthy that quercetin derivatives can be readily synthesized and modified under mild conditions. The derivatives have small molecular volumes and ideal logP values (<5) to act as "drug-like" candidates. Tethering a side chain to a flavonoid scaffold opens a new direction for designing novel triplex binding ligands for applications in antigene therapy.

References

1. Dahm, R. Friedrich Miescher and the discovery of DNA. *Dev. Biol.* **2005***, 278*, 274-288.

2. Choudhuri, S. The Path from Nuclein to Human Genome: A Brief History of DNA with a Note on Human Genome Sequencing and Its Impact on Future Research in Biology. *Bulletin of Science, Technology & Society* **2003***, 23*, 360-367.

3. Avery, O. T.; MacLeod, C. M.; McCarty, M. Studies on the Chemical Nature of the Substance Inducing Transformation of Pneumococcal Types: Induction of Transformation by a Desoxyribonucleic Acid Fraction Isolated from Pneumococcus Type III. *J. Exp. Med.* **1944***, 79*, 137-158.

4. Watson, J. D.; Crick, F. H. C. Molecular Structure of Nucleic Acids: A Structure for Deoxyribose Nucleic Acid. *Nature* **1953***, 171*, 737-738.

5. Klug, A. Rosalind Franklin and the Discovery of the Structure of DNA. *Nature* **1968***, 219*, 808-810.

6. CRICK, F. Central Dogma of Molecular Biology. *Nature* **1970***, 227*, 561-563.

7. González-Pardo, H.; Pérez Álvarez, M. Epigenetics and its implications for Psychology. *Psicothema* **2013***, 25*, 3-12.

8. Wang, S. Development of Novel Phenanthroline and Thiazole Orange Derived G-quadruplex Ligands and Telomerase Inhibitors, University of the Pacific, 2018.

9. Mauroesguerroto A-DNA, B-DNA, and Z-DNA conformations of DNA. *https://commons.wikimedia.org/wiki/File:Dnaconformations.png*.

10. Wang, L.; Keiderling, T. A. Vibrational circular dichroism studies of the A-to-B conformational transition in DNA. *Biochemistry (Easton)* **1992***, 31*, 10265-10271.

11. Doluca, O.; Withers, J. M.; Filichev, V. V. Molecular Engineering of Guanine-Rich Sequences: Z-DNA, DNA Triplexes, and G-Quadruplexes. *Chem. Rev.* **2013**, *113*, 3044-3083.

12. Mergny, J.; Hélène, C. G-quadruplex DNA: A target for drug design. *Nat. Med.* **1998**, *4*, 1366-1367.

13. Lipps, H. J.; Rhodes, D. G-quadruplex structures: in vivo evidence and function. *Trends Cell Biol.* **2009**, *19*, 414-422.

14. Burge, S.; Parkinson, G. N.; Hazel, P.; Todd, A. K.; Neidle, S. Quadruplex DNA: sequence, topology and structure. *Nucleic Acids Res.* **2006**, *34*, 5402-5415.

15. Brown, S. L.; Kendrick, S. The i-Motif as a Molecular Target: More Than a Complementary DNA Secondary Structure. *Pharmaceuticals (Basel)* **2021**, *14*, 96. doi: 10.3390/ph14020096.

16. Abou Assi, H.; Garavís, M.; González, C.; Damha, M. J. i-Motif DNA: structural features and significance to cell biology. *Nucleic Acids Res.* **2018**, *46*, 8038-8056.

17. Felsenfeld, G.; Rich, A. Studies on the formation of two- and three-stranded polyribonucleotides. *Biochim. Biophys. Acta* **1957**, *26*, 457-468.

18. Hoogsteen, K. The structure of crystals containing a hydrogen-bonded complex of 1-methylthymine and 9-methyladenine. *Acta crystallographica* **1959**, *12*, 822-823.

19. Hoogsteen, K. The crystal and molecular structure of a hydrogen-bonded complex between 1-methylthymine and 9-methyladenine. *Acta crystallographica* **1963**, *16*, 907-916.

20. Radhakrishnan, I.; Patel, D. J. DNA Triplexes: Solution Structures, Hydration Sites, Energetics, Interactions, and Function. *Biochemistry (Easton)* **1994**, *33*, 11405-11416.

21. Beal, P. A.; Dervan, P. B. Second structural motif for recognition of DNA by oligonucleotide-directed triple-helix formation. *Science* **1991***, 251*, 1360-1363.

22. Moser, H. E.; Dervan, P. B. Sequence-specific cleavage of double helical DNA by triple helix formation. *Science* **1987***, 238*, 645-650.

23. Phipps, A. K.; Tarköy, M.; Schultze, P.; Feigon, J. Solution Structure of an Intramolecular DNA Triplex Containing 5-(1-Propynyl)-2'-deoxyuridine Residues in the Third Strand, *Biochemistry (N. Y.)* **1998***, 37*, 5820-5830.

24. Asensio, J. L.; Brown, T.; Lane, A. N. Solution conformation of a parallel DNA triple helix with 5′ and 3′ triplex–duplex junctions. *Structure* **1999***, 7*, 1-11.

25. HOLLAND, J. A.; HANSEN, M. R.; DU, Z.; HOFFMAN, D. W. An examination of coaxial stacking of helical stems in a pseudoknot motif: The gene 32 messenger RNA pseudoknot of bacteriophage T2. *RNA* **1999***, 5*, 257-271.

26. Fire, A.; Xu, S.; Montgomery, M. K.; Kostas, S. A.; Driver, S. E.; Mello, C. C. Potent and specific genetic interference by double-stranded RNA in Caenorhabditis elegans. *Nature* **1998***, 391*, 806-811.

27. Dana, H.; Chalbatani, G. M.; Mahmoodzadeh, H.; Karimloo, R.; Rezaiean, O.; Moradzadeh, A.; Mehmandoost, N.; Moazzen, F.; Mazraeh, A.; Marmari, V.; Ebrahimi, M.; Rashno, M. M.; Abadi, S. J.; Gharagouzlo, E. Molecular Mechanisms and Biological Functions of siRNA. *Int. J. Biomed. Sci.* **2017***, 13*, 48-57.

28. Lu, M.; Zhang, Q.; Deng, M.; Miao, J.; Guo, Y.; Gao, W.; Cui, Q. An Analysis of Human MicroRNA and Disease Associations. *PLOS ONE* **2008***, 3*, e3420.

29. Ambros, V. The functions of animal microRNAs. *Nature* **2004***, 431*, 350-355.

30. Bartel, D. P. MicroRNAs: genomics, biogenesis, mechanism, and function. *Cell* **2004***, 116*, 281-297.

31. Chalk, A. M.; Wahlestedt, C.; Sonnhammer, E. L. Improved and automated prediction of effective siRNA. *Biochem. Biophys. Res. Commun.* **2004***, 319*, 264-274.

32. Birmingham, A.; Anderson, E. M.; Reynolds, A.; Ilsley-Tyree, D.; Leake, D.; Fedorov, Y.; Baskerville, S.; Maksimova, E.; Robinson, K.; Karpilow, J.; Marshall, W. S.; Khvorova, A. Addendum: 3′ UTR seed matches, but not overall identity, are associated with RNAi off-targets. *Nature Methods* **2006***, 3*, 487.

33. Watts, J. K.; Deleavey, G. F.; Damha, M. J. Chemically modified siRNA: tools and applications. *Drug Discov. Today* **2008***, 13*, 842-855.

34. Kim, H.; Miller, D. Inhibition of in Vitro Transcription by a Triplex-Forming Oligonucleotide Targeted to Human c-myc P2 Promoter. *Biochemistry* **1995***, 34*, 8165-8171.

35. Cooney, M.; Czernuszewicz, G.; Postel, E. H.; Flint, S. J.; Hogan, M. E. Site-Specific Oligonucleotide Binding Represses Transcription of the Human c-myc Gene in Vitro. *Science* **1988***, 241*, 456-459.

36. Praseuth, D.; Guieysse, A. L.; Hélène, C. Triple helix formation and the antigene strategy for sequence-specific control of gene expression. *Biochimica et Biophysica Acta (BBA) - Gene Structure and Expression* **1999***, 1489*, 181-206.

37. Noonberg, S. B.; François, J. C.; Praseuth, D.; Guieysse-Peugeot, A. L.; Lacoste, J.; Garestier, T.; Hélène, C. Triplex formation with alpha anomers of purine-rich and pyrimidine-rich oligodeoxynucleotides. *Nucleic Acids Res.* **1995***, 23*, 4042-4049.

38. Thuong, N. T.; Hélène, C. Sequence-Specific Recognition and Modification of Double-Helical DNA by Oligonucleotides. *Angewandte Chemie (International ed.)* **1993***, 32*, 666-690.

39. Giovannangeli, C.; Perrouault, L.; Escudé, C.; Thuong, N.; Hélène, C. Specific Inhibition of in Vitro Transcription Elongation by Triplex-Forming Oligonucleotide−Intercalator Conjugates Targeted to HIV Proviral DNA. *Biochemistry* **1996***, 35*, 10539-10548.

40. Taniguchi, Y.; Sasaki, S. An efficient antigene activity and antiproliferative effect by targeting the Bcl-2 or survivin gene with triplex forming oligonucleotides containing a W-shaped nucleoside analogue (WNA-βT). *Org. Biomol. Chem.* **2012***, 10*, 8336-8341.

41. Notomi, R.; Wang, L.; Sasaki, S.; Taniguchi, Y. Design and synthesis of purine nucleoside analogues for the formation of stable anti-parallel-type triplex DNA with duplex DNA bearing the (5m)CG base pair. *RSC Adv.* **2021***, 11*, 21390-21396.

42. Sasaki, S.; Yamauchi, H.; Takahasi, R.; Taniguchi, Y.; Maeda, M. New base analogs for the formation of non-natural triplexes. *Nucleic Acids Symp Ser (Oxf)* **2001***, 1*, 23-24.

43. Rusling, D. A. Triplex-forming properties and enzymatic incorporation of a base-modified nucleotide capable of duplex DNA recognition at neutral pH. *Nucleic Acids Res.* **2021***, 49*, 7256-7266.

44. Buchini, S.; Leumann, C. J. New Nucleoside Analogues for the Recognition of Pyrimidine-Purine Inversion Sites. *Nucleosides Nucleotides Nucleic Acids* **2003***, 22*, 1199-1201.

45. Arya, D. P.; Micovic, L.; Charles, I.; Coffee, R. L.,Jr; Willis, B.; Xue, L. Neomycin binding to Watson-Hoogsteen (W-H) DNA triplex groove: a model. *J. Am. Chem. Soc.* **2003***, 125*, 3733-3744.

46. Pilch, D. S.; Breslauer, K. J. Ligand-Induced Formation of Nucleic Acid Triple Helices. *Proc. Natl. Acad. Sci. U. S. A.* **1994**, *91*, 9332-9336.

47. Mergny, J. L.; Duval-Valentin, G.; Nguyen, C. H.; Perrouault, L.; Faucon, B.; Rougée, M.; Montenay-Garestier, T.; Bisagni, E.; Hélène, C. Triple helix-specific ligands. *Science* **1992**, *256*, 1681-1684.

48. Lee, Y. K.; Yuk, D. Y.; Lee, J. W.; Lee, S. Y.; Ha, T. Y.; Oh, K. W.; Yun, Y. P.; Hong, J. T. (-)-Epigallocatechin-3-gallate prevents lipopolysaccharide-induced elevation of beta-amyloid generation and memory deficiency. *Brain Res.* **2009**, *1250*, 164-174.

49. Justesen, U.; Knuthsen, P. Composition of flavonoids in fresh herbs and calculation of flavonoid intake by use of herbs in traditional Danish dishes. *Food Chem.* **2001**, *73*, 245-250.

50. Li, Y.; Yao, J.; Han, C.; Yang, J.; Chaudhry, M. T.; Wang, S.; Liu, H.; Yin, Y. Quercetin, Inflammation and Immunity. *Nutrients* **2016**, *8*, 167.

51. Hodek, P.; Trefil, P.; Stiborová, M. Flavonoids-potent and versatile biologically active compounds interacting with cytochromes P450. *Chem. Biol. Interact.* **2002**, *139*, 1-21.

52. Mitchell, A. E.; Hong, Y.; Koh, E.; Barrett, D. M.; Bryant, D. E.; Denison, R. F.; Kaffka, S. Ten-year comparison of the influence of organic and conventional crop management practices on the content of flavonoids in tomatoes. *J. Agric. Food Chem.* **2007**, *55*, 6154-6159.

53. Kobori, M.; Takahashi, Y.; Akimoto, Y.; Sakurai, M.; Matsunaga, I.; Nishimuro, H.; Ippoushi, K.; Oike, H.; Ohnishi-Kameyama, M. Chronic high intake of quercetin reduces oxidative stress and induces expression of the antioxidant enzymes in the liver and visceral adipose tissues in mice. *Journal of Functional Foods* **2015**, *15*, 551-560.

54. Granado-Serrano, A. B.; Martín, M. A.; Bravo, L.; Goya, L.; Ramos, S. Quercetin modulates Nrf2 and glutathione-related defenses in HepG2 cells: Involvement of p38. *Chem. Biol. Interact.* **2012***, 195*, 154-164.

55. Adedara, I. A.; Ego, V. C.; Subair, T. I.; Oyediran, O.; Farombi, E. O. Quercetin Improves Neurobehavioral Performance Through Restoration of Brain Antioxidant Status and Acetylcholinesterase Activity in Manganese-Treated Rats. *Neurochem. Res.* **2017***, 42*, 1219-1229.

56. Schültke, E.; Kamencic, H.; Skihar, V. M.; Griebel, R.; Juurlink, B. Quercetin in an animal model of spinal cord compression injury: correlation of treatment duration with recovery of motor function. *Spinal Cord* **2010***, 48*, 112-117.

57. Schültke, E.; Kendall, E.; Kamencic, H.; Ghong, Z.; Griebel, R. W.; Juurlink, B. H. J. Quercetin promotes functional recovery following acute spinal cord injury. *J. Neurotrauma* **2003***, 20*, 583-591.

58. Colunga Biancatelli, R. M. L.; Berrill, M.; Catravas, J. D.; Marik, P. E. Quercetin and Vitamin C: An Experimental, Synergistic Therapy for the Prevention and Treatment of SARS-CoV-2 Related Disease (COVID-19). *Front. Immunol.* **2020***, 11*, 1451.

59. Shinozuka, K.; Kikuchi, Y.; Nishino, C.; Mori, A.; Tawata, S. Inhibitory effect of flavonoids on DNA-dependent DNA and RNA polymerases. *Experientia* **1988***, 44*, 882-885.

60. Bachmetov, L.; Gal-Tanamy, M.; Shapira, A.; Vorobeychik, M.; Giterman-Galam, T.; Sathiyamoorthy, P.; Golan-Goldhirsh, A.; Benhar, I.; Tur-Kaspa, R.; Zemel, R. Suppression of hepatitis C virus by the flavonoid quercetin is mediated by inhibition of NS3 protease activity. *J. Viral Hepat.* **2012***, 19*, 81.

61. Spedding, G.; Ratty, A.; Middleton, E. J. Inhibition of reverse transcriptases by flavonoids. *Antiviral Res.* **1989***, 12*, 99-110.

62. Schültke, E.; Kendall, E.; Kamencic, H.; Ghong, Z.; Griebel, R. W.; Juurlink, B. H. J. Quercetin promotes functional recovery following acute spinal cord injury. *J. Neurotrauma* **2003***, 20*, 583-591.

63. Cushnie, T. P. T.; Lamb, A. J. Antimicrobial activity of flavonoids. *Int. J. Antimicrob. Agents* **2005***, 26*, 343-356.

64. Srivastava, S.; Somasagara, R. R.; Hegde, M.; Nishana, M.; Tadi, S. K.; Srivastava, M.; Choudhary, B.; Raghavan, S. C. Quercetin, a Natural Flavonoid Interacts with DNA, Arrests Cell Cycle and Causes Tumor Regression by Activating Mitochondrial Pathway of Apoptosis. *Scientific Reports* **2016***, 6*, 24049.

65. Reyes-Farias, M.; Carrasco-Pozo, C. The Anti-Cancer Effect of Quercetin: Molecular Implications in Cancer Metabolism. *Int. J. Mol. Sci.* **2019***, 20*, 3177. doi: 10.3390/ijms20133177.

66. Chowdhury, A. R.; Sharma, S.; Mandal, S.; Goswami, A.; Mukhopadhyay, S.; Majumder, H. K. Luteolin, an emerging anti-cancer flavonoid, poisons eukaryotic DNA topoisomerase I. *Biochem. J.* **2002***, 366*, 653-661.

67. Wan, C.; Cui, M.; Song, F.; Liu, Z.; Liu, S. A study of the non-covalent interaction between flavonoids and DNA triplexes by electrospray ionization mass spectrometry. *International Journal of Mass Spectrometry* **2009***, 283*, 48-55.

68. Raza, A.; Xu, X.; Xia, L.; Xia, C.; Tang, J.; Ouyang, Z. Quercetin-Iron Complex: Synthesis, Characterization, Antioxidant, DNA Binding, DNA Cleavage, and Antibacterial Activity Studies. *J. Fluoresc.* **2016***, 26*, 2023-2031.

69. Dolatabadi, J. E. N. Molecular aspects on the interaction of quercetin and its metal complexes with DNA. *Int. J. Biol. Macromol.* **2011**, *48*, 227-233.

70. Tan, J.; Wang, B.; Zhu, L. DNA binding, cytotoxicity, apoptotic inducing activity, and molecular modeling study of quercetin zinc(II) complex. *Bioorganic & medicinal chemistry* **2009**, *17*, 614-620.

71. Bravo, A.; Anacona, J. R. Metal complexes of the flavonoid quercetin: antibacterial properties. *Transition Metal Chemistry* **2001**, *26*, 20-23.

72. Tan, J.; Zhu, L.; Wang, B. From GC-rich DNA binding to the repression of survivin gene for quercetin nickel (II) complex: implications for cancer therapy. *Biometals* **2010**, *23*, 1075-1084.

73. Rangel, V. M.; Gu, L.; Chen, G.; Chen, Q.; Xue, L. 5-Substituted 3, 3′, 4′, 7-tetramethoxyflavonoids – A novel class of potent DNA triplex specific binding ligands. *Bioorg. Med. Chem. Lett.* **2022**, *61*, 128608.

74. Siegel, R. L.; Miller, K. D.; Fuchs, H. E.; Jemal, A. Cancer statistics, 2022. *CA Cancer. J. Clin.* **2022**, *72*, 7-33.

75. Zella, D.; Gallo, R. C. Viruses and Bacteria Associated with Cancer: An Overview. *Viruses* **2021**, *13*, 1039. doi: 10.3390/v13061039.

76. Basu, A. K. DNA Damage, Mutagenesis and Cancer. *Int. J. Mol. Sci.* **2018**, *19*, 970. doi: 10.3390/ijms19040970.

77. Bacolla, A.; Collins, J. R.; Gold, B.; Chuzhanova, N.; Yi, M.; Stephens, R. M.; Stefanov, S.; Olsh, A.; Jakupciak, J. P.; Dean, M.; Lempicki, R. A.; Cooper, D. N.; Wells, R. D. Long homopurine•homopyrimidine sequences are characteristic of genes expressed in brain and the pseudoautosomal region. *Nucleic Acids Res.* **2006**, *34*, 2663-2675.

78. Vasquez, K. M.; Narayanan, L.; Glazer, P. M. Specific Mutations Induced by Triplex-Forming Oligonucleotides in Mice. *Science* **2000***, 290*, 530-533.

79. Knauert, M. P.; Glazer, P. M. Triplex forming oligonucleotides: sequence-specific tools for gene targeting. *Hum. Mol. Genet.* **2001***, 10*, 2243-2251.

80. Faria, M.; Giovannangeli, C. Triplex-forming molecules: from concepts to applications. *J. Gene Med.* **2001***, 3*, 299-310.

81. Ljubimova, J. Y.; Sun, T.; Mashouf, L.; Ljubimov, A. V.; Israel, L. L.; Ljubimov, V. A.; Falahatian, V.; Holler, E. Covalent nano delivery systems for selective imaging and treatment of brain tumors. *Adv. Drug Deliv. Rev.* **2017***, 113*, 177-200.

82. Wang, J.; Ni, Q.; Wang, Y.; Zhang, Y.; He, H.; Gao, D.; Ma, X.; Liang, X. Nanoscale drug delivery systems for controllable drug behaviors by multi-stage barrier penetration. *J. Controlled Release* **2021***, 331*, 282-295.

83. Hughes, J. F.; Skaletsky, H.; Pyntikova, T.; Minx, P. J.; Graves, T.; Rozen, S.; Wilson, R. K.; Page, D. C. Conservation of Y-linked genes during human evolution revealed by comparative sequencing in chimpanzee. *Nature* **2005***, 437*, 100-103.

84. Carbone, G. M.; Napoli, S.; Valentini, A.; Cavalli, F.; Watson, D. K.; Catapano, C. V. Triplex DNA-mediated downregulation of Ets2 expression results in growth inhibition and apoptosis in human prostate cancer cells. *Nucleic Acids Res.* **2004***, 32*, 4358-4367.

85. Jain, A.; Bacolla, A.; Chakraborty, P.; Grosse, F.; Vasquez, K. M. Human DHX9 helicase unwinds triple-helical DNA structures. *Biochemistry* **2010***, 49*, 6992-6999.

86. Napoli, S.; Negri, U.; Arcamone, F.; Capobianco, M. L.; Carbone, G. M.; Catapano, C. V. Growth inhibition and apoptosis induced by daunomycin-conjugated triplex-forming

oligonucleotides targeting the c-myc gene in prostate cancer cells. *Nucleic Acids Res.* **2006**, *34*, 734-744.

87. Boulware, S. B.; Christensen, L. A.; Thames, H.; Coghlan, L.; Vasquez, K. M.; Finch, R. A. Triplex-forming oligonucleotides targeting c-MYC potentiate the anti-tumor activity of gemcitabine in a mouse model of human cancer. *Mol. Carcinog.* **2014**, *53*, 744-752.

88. Wang, S. Q.; Setlow, R.; Berwick, M.; Polsky, D.; Marghoob, A. A.; Kopf, A. W.; Bart, R. S. Ultraviolet A and melanoma: a review. *J. Am. Acad. Dermatol.* **2001**, *44*, 837-846.

89. Vasquez, K. M. Targeting and processing of site-specific DNA interstrand crosslinks. *Environ. Mol. Mutagen.* **2010**, *51*, 527-539.

90. Vue, B.; Zhang, S.; Chen, Q. H. Flavonoids with Therapeutic Potential in Prostate Cancer. *Anticancer Agents Med. Chem.* **2016**, *16*, 1205-1229.

91. Rajaram, P.; Jiang, Z.; Chen, G.; Rivera, A.; Phasakda, A.; Zhang, Q.; Zheng, S.; Wang, G.; Chen, Q. Nitrogen-containing derivatives of O-tetramethylquercetin: Synthesis and biological profiles in prostate cancer cell models. *Bioorg. Chem.* **2019**, *87*, 227-239.

92. Dedon, P. C. Determination of Binding Mode: Intercalation. *Current Protocols in Nucleic Acid Chemistry* **2000**, *00*, 8.1.1-8.1.13.

93. Arya, D. P.; Micovic, L.; Charles, I.; Coffee, R. L.,Jr; Willis, B.; Xue, L. Neomycin binding to Watson-Hoogsteen (W-H) DNA triplex groove: a model. *J. Am. Chem. Soc.* **2003**, *125*, 3733-3744.

94. Chiu, M. H.; Prenner, E. J. Differential scanning calorimetry: An invaluable tool for a detailed thermodynamic characterization of macromolecules and their interactions. *J. Pharm. Bioallied Sci.* **2011**, *3*, 39-59.

95. Pilch, D. S.; Kirolos, M. A.; Liu, X.; Plum, G. E.; Breslauer, K. J. Berenil [1,3-bis(4'-amidinophenyl)triazene] binding to DNA duplexes and to a RNA duplex: evidence for both intercalative and minor groove binding properties. *Biochemistry* **1995**, *34*, 9962-9976.

96. Rajeswari, M. R. DNA triplex structures in neurodegenerative disorder, Friedreich's ataxia. *J. Biosci.* **2012**, *37*, 519-532.

97. Greschner, A. A.; Bujold, K. E.; Sleiman, H. F. Intercalators as molecular chaperones in DNA self-assembly. *J. Am. Chem. Soc.* **2013**, *135*, 11283-11288.

98. Chitranshi, P.; Chen, C.; Jones, P. R.; Faridi, J. S.; Xue, L. Investigation on the Interactions of NiCR and NiCR-2H with DNA. *Bioinorganic Chemistry and Applications* **2010**, *2010*, 619436-10.

99. Arya, D. P. New approaches toward recognition of nucleic acid triple helices. *Acc. Chem. Res.* **2011**, *44*, 134-146.

100. Buurma, N. J.; Haq, I. Advances in the analysis of isothermal titration calorimetry data for ligand-DNA interactions. *Methods* **2007**, *42*, 162-172.

101. Singh, M.; Wang, S.; Joo, H.; Ye, Z.; Christison, K. M.; Hekman, R.; Vierra, C.; Xue, L. Use of neomycin as a structured amino-containing side chain motif for phenanthroline-based G-quadruplex ligands and telomerase inhibitors. *Chem. Biol. Drug Des.* **2020**, *96*, 1292-1304.

102. Chaires, J. B. A thermodynamic signature for drug-DNA binding mode. *Arch. Biochem. Biophys.* **2006**, *453*, 26-31.

103. Wilson, W. D.; Tanious, F. A.; Mizan, S.; Yao, S.; Kiselyov, A. S.; Zon, G.; Strekowski, L. DNA triple-helix specific intercalators as antigene enhancers: Unfused aromatic cations. *Biochemistry (Easton)* **1993**, *32*, 10614-10621.

104. Chaires, J. B.; Ren, J.; Henary, M.; Zegrocka, O.; Bishop, G. R.; Strekowski, L. Triplex Selective 2-(2-Naphthyl)quinoline Compounds: Origins of Affinity and New Design Principles. *J. Am. Chem. Soc.* **2003***, 125*, 7272-7283.

105. Israels, E. D.; Israels, L. G. The Cell Cycle. *Oncologist* **2000***, 5*, 510-513.

106. Robbins, E.; Pederson, T. On the Role of Ions in Mitosis. *In Vitro* **1971***, 6*, 323-334.

107. Michea, L.; Ferguson, D. R.; Peters, E. M.; Andrews, P. M.; Kirby, M. R.; Burg, M. B. Cell cycle delay and apoptosis are induced by high salt and urea in renal medullary cells. *American Journal of Physiology-Renal Physiology* **2000***, 278*, F209-F218.

108. Demaurex, N. pH Homeostasis of Cellular Organelles. *Physiology* **2002***, 17*, 1-5.

109. Caceres-Cortes, J.; Rajotte, D.; Dumouchel, J.; Haddad, P.; Hoang, T. Product of the steel locus suppresses apoptosis in hemopoietic cells. Comparison with pathways activated by granulocyte macrophage colony-stimulating factor. *J. Biol. Chem.* **1994***, 269*, 12084-12091.

110. Barry, M. A.; Reynolds, J. E.; Eastman, A. Etoposide-induced apoptosis in human HL-60 cells is associated with intracellular acidification. *Cancer Res.* **1993***, 53*, 2349-2357.

111. Hopkins, E.; Sanvictores, T.; Sharma, S. Physiology, Acid Base Balance. In *StatPearls*StatPearls Publishing LLC: Treasure Island (FL), 2022; .

112. Gerweck, L. E.; Seetharaman, K. Cellular pH Gradient in Tumor versus Normal Tissue: Potential Exploitation for the Treatment of Cancer1. *Cancer Res.* **1996***, 56*, 1194-1198.

113. Peng, J.; He, X.; Wang, K.; Tan, W.; Wang, Y.; Liu, Y. Noninvasive monitoring of intracellular pH change induced by drug stimulation using silica nanoparticle sensors. *Analytical and Bioanalytical Chemistry* **2007***, 388*, 645-654.

114. Spink, C. H.; Chaires, J. B. Selective Stabilization of Triplex DNA by Poly(ethylene glycols). *J. Am. Chem. Soc.* **1995**, *117*, 12887-12888.

115. Tyrrell, J.; Weeks, K. M.; Pielak, G. J. Challenge of mimicking the influences of the cellular environment on RNA structure by PEG-induced macromolecular crowding. *Biochemistry* **2015**, *54*, 6447-6453.

116. Lipinski, C. A.; Lombardo, F.; Dominy, B. W.; Feeney, P. J. Experimental and computational approaches to estimate solubility and permeability in drug discovery and development settings. *Advanced drug delivery reviews* **2001**, *46*, 3-26.

117. Di, L.; Kerns, E. H.; Carter, G. T. Drug-Like Property Concepts in Pharmaceutical Design. *Current pharmaceutical design* **2009**, *15*, 2184-2194.

Appendix A: Figures

Figure A-1

Thermal Denaturation of poly(dA)●2poly(dT) in the Presence of Tetramethoxyquercetin Four-
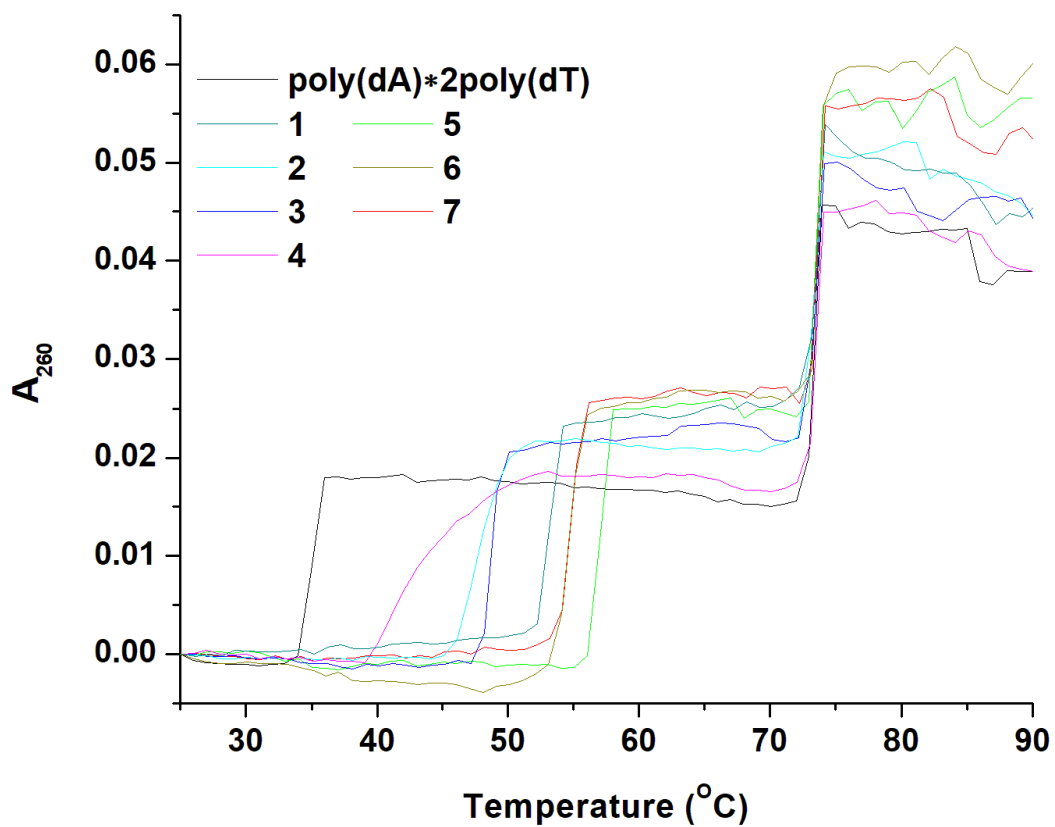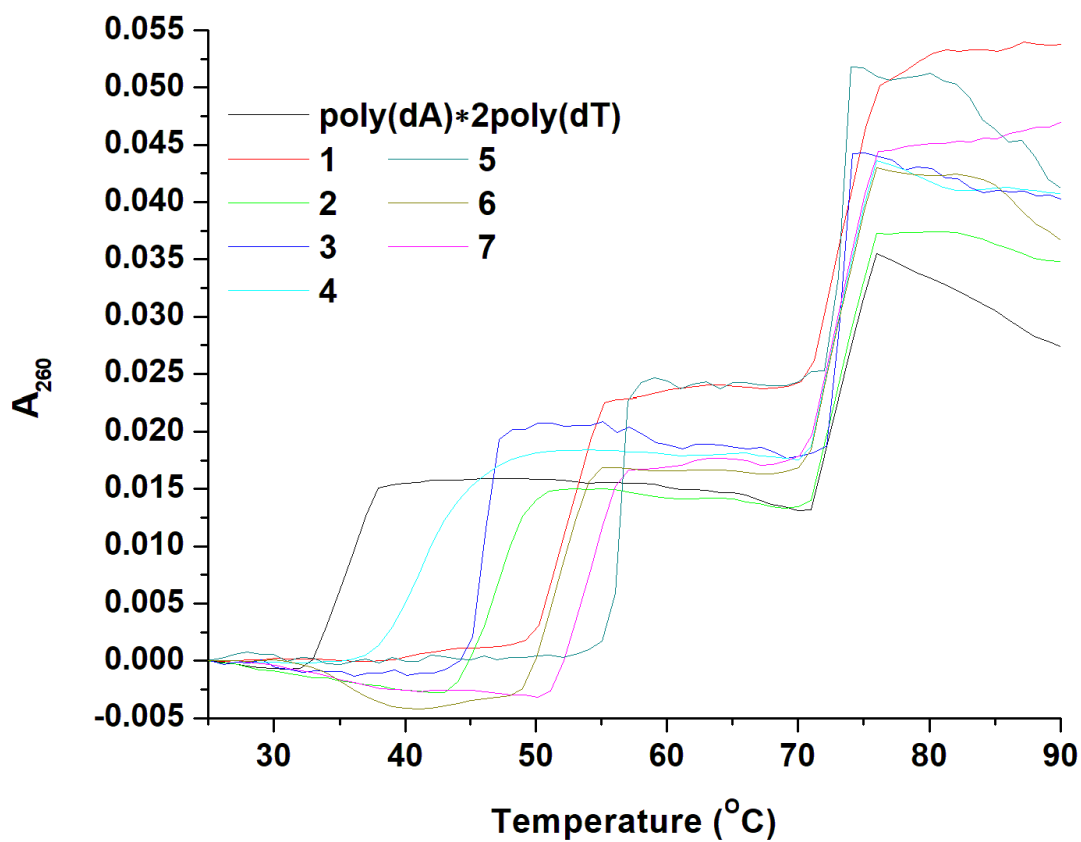
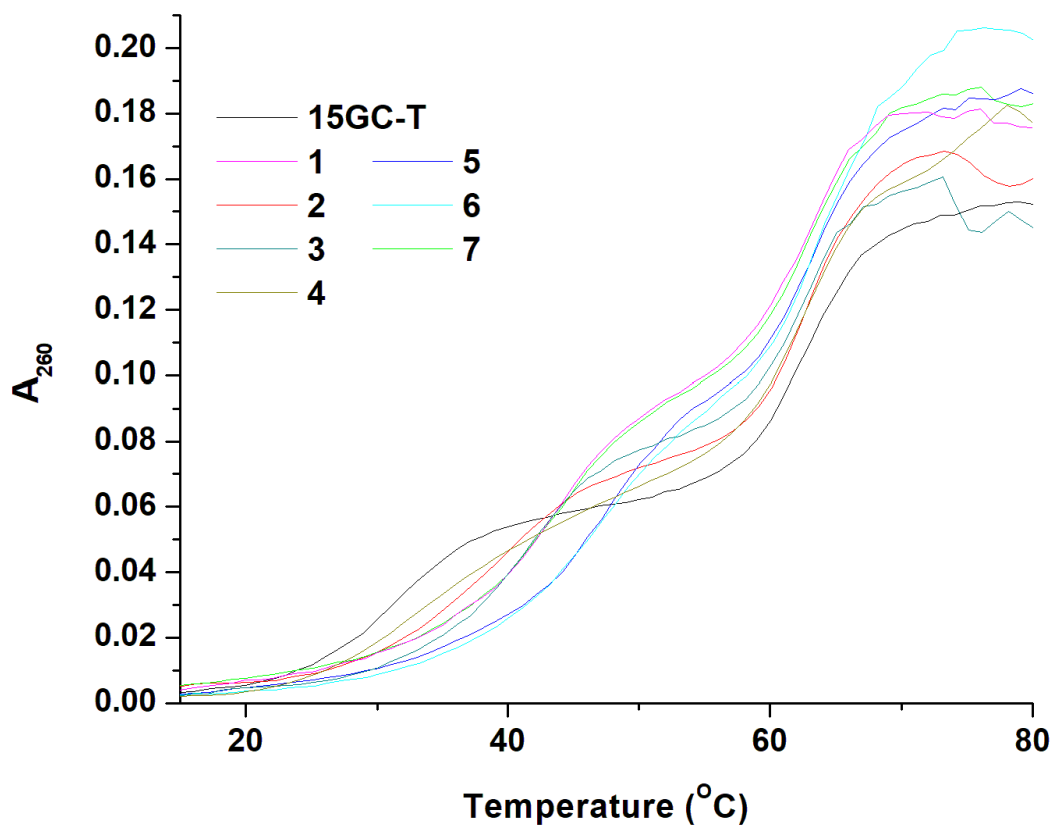*Carbon Linker Derivatives in 50 mM KCl*
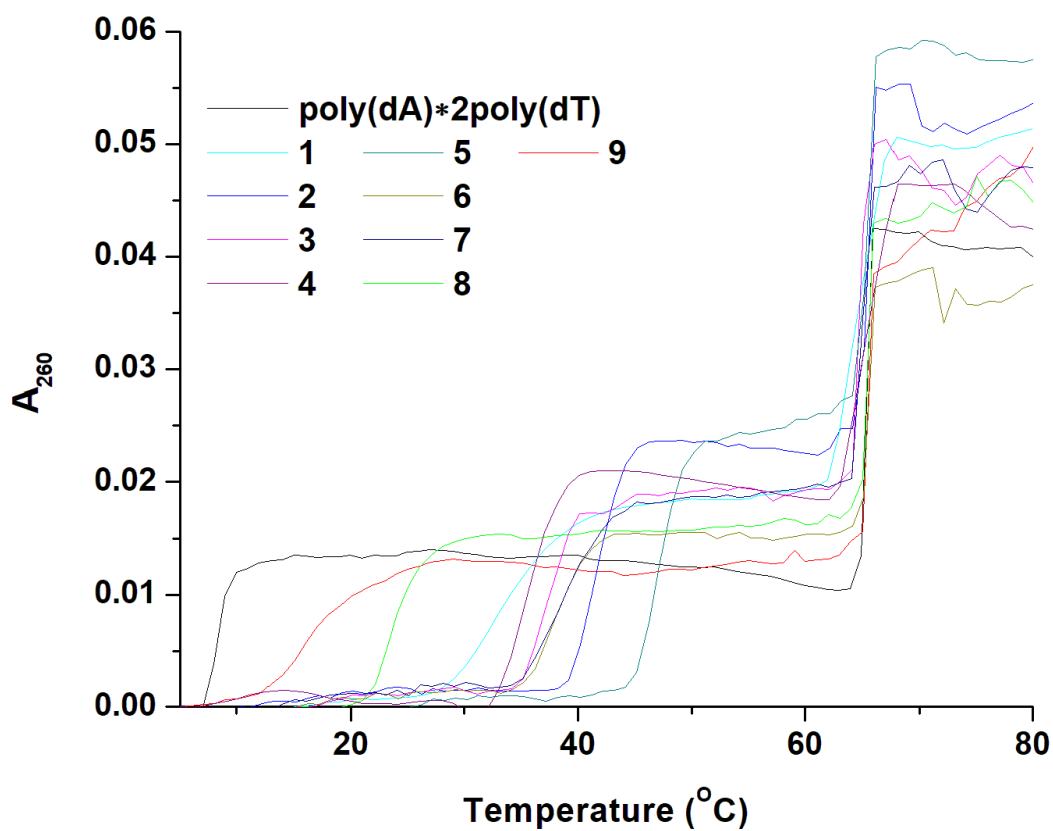
Y-axis adjusted to zero for better presentation. Buffer conditions: 10 mM sodium cacodylate and 50 mM KCl, pH 7.

Figure A-2

Thermal Denaturation of poly(dA)●2poly(dT) in the Presence of Tetramethoxyquercetin Four-

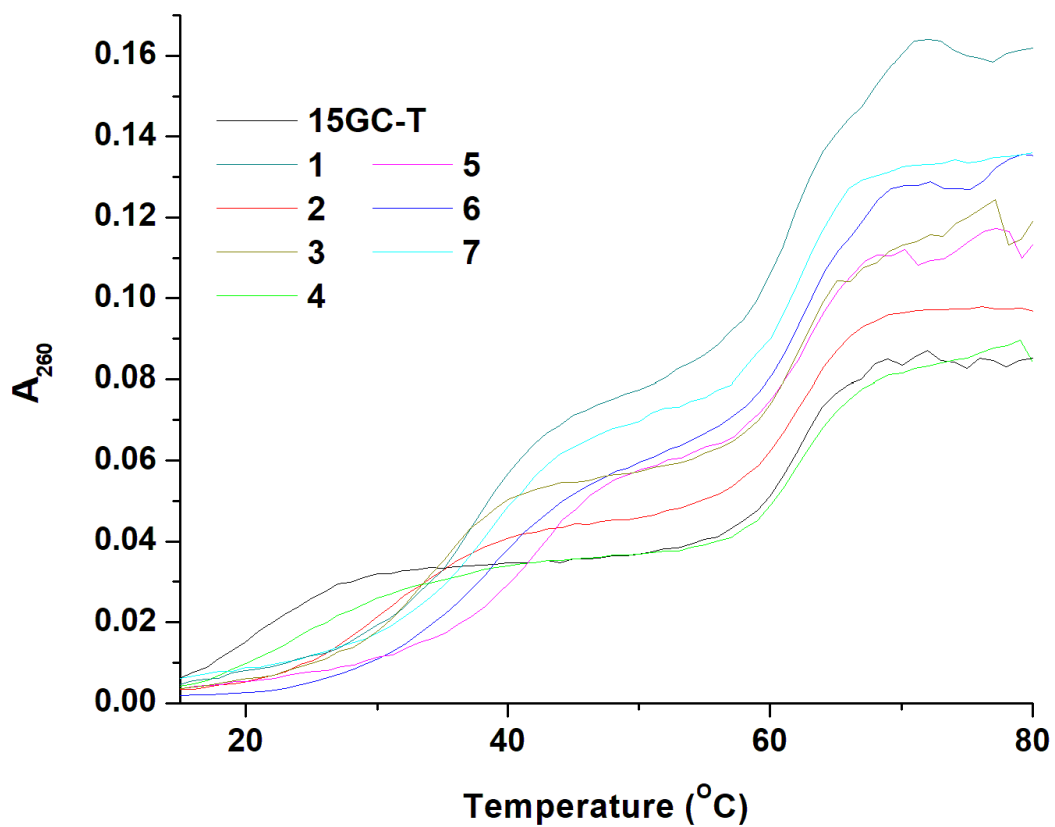*Carbon Linker Derivatives in 250 mM KCl*
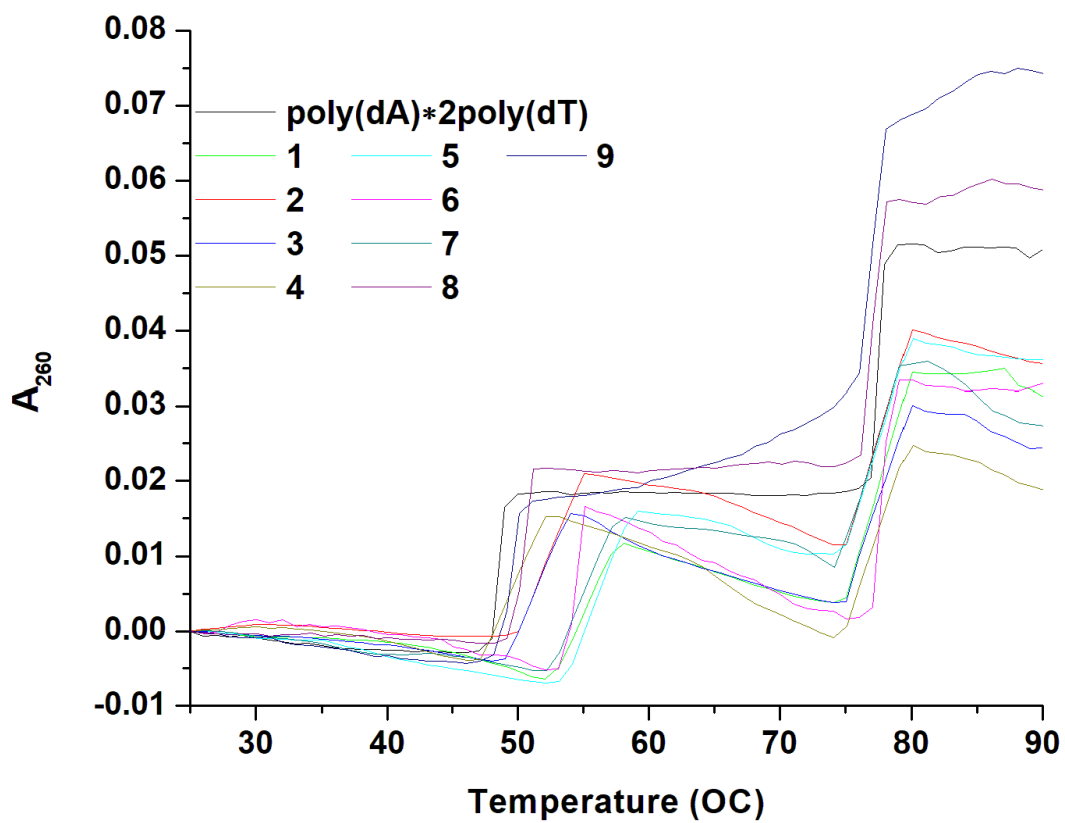
Y-axis adjusted to zero for better presentation. Buffer conditions: 10 mM sodium cacodylate and 250 mM KCl, pH

7.

Figure A-3

Thermal Denaturation of 15GC-T in the Presence of Tetramethoxyquercetin Four-Carbon Linker

Derivatives in 25mM NaCl
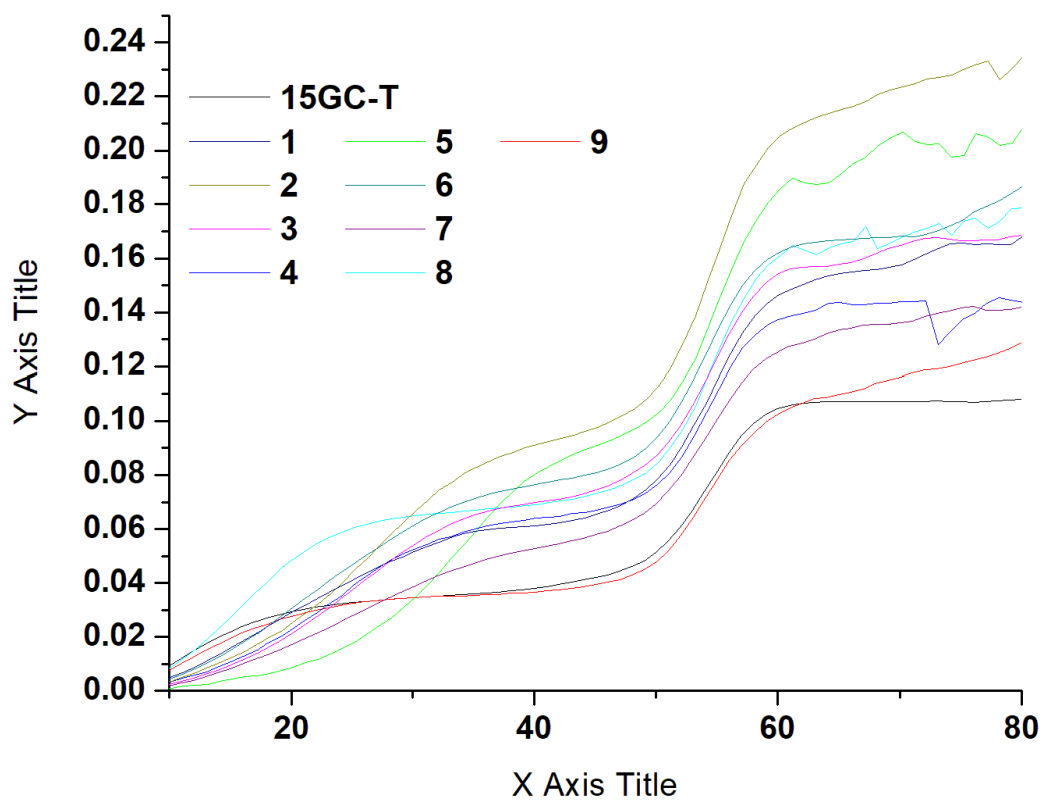
Y-axis adjusted to zero for better presentation. Buffer conditions: 10 mM sodium cacodylate and 25 mM NaCl, pH
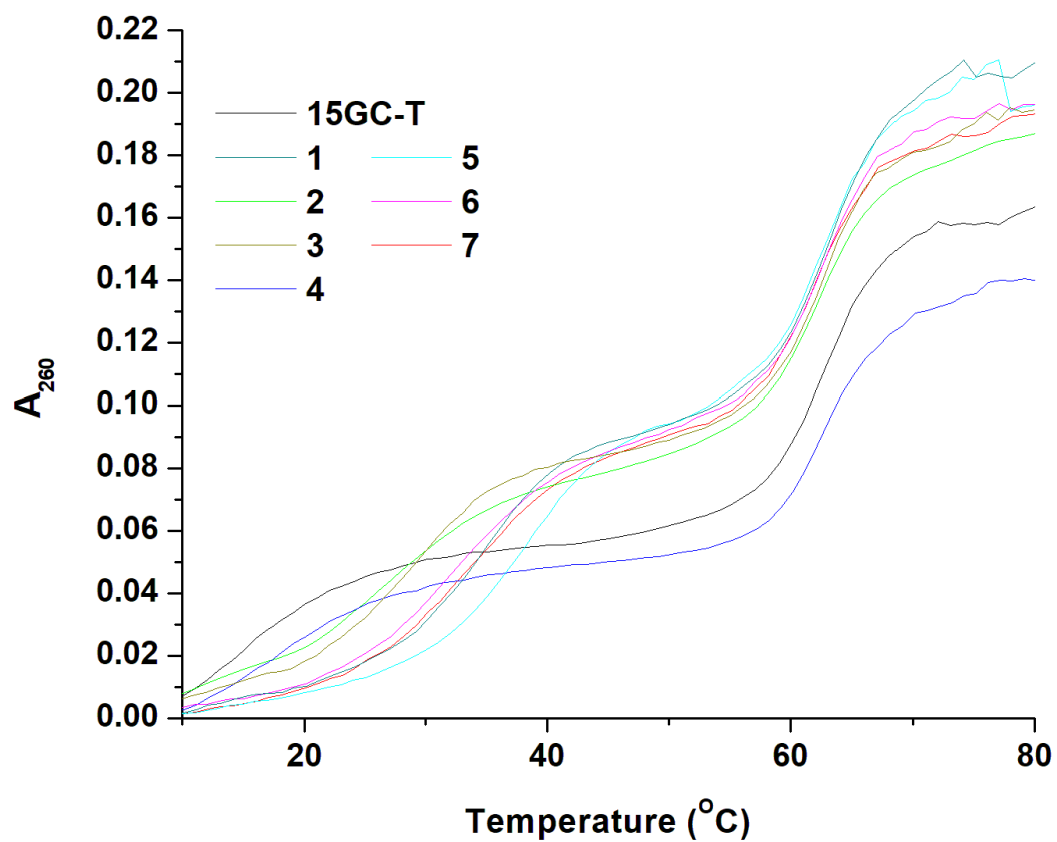
7.

Figure A-4

Thermal Denaturation of 15GC-T in the Presence of Tetramethoxyquercetin Four-Carbon Linker

Derivatives in 200 mM NaCl
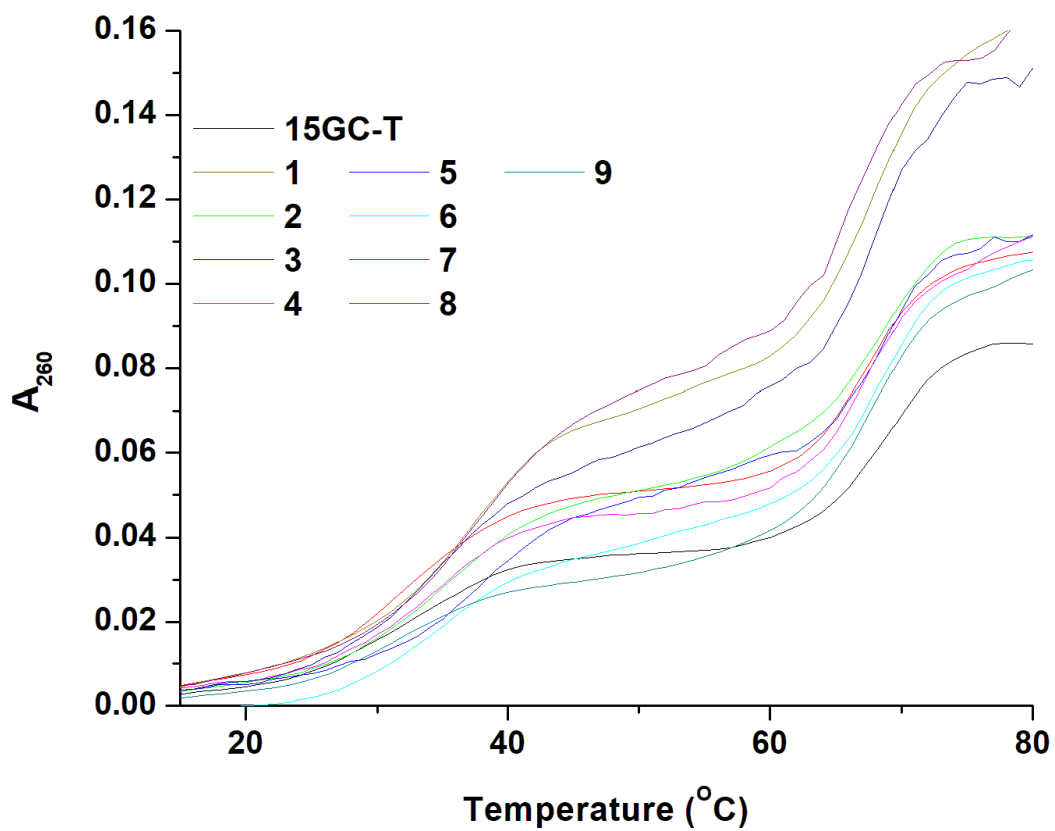
Y-axis adjusted to zero for better presentation. Buffer conditions: 10 mM sodium cacodylate and 200 mM NaCl, pH 7.

Figure A-5

Thermal Denaturation of 10GC-T in the Presence of Tetramethoxyquercetin Four-Carbon Linker

Derivatives in 25 mM NaCl
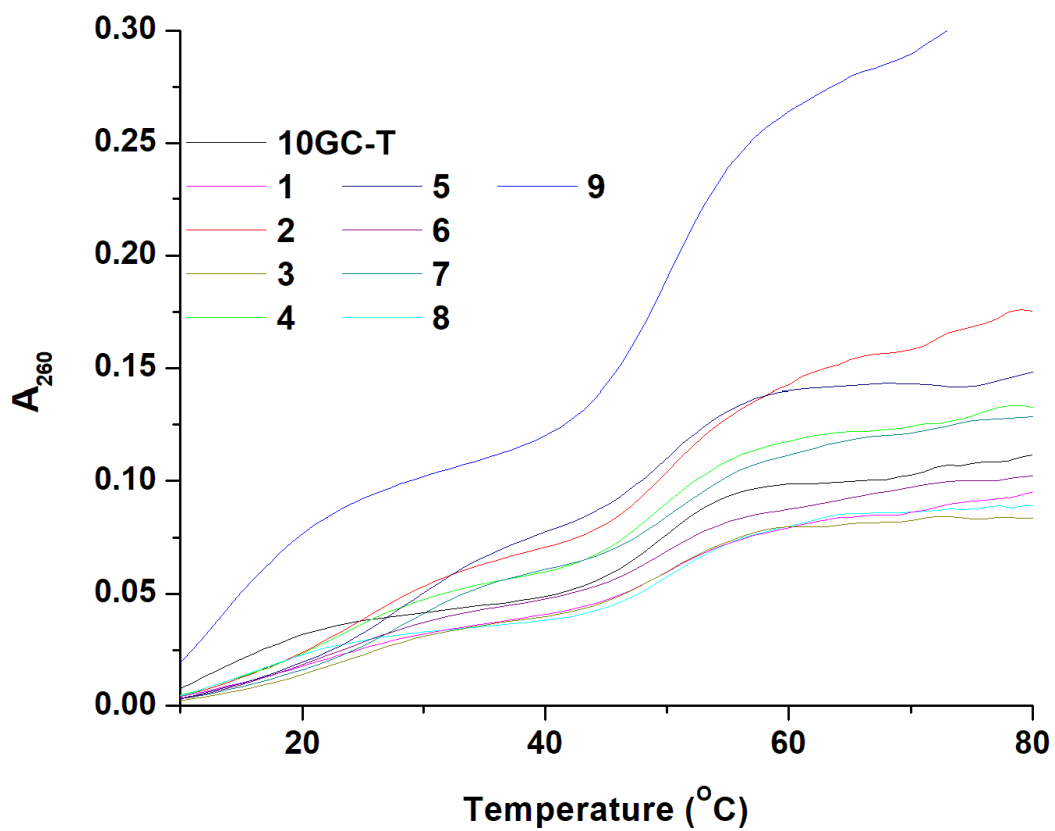
Y-axis adjusted to zero for better presentation. Buffer conditions: 10 mM sodium cacodylate and 25 mM NaCl, pH
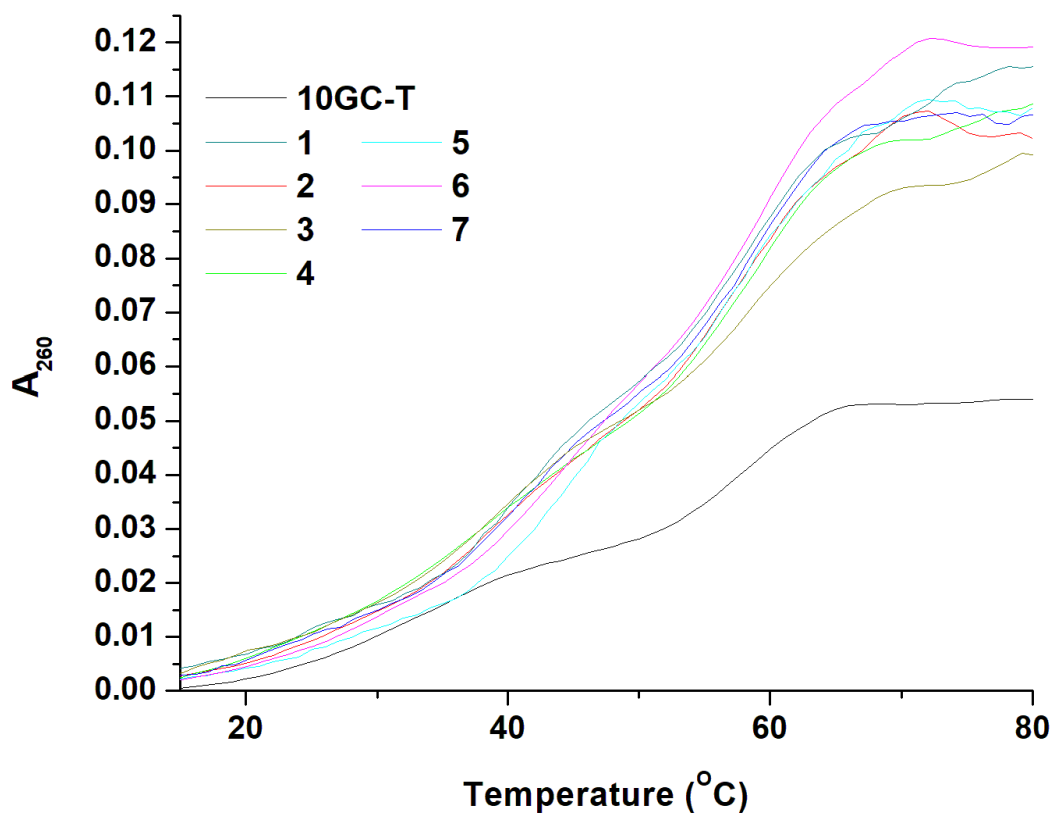
7.

Figure A-6

Thermal Denaturation of 10GC-T in the Presence of Tetramethoxyquercetin Four-Carbon Linker

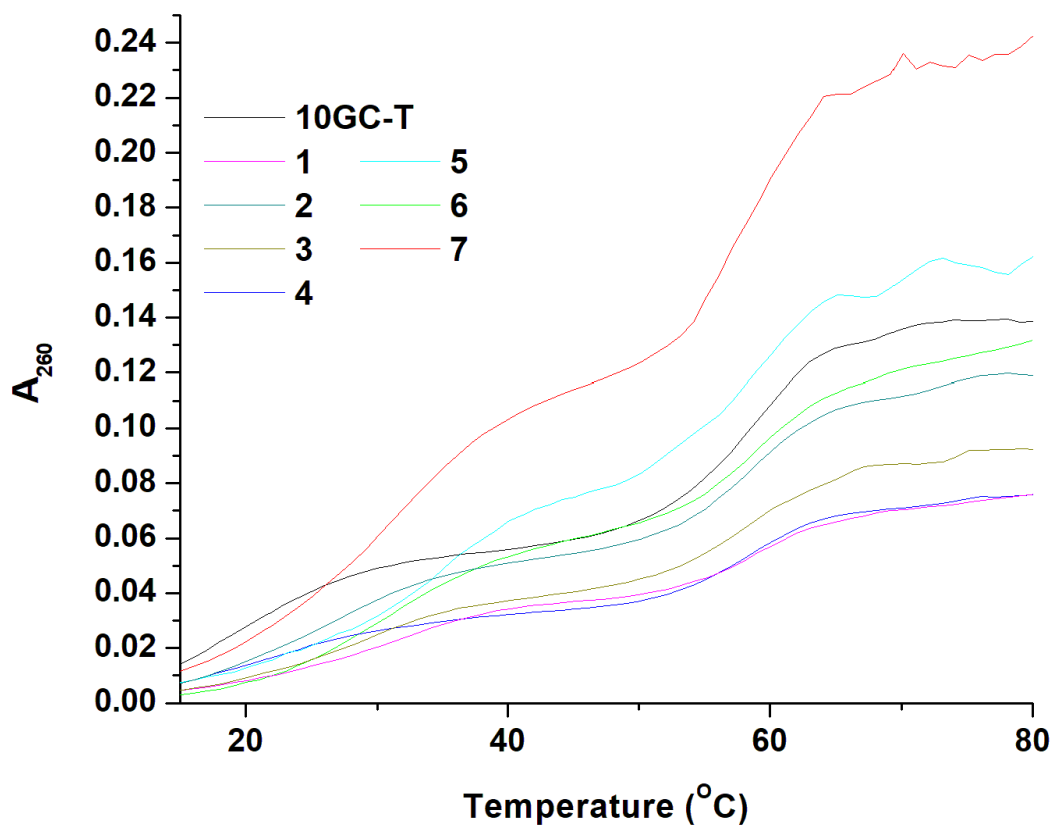*Derivatives in 200 mM NaCl*
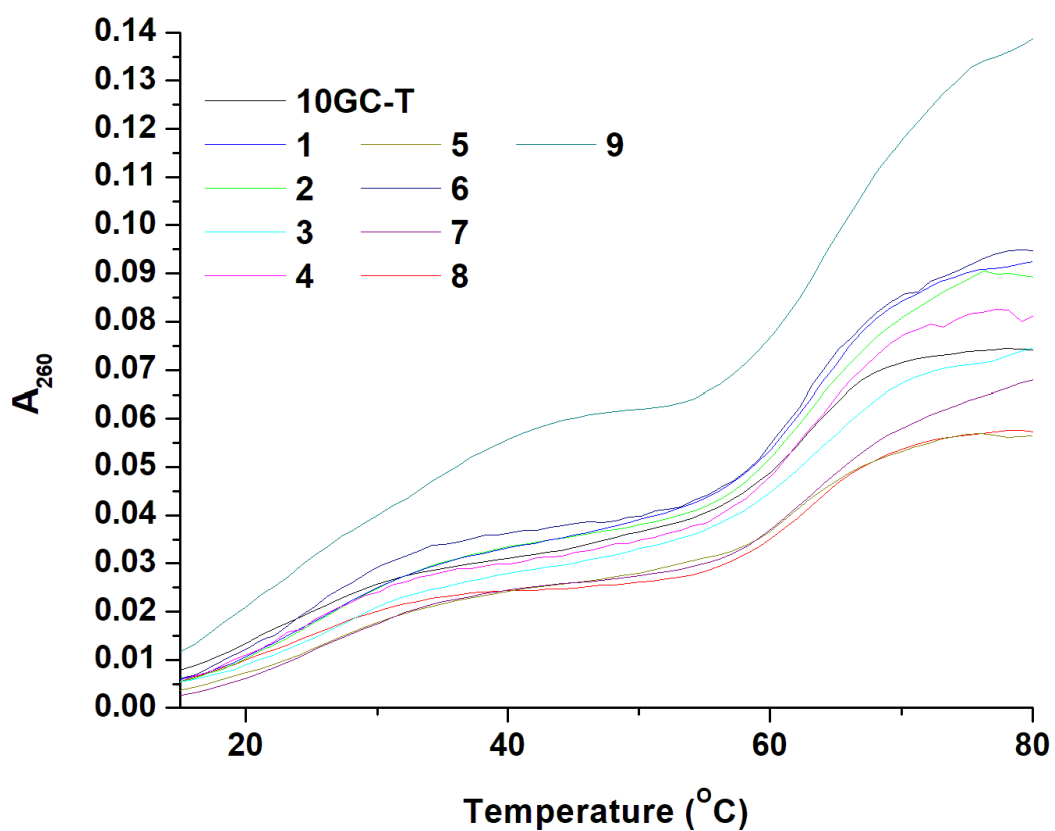
Y-axis adjusted to zero for better presentation. Buffer conditions: 10 mM sodium cacodylate and 200 mM NaCl, pH

7.

Figure A-7

Thermal Denaturation of poly(dA)•2poly(dT) in the Presence of Tetramethoxyquercetin Three-

Carbon Linker Derivatives at pH 6
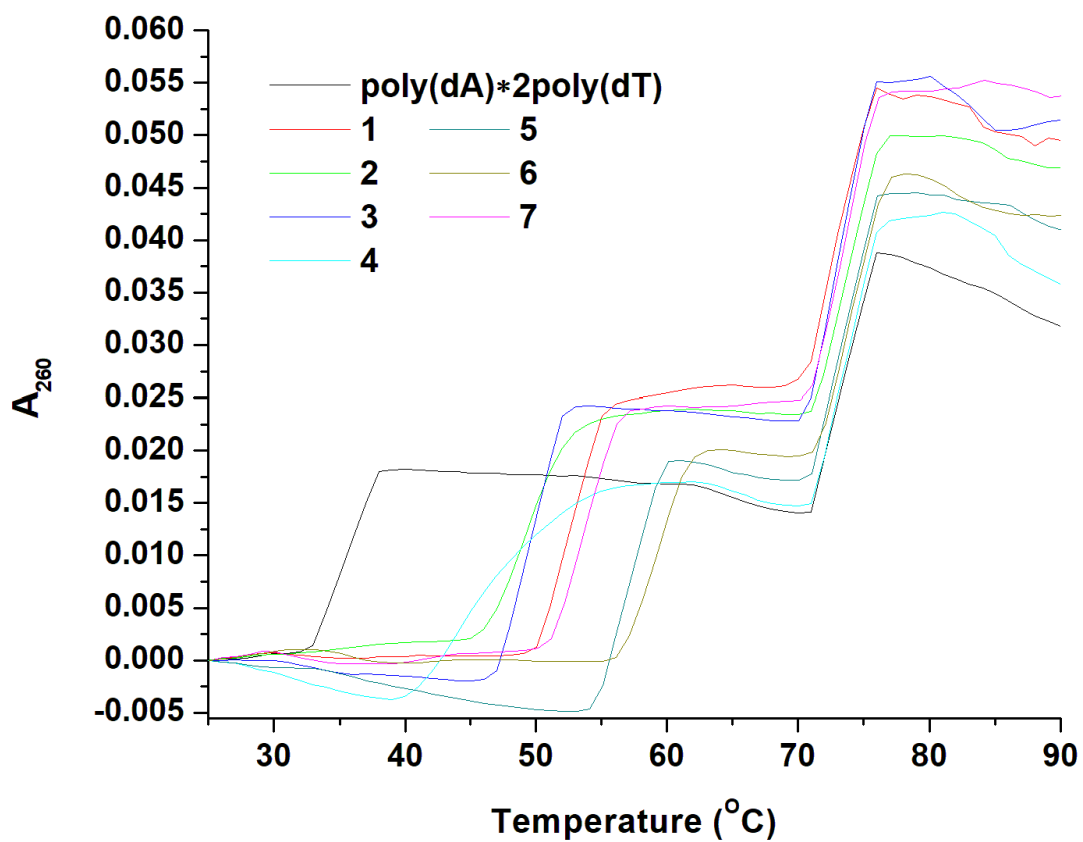
Y-axis adjusted to zero for better presentation. Buffer conditions: 10 mM sodium cacodylate and 150 mM KCl, pH

6.

Figure A-8

Thermal Denaturation of poly(dA)●2poly(dT) in the Presence of Tetramethoxyquercetin Three-

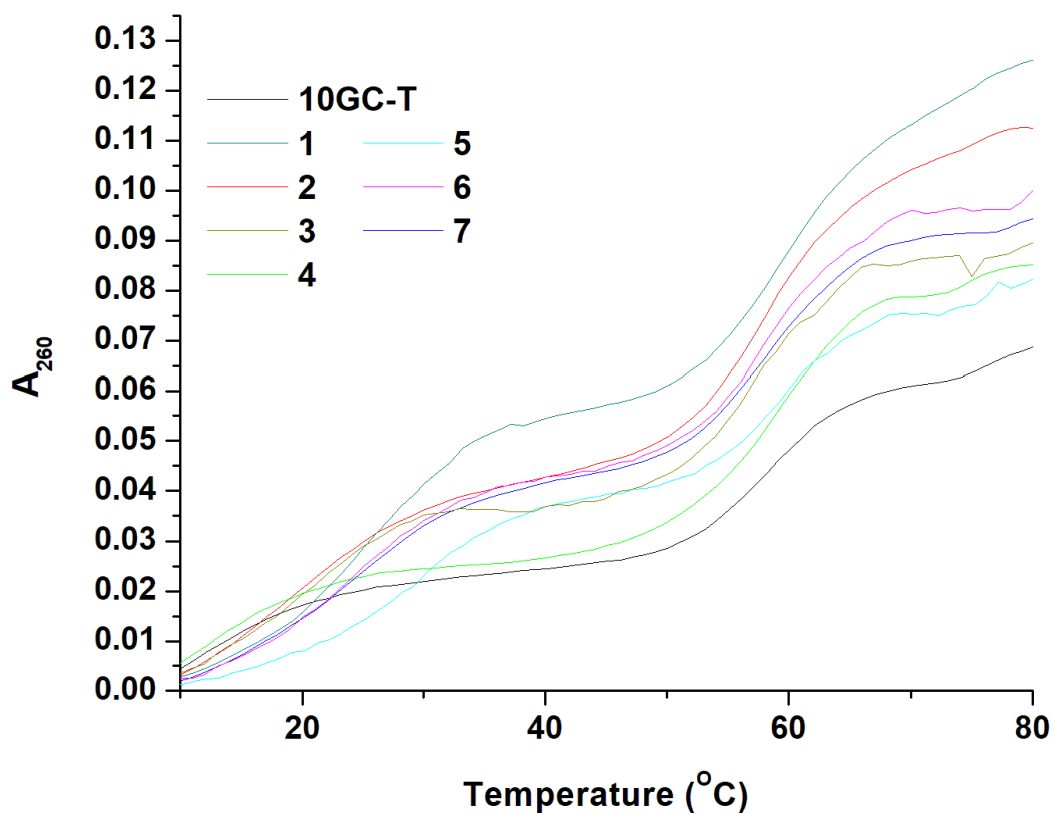*Carbon Linker Derivatives at pH 7*

Y-axis adjusted to zero for better presentation. Buffer conditions: 10 mM sodium cacodylate and 150 mM KCl, pH

7.

Figure A-9

Thermal Denaturation of poly(dA)●2poly(dT) in the Presence of Tetramethoxyquercetin Three-

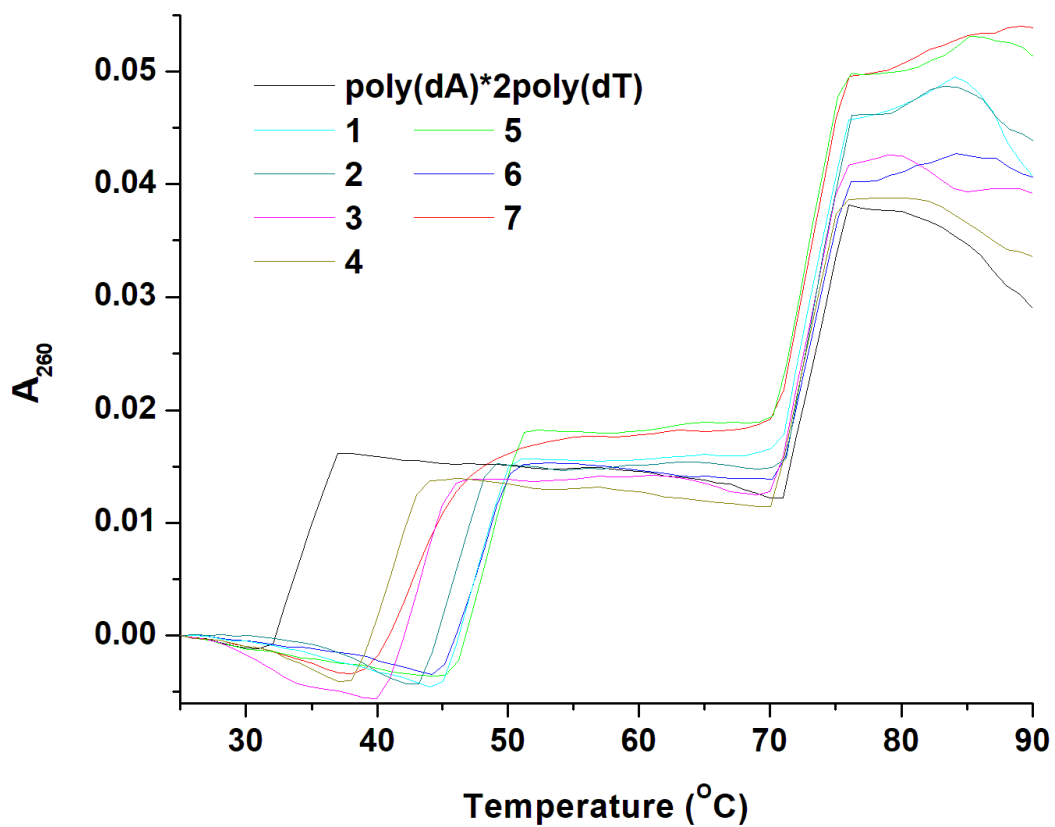*Carbon Linker Derivatives at pH 8*

Y-axis adjusted to zero for better presentation. Buffer conditions: 10 mM sodium cacodylate and 150 mM KCl, pH

8.

Figure A-10

Thermal Denaturation of 15GC-T in the Presence of Tetramethoxyquercetin Three-Carbon

Linker Derivatives at pH 6

Y-axis adjusted to zero for better presentation. Buffer conditions: 10 mM sodium cacodylate and 100 mM NaCl, pH

6.

Figure A-11

Thermal Denaturation of 15GC-T in the Presence of Tetramethoxyquercetin Three-Carbon
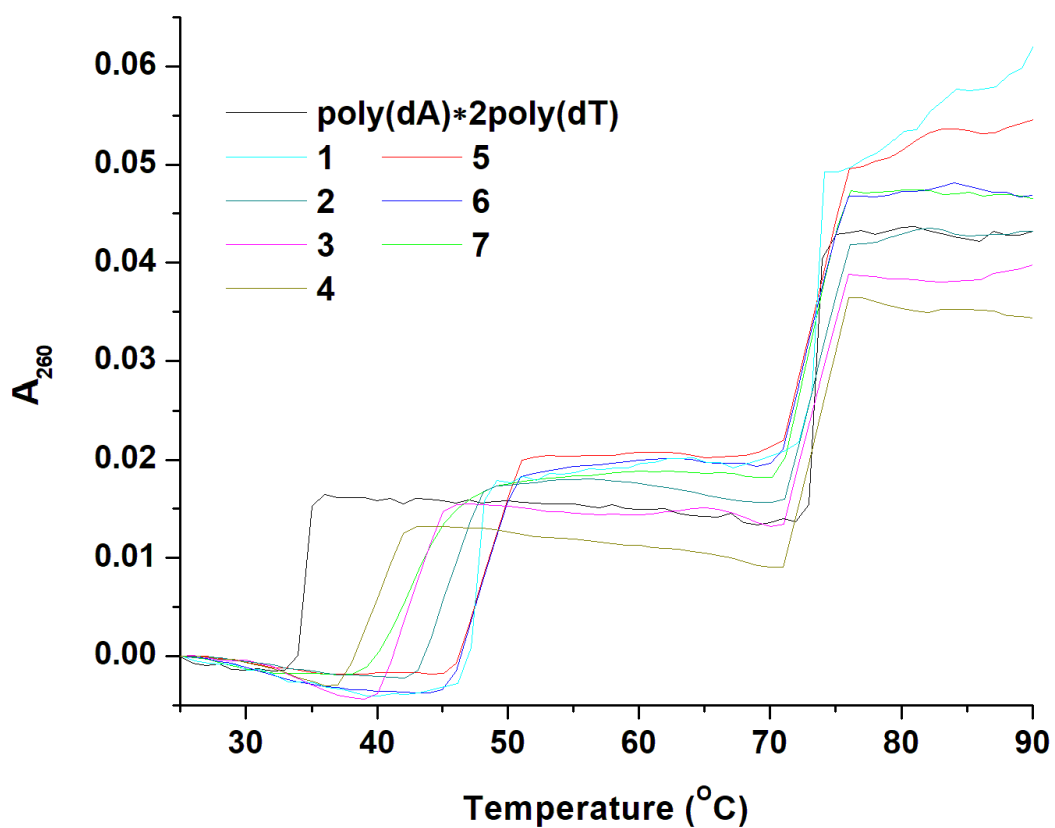
Linker Derivatives at pH 7

Y-axis adjusted to zero for better presentation. Buffer conditions: 10 mM sodium cacodylate and 100 mM NaCl, pH 7.

Figure A-12

Thermal Denaturation of 15GC-T in the Presence of Tetramethoxyquercetin Three-Carbon
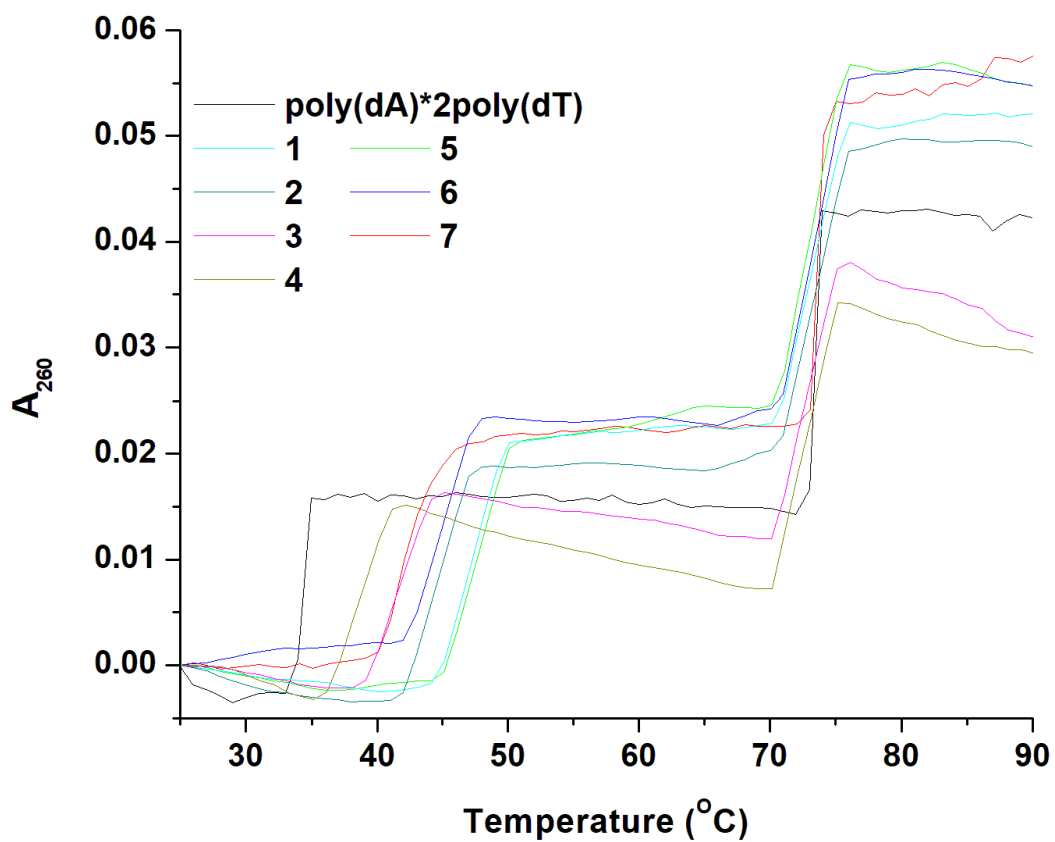
Linker Derivatives at pH 8

Y-axis adjusted to zero for better presentation. Buffer conditions: 10 mM sodium cacodylate and 100 mM NaCl, pH

8.

Figure A-13

Thermal Denaturation of 10GC-T in the Presence of Tetramethoxyquercetin Three-Carbon

Linker Derivatives at pH 6

Y-axis adjusted to zero for better presentation. Buffer conditions: 10 mM sodium cacodylate and 100 mM NaCl, pH

6.

Figure A-14

Thermal Denaturation of 10GC-T in the Presence of Tetramethoxyquercetin Three-Carbon

Linker Derivatives at pH 7

Y-axis adjusted to zero for better presentation. Buffer conditions: 10 mM sodium cacodylate and 100 mM NaCl, pH 7.

Figure A-15

Thermal Denaturation of 10GC-T in the Presence of Tetramethoxyquercetin Three-Carbon

Linker Derivatives at pH 8

Y-axis adjusted to zero for better presentation. Buffer conditions: 10 mM sodium cacodylate and 100 mM NaCl, pH

8.

Figure A-16

Thermal Denaturation of poly(dA)•2poly(dT) in the Presence of Tetramethoxyquercetin Five-
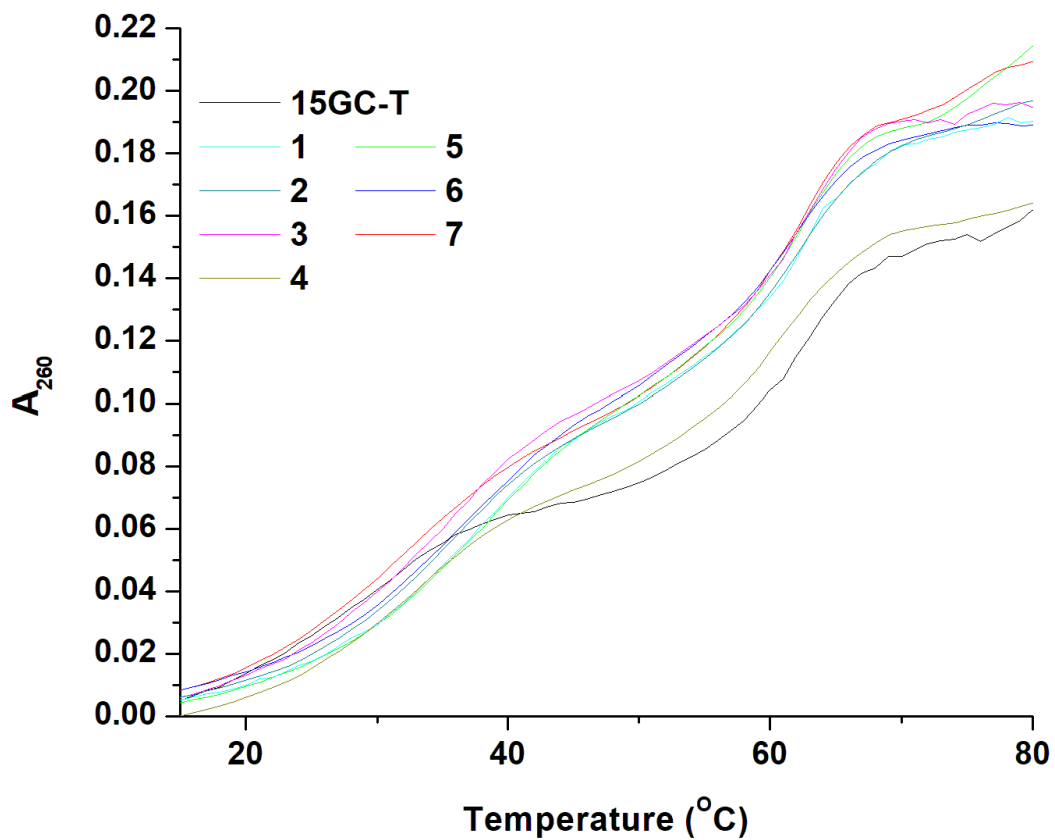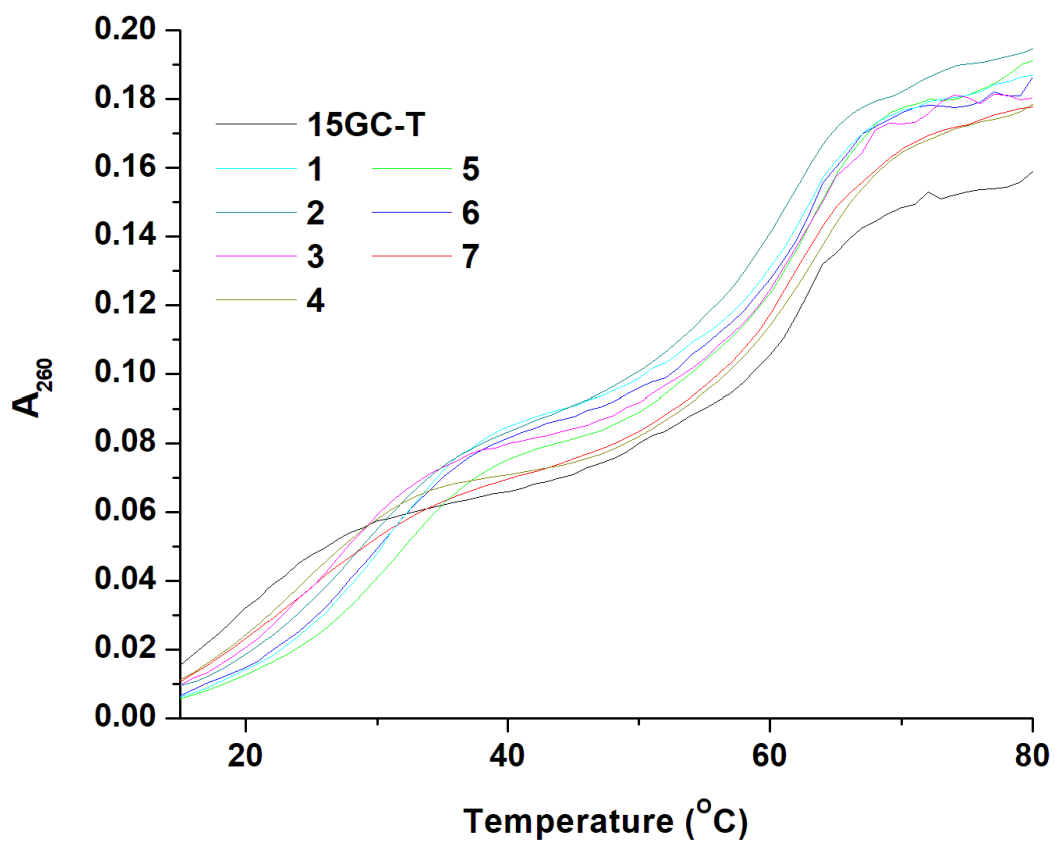
Carbon Linker Derivatives at pH 6

Y-axis adjusted to zero for better presentation. Buffer conditions: 10 mM sodium cacodylate and 150 mM KCl, pH

6.

Figure A-17

Thermal Denaturation of poly(dA)●2poly(dT) in the Presence of Tetramethoxyquercetin Five-

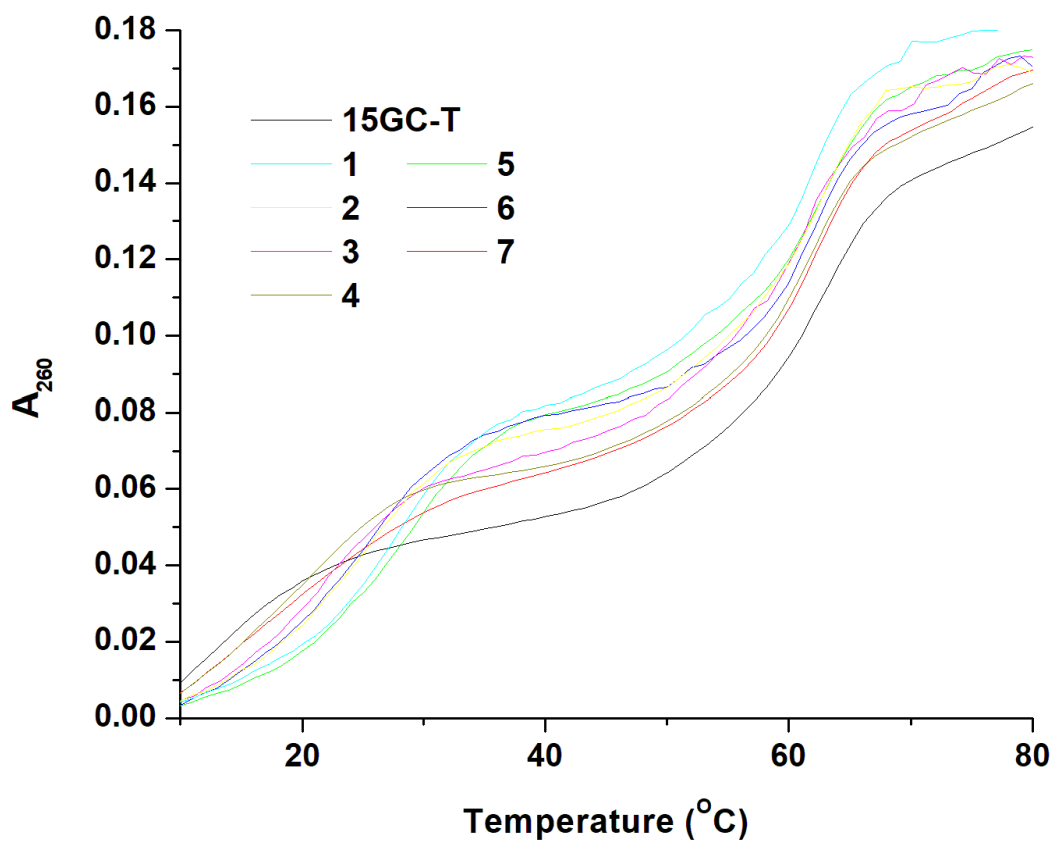*Carbon Linker Derivatives at pH 7*

Y-axis adjusted to zero for better presentation. Buffer conditions: 10 mM sodium cacodylate and 150 mM KCl, pH

7.

Figure A-18

Thermal Denaturation of poly(dA)●2poly(dT) in the Presence of Tetramethoxyquercetin Five-Carbon Linker Derivatives at pH 8
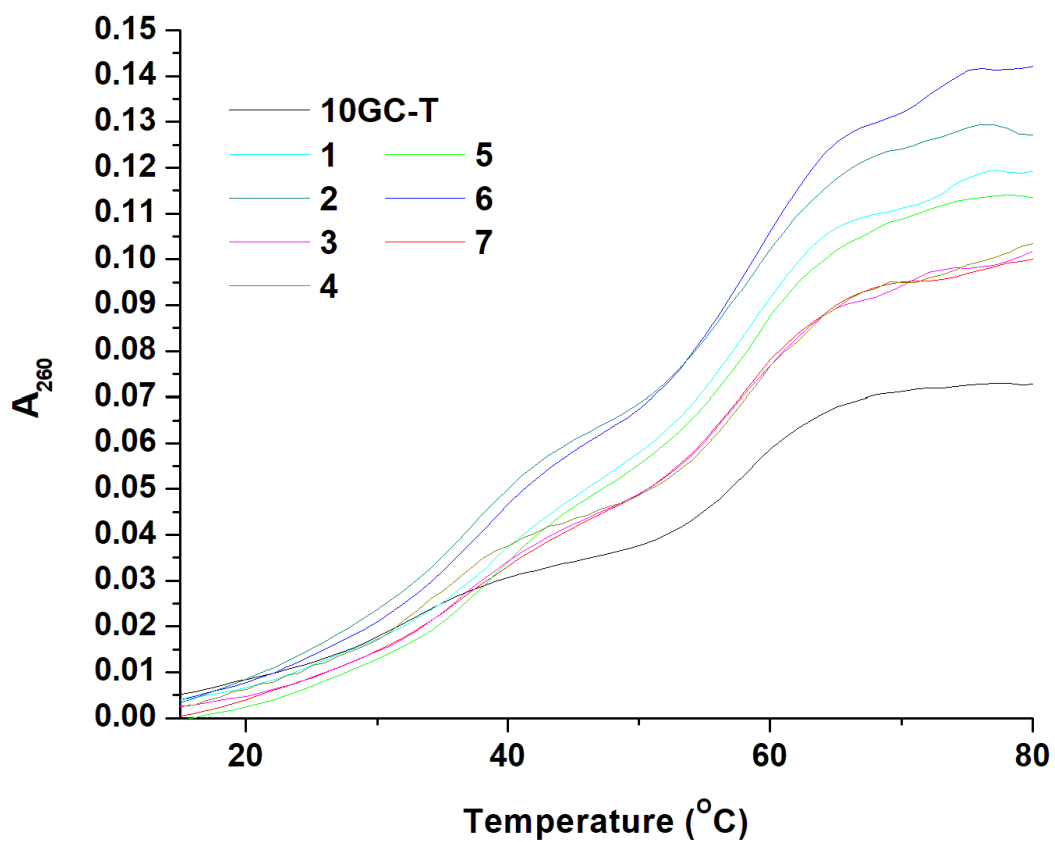

Y-axis adjusted to zero for better presentation. Buffer conditions: 10 mM sodium cacodylate and 150 mM KCl, pH 8.

Figure A-19

Thermal Denaturation of 15GC-T in the Presence of Tetramethoxyquercetin Five-Carbon Linker

Derivatives at pH 6

Y-axis adjusted to zero for better presentation. Buffer conditions: 10 mM sodium cacodylate and 100 mM NaCl, pH

6.

Figure A-20

Thermal Denaturation of 15GC-T in the Presence of Tetramethoxyquercetin Five-Carbon Linker
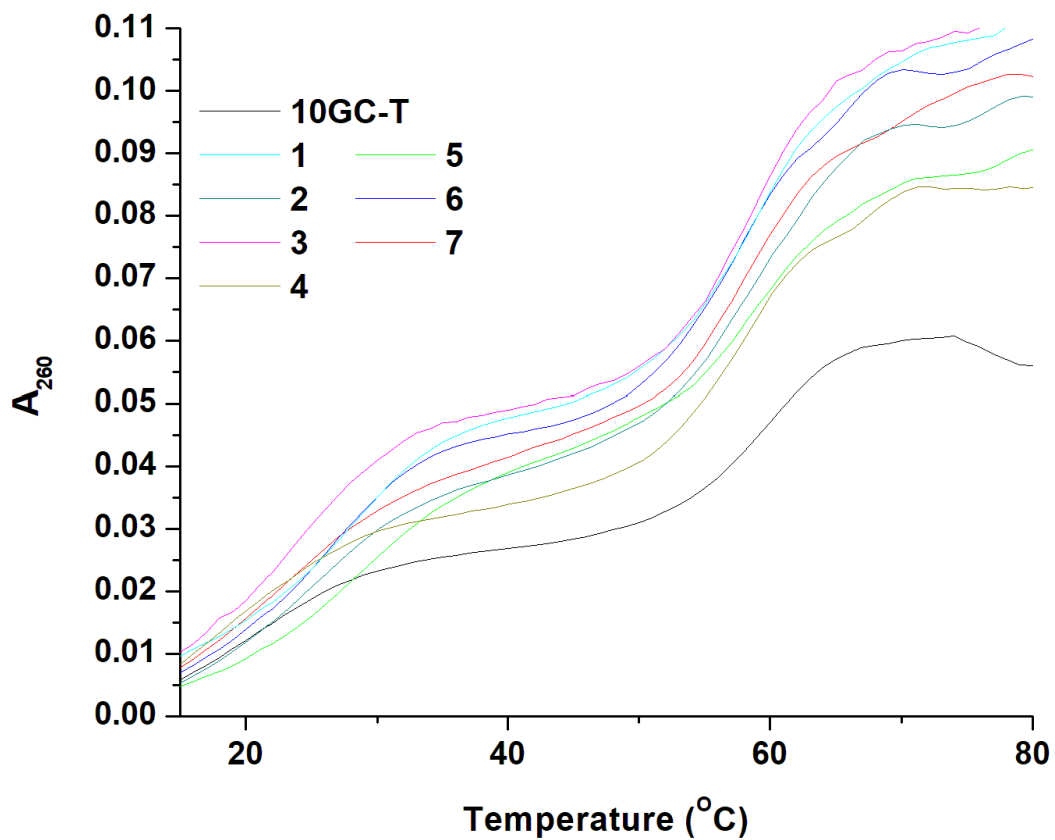
Derivatives at pH 7

Y-axis adjusted to zero for better presentation. Buffer conditions: 10 mM sodium cacodylate and 100 mM NaCl, pH

7.

Figure A-21

Thermal Denaturation of 15GC-T in the Presence of Tetramethoxyquercetin Five-Carbon Linker
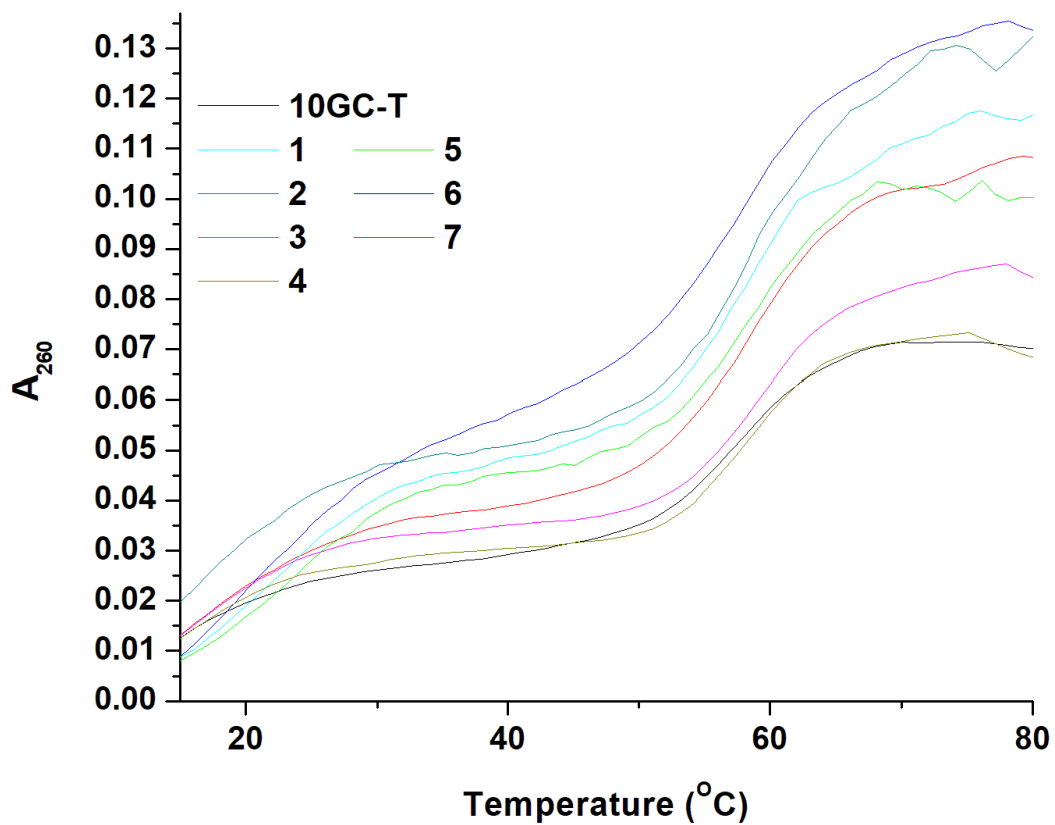
Derivatives at pH 8

Y-axis adjusted to zero for better presentation. Buffer conditions: 10 mM sodium cacodylate and 100 mM NaCl, pH 8.

Figure A-22

Thermal Denaturation of 10GC-T in the Presence of Tetramethoxyquercetin Five-Carbon Linker

Derivatives at pH 6

Y-axis adjusted to zero for better presentation. Buffer conditions: 10 mM sodium cacodylate and 100 mM NaCl, pH 6.

Figure A-23

Thermal Denaturation of 10GC-T in the Presence of Tetramethoxyquercetin Five-Carbon Linker
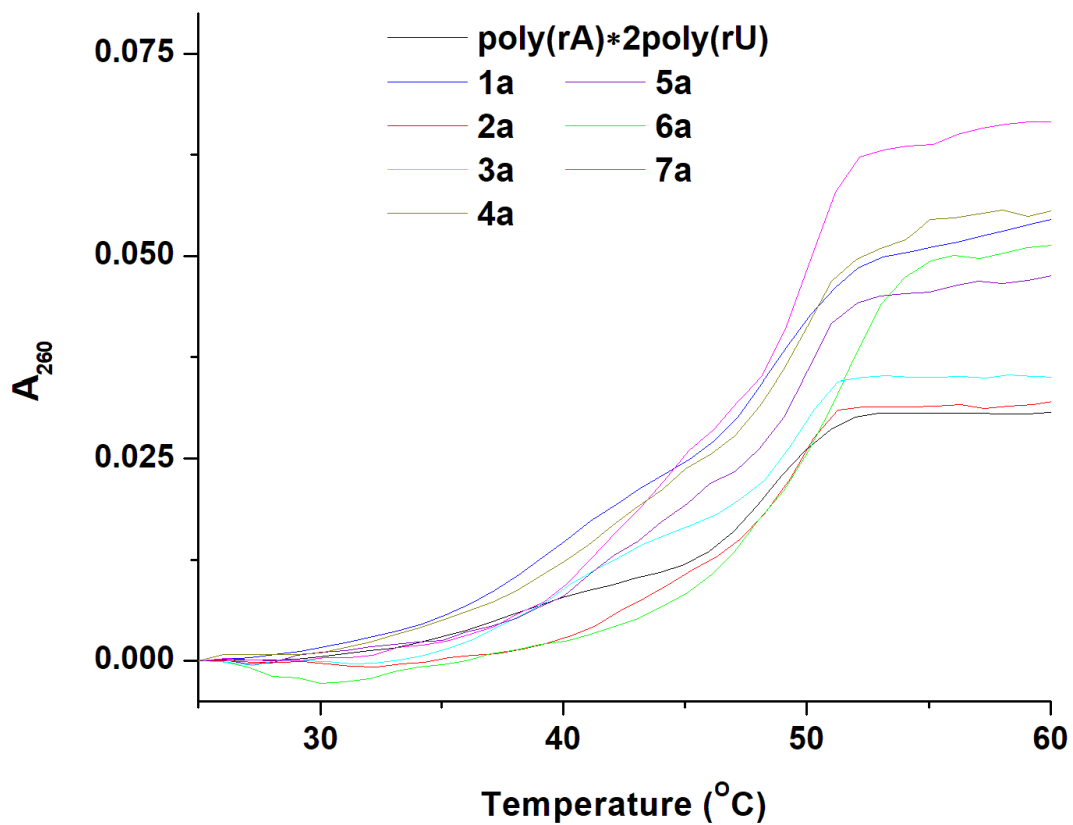
Derivatives at pH 7

Y-axis adjusted to zero for better presentation. Buffer conditions: 10 mM sodium cacodylate and 100 mM NaCl, pH 7.

Figure A-24

Thermal Denaturation of 10GC-T in the Presence of Tetramethoxyquercetin Five-Carbon Linker

Derivatives at pH 8

Y-axis adjusted to zero for better presentation. Buffer conditions: 10 mM sodium cacodylate and 100 mM NaCl, pH
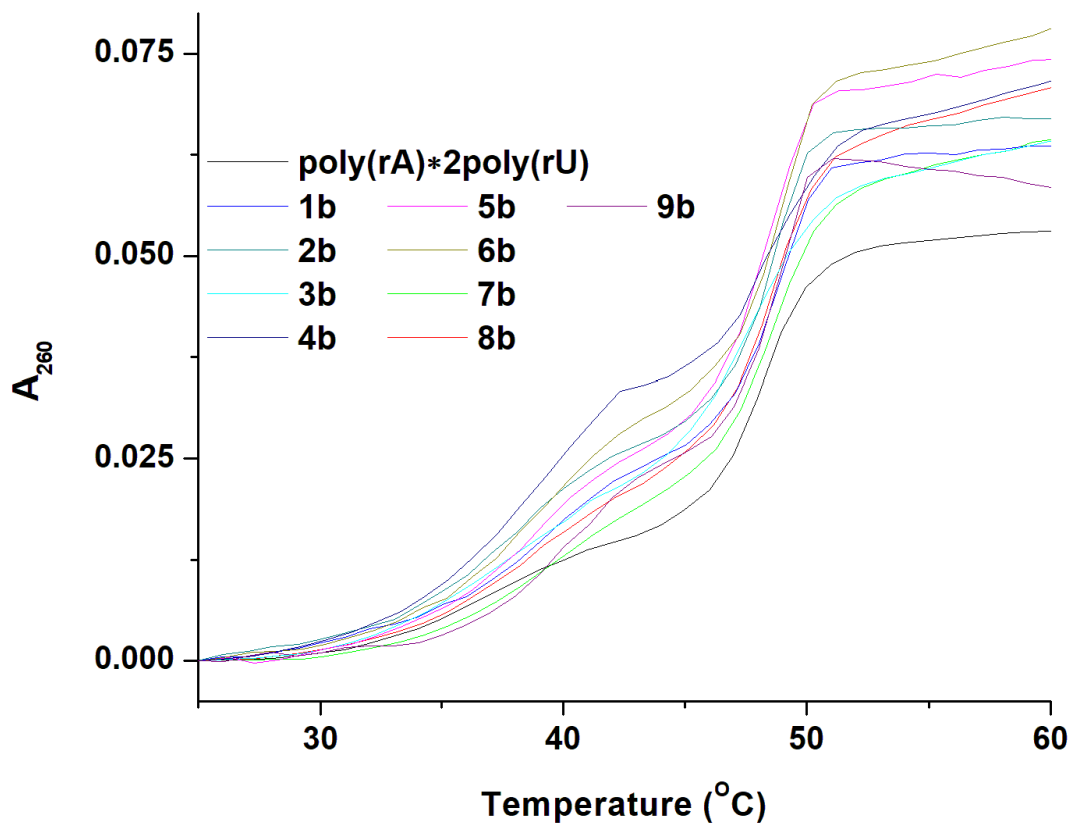
8.

Figure A-25

Thermal Denaturation of poly(rA)•2poly(rU) in the Presence of Tetramethoxyquercetin Three-Carbon Linker Derivatives

Y-axis adjusted to zero for better presentation. Buffer conditions: 10 mM sodium cacodylate, 0.1 mM Na$_2$EDTA and 25 mM NaCl, pH 6.8.
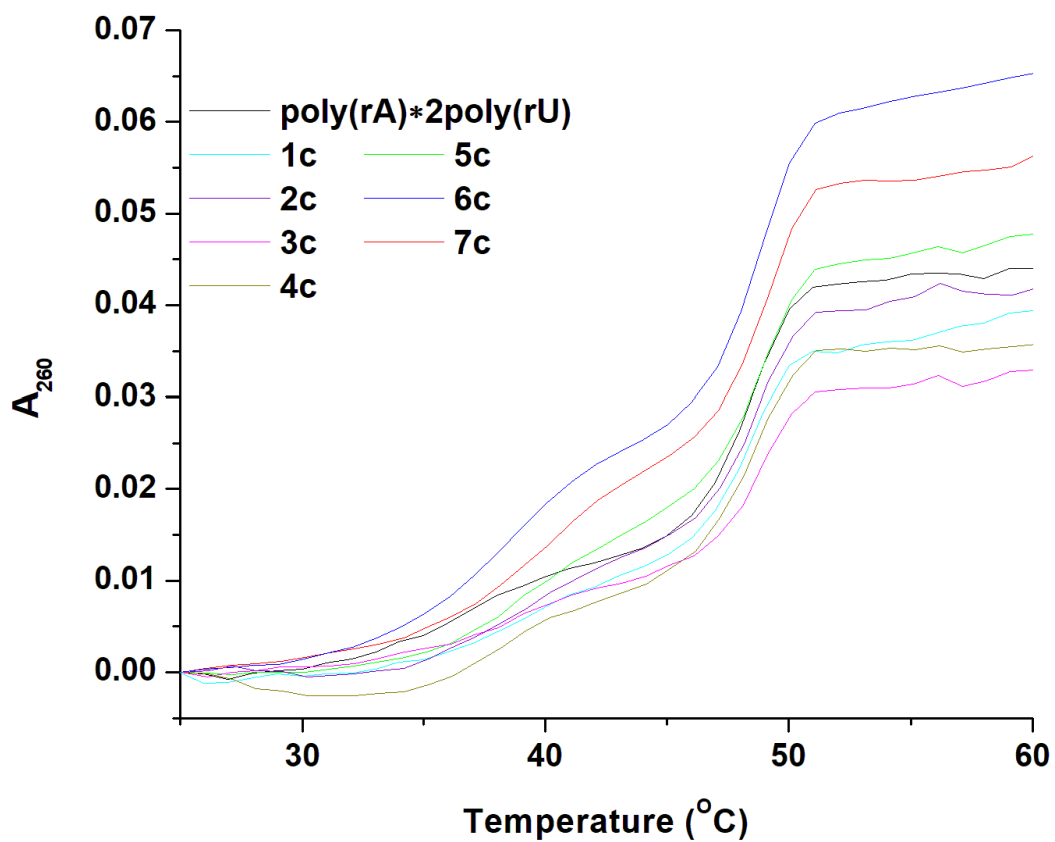
Figure A-26

Thermal Denaturation of poly(rA)●2poly(rU) in the Presence of Tetramethoxyquercetin Four-

Carbon Linker Derivatives

Y-axis adjusted to zero for better presentation. Buffer conditions: 10 mM sodium cacodylate, 0.1 mM Na$_2$EDTA

and 25 mM NaCl, pH 6.8.

Figure A-27

Thermal Denaturation of poly(rA)●2poly(rU) in the Presence of Tetramethoxyquercetin Five-

Carbon Linker Derivatives

Y-axis adjusted to zero for better presentation. Buffer conditions: 10 mM sodium cacodylate, 0.1 mM Na_2EDTA

and 25 mM NaCl, pH 6.8.